2010

Isotopic Composition of Mercury in the Atmosphere

Sulata Ghosh

THE FLORIDA STATE UNIVERSITY

COLLEGE OF ARTS AND SCIENCES

ISOTOPIC COMPOSITION OF MERCURY IN THE ATMOSPHERE

By

SULATA GHOSH

A Dissertation submitted to the
Department of Earth Ocean and Atmospheric Sciences
in partial fulfillment of the
requirements for the degree of
Doctor of Philosophy

Degree Awarded:
Summer Semester, 2010

The members of the committee approve the dissertation of Sulata Ghosh defended on April 27, 2010

_____
A. Leroy Odom
Professor Directing Dissertation

_____
William Landing
University Representative

_____
Yang Wang
Committee Member

_____
Stephen Kish
Committee Member

Approved:

_____
Lynn Dudley, Chair, Department of Earth Ocean and Atmospheric Sciences

_____
Joseph Travis, Dean, College of Arts and Sciences

The Graduate School has verified and approved the above-named committee members.

To Baba,
for all that you do

ACKNOWLEDGEMENTS

Many people are responsible for the success of this dissertation and I would like to thank everyone that has helped me through it.

Firstly, I would like to thank my advisor, Dr A Leroy Odom, for supervising this dissertation. I am truly grateful for his guidance, support and encouragement. His enthusiasm is contagious and is a great motivator. I would like to thank him for his never ending patience, for listening to my constant whining and for feeding this hungry grad student.

I would also like to thank my committee members Dr Stephen Kish, Dr William Landing and Dr Yang Wang, for being extremely helpful and being very generous with their time and suggestions towards my research. I am grateful to all the professors at FSU that have taught me over the years. I admire their commitment to their students.

To my wonderful friends, I cherish all the laughter and support. I would also like to acknowledge Jorge Cham for the much needed comic relief.

I thank my family especially my father, sister, mother, brother-in-law and niece. Huge thanks to Raoul, for staying with me in the lab while I ran my samples through the night. You all have been pillars of support. But for your love and encouragement, this journey would not have been possible.

Big thanks to Baba, my role model in life, for always believing in me and even to this day explaining the fundamentals of physics over the phone. This is for you.

TABLE OF CONTENTS

LIST OF TABLES

LIST OF FIGURES

ABSTRACT

The cardinal role of the atmosphere in the global dispersion of mercury and its deposition in aquatic environments and on land is well established. Re-emission of mercury from waters and land is the major source of atmospheric mercury. If isotopic variations in Hg are to be used in developing a better understanding of the mercury cycle, experimental studies of the isotopic effects of those processes that induce mercury transformations from one species to another and its transition in and out of the atmosphere are critical. Knowledge of the isotopic composition of atmospheric mercury is also a key. This study has attempted to determine the isotopic signature of Hg in the atmosphere to provide an anchor for geochemical models of mercury.

The residence time of Hg^0 which comprises of approximately 98% of the total mercury in the atmosphere has been variously estimated to be between 0.6 and 2.0 years. Both the horizontal and vertical mixing times of the troposphere are approximately one month (vertical mixing can be much faster). Accordingly, we suspect that atmospheric mercury might closely approach isotopic homogeneity on a hemispherical scale (mixing times between the northern and southern hemispheres might well exceed a year). We have analyzed atmospheric mercury collected in our local area along the Gulf of Mexico coast at various times, elsewhere in the U.S. and at NOAA Global Baseline Observatories.

Mercury is trapped on gold plated sand in a quartz tube. Air is passed through this gold trap by a pump, and a flow meter is used to monitor the flow rate. A desiccant ($CaSO_4$) is used to absorb the moisture from the air and does not interfere with the Hg collection. To ensure that anthropogenic input was at it its minimum, sampling was not conducted in industrialized areas, or near coal powered plants and remote locations were preferred. Once the sampling is complete, mercury is thermally purged from the gold trap, and carried by a helium stream into concentrated nitric acid containing chloride, where it is completely oxidized to Hg (II). Hg (II) is reduced in a CETAC HGX 200 Cold vapor generator, and the evolving cold mercury vapor is analyzed in a NEPTUNE MC-

ICP-MS. To minimize the effects of instrumental fractionation, isotope ratios were determined by sample standard bracketing technique and reported in δ (‰) notation relative to NIST SRM 3133. Where as δ^{A}Hg = $(\frac{Rsample}{Rstd} - 1)1000$ ‰, where R= $\frac{^{A}Hg}{^{200}Hg}$.

Samples of atmospheric mercury exhibit a mass dependent fractionation effect with light isotope enrichment in ^{198}Hg/^{200}Hg ratios (relative to NIST-SRM 3133) of the order of 1.3 $\pm$ 0.8 ‰ (2σ), and small but reproducible mass independent fractionation effects with positive ^{199}Hg and ^{201}Hg anomalies of +0.1 to +0.3 ‰. From this study it is concluded that the atmosphere comes close to an isotopically uniform reservoir of mercury $(IUR)_{Hg}$, on which local and temporary effects are likely imposed. This $(IUR)_{Hg}$ provides an anchor around which models of the global mercury cycle could be constrained.

In atmospheric waters and precipitation, mercury is present in the form Hg (II). Rainwater was collected in Tallahassee, FL for isotopic analysis of mercury. Due to low concentration of mercury in rainwater, samples were pre-concentrated by adding chloride and subsequent evaporation. All samples analyzed show a small positive odd isotope anomaly of the order of 0.213 +/- 0.28 (2σ) ‰ for ^{199}Hg and 0.18 +/- 0.24 (2σ) ‰ for ^{201}Hg.

A network of *Tillandsia usneoides* (common name: Spanish Moss), an epiphyte, was collected along the eastern Coastal Plain of the U.S. from northern Florida to North Carolina and analyzed for its isotopic composition to determine its effectiveness as a natural monitor of isotopic composition of the atmosphere in which it grows. The Spanish moss exhibits a clear negative mass independent isotope effect which is distinct from the isotopic composition of the Hg-vapor in the ambient air and Hg (II) in the rain measured. Moreover all samples plot within analytical uncertainty of the theoretical fractionation line for magnetic isotope effect with a Δ^{201}Hg/Δ^{199}Hg ratio of 1:1.1. This clearly indicates towards a biological origin of the isotope effect seen in the moss.

CHAPTER 1

The use of mercury isotopes as a tool to study the geochemical cycling of mercury

1.1 Introduction and statement of purpose

In wake of the Minamata Bay disaster (Japan) of the 1950's and 1960's there has been a tremendous amount of effort to understand the behavior of mercury in the biosphere. Inorganic forms of mercury released into the atmosphere can be converted to methyl mercury by sulfate reducing bacteria. Methyl mercury is a very toxic substance, which can bio-accumulate in the lowest level organisms in the aquatic food chain and bio-magnify all the way up to upper level wildlife and humans.

Atmospheric deposition is the most important source of Hg to water bodies. Several anthropogenic and natural sources have been identified for atmospheric mercury. Models that have greatly contributed to the understanding of the mercury cycle are based on concentration and fluxes. However, there still remain uncertainties regarding the relative amounts of natural and anthropogenic emissions, the atmospheric depositional rates and the spatial variations of atmospheric mercury (Schroeder and Munthe, 1997).

The recent discovery of mass independent fractionation (MIF) of mercury isotopes (Bergquist and Blum, 2007) and multiple MIF isotope effects (Ghosh and Odom, 2007; Das and Odom, 2007; Ghosh et al. 2008; Gehrke et al.,2009; Biswas et al, 2008; Das et al, 2009; Carignan et al 2009) provides promise of new understanding of the dynamics of the mercury environmental cycle. The cardinal role of the atmosphere in the transport and deposition of mercury, indeed in its global dispersion calls for an investigation of the isotope systematics of atmospheric mercury, before this promise is fulfilled. In particular the following questions need be answered:

1) Can atmospheric mercury be characterized in terms of isotope effects?

2) What is the scale of isotopic homogeneity/heterogeneity (local, regional, hemispherical, global)? Primarily, is the atmosphere an isotopically uniform reservoir of mercury that can serve as an anchor in mercury cycling models, or do heterogeneities exists that can provide information on atmospheric inputs, local sources or large scale atmospheric patterns?

3) What isotopic differences exists between Hg(0) and Hg(+2) and what isotope effects are induced in redox reactions involved in atmospheric inputs and deposition?

4) How well does mercury in epiphytes represent atmospheric mercury? Can mercury in epiphytes be used as convenient, inexpensive, and abundant proxies? Does it represent the mercury of dry or wet deposition, or both, or can enzymes in plants be responsible for the isotope effects observed in epiphytes.

The following research represents an attempt to answer these important questions and provide a foundation for future studies.

1.2 General Considerations

Mercury is a transition group heavy metal and has an atomic number 80. It is the only metal which is liquid at STP. Mercury (Hg) has seven stable isotopes. Relative isotope abundances are ^{196}Hg (0.15%), ^{198}Hg (9.97%), ^{199}Hg (16.87%), ^{200}Hg (23.10%), ^{201}Hg (13.18%), ^{202}Hg (29.86%), and ^{204}Hg (6.86%). The most important ore of mercury is cinnabar (HgS) which has been mined extensively from its chief deposits in Almaden (Spain), Idria (Slovenia), Monte Amiata (Italy), British Columbia (Canada) and California (USA) for its use in many industries such as mining, metallurgy and dentistry. The most important source of juvenile mercury is through the outgassing of earth's crust and mantle, volcanism and geothermal processes. Once released into the atmosphere, it may be subjected to a variety of geochemical processes and pathways. The fate of mercury in the atmosphere depends on several factors such as environmental conditions and chemical as well as physical properties of the particular species of mercury.

1.3 Global Mercury Cycle

Inorganic forms of mercury deposited from the atmosphere can be converted to methylmercury by naturally occurring biological processes. Mehylmercury is a very toxic substance which can concentrate a million fold in the aquatic food chain. Exposure to methylmercury can cause severe birth defects and neurological impairment in children as it can break through the placenta. Extreme cases of the Minamata disease cause convulsions, coma and an eventual death. Health advisories have been issued to many communities advising them to limit their consumption of fish, fresh water as well as seawater. This is the main reason for concern about emission and mobilization of mercury into the biosphere (Schroeder and Munthe, 1997). Since the 1970's, when chlor alkali plants were a huge source of mercury emissions into the atmosphere in the industrialized nations, there have been regulatory controls on this and other types of

anthropogenic mercury emissions. Coal combustion, metal smelting, refining and manufacturing, as well as waste incineration are currently major sources of anthropogenic emissions (Schroeder and Munthe, 1997).The way mercury is emitted and recycled in the atmosphere has therefore been extensively studied and documented.

Mercury is highly volatile and enters the atmosphere via processes such as outgassing of the earth's crust or mantle, from surficial soils, water bodies, volcanoes and geothermal sources (Schroeder and Munthe, 1997). It can be readily reemitted to the atmosphere once it is deposited to the earth's surface.In the air, mercury predominantly exists in the vapor phase as Hg (0). It is relatively inert to chemical attack by atmospheric constituents and only slightly soluble in water (Schroeder and Munthe, 1997). The key factors driving the global mercury cycle are wet deposition of Hg (II), dry particle deposition and adsorption of Hg vapor onto surfaces from the atmosphere and evasion of dissolved gaseous mercury from water bodies such as oceans and lakes as well as evasion from lands (Mason and Sheu, 2002). Figure 1 is a schematic diagram of the mercury cycle as described by Mason and Sheu (2002). In forested areas, mercury can be exchanged through leaves that can be both a source and a sink for Hg (0). Here, dry deposition is of similar or greater importance than wet deposition (Lindberg 1996, Schroeder and Munthe, 1997). From some natural sources like volcanoes and soil erosion, mercury can be associated with particulate matter. Air can be enriched with reactive gaseous mercury (RGHg) and particulate mercury (Hg-P) in close proximity of these point sources. In this case, dry deposition of RGHg dominates the overall flux (Schroeder and Munthe, 1997). This dry deposition can have an impact on a local or regional scale. The speciation of RGHg (Reactive Hg) is assumed to be gaseous $HgCl_2$ or other Mercuric Halides. The compounds have a high surface reactivity and water solubility compared to Hg (0) and they are rapidly removed from the atmosphere by deposition processes.

Mason and Sheu (2002) have studied the deposition of RGHg formed in remote regions by all the potential gas phase or heterogeneous reactions in the atmosphere, especially the oxidation of Hg (0) by halogen radicals (Lin and Pehkonen, 1999). The imbalance between the evasion and deposition estimates suggests that oxidation or some other removal mechanism for atmospheric Hg (0). From their study of atmospheric collections over the North Atlantic Ocean, they propose enhanced oxidation above the sea surface.

The three predominant mercury species in the atmosphere exhibit different transport characteristics (Schroeder and Munthe, 1997). Elemental Hg is capable of being transported for very long distances from tens to thousands of kilometers. Hg (+2) species in the gas phase can be transported from a few tens to a few hundreds of kilometers from their source. Hg associated with particulate matter is generally deposited at intermediate distances depending on the size and density of the aerosol (Schroeder and Munthe, 1997).

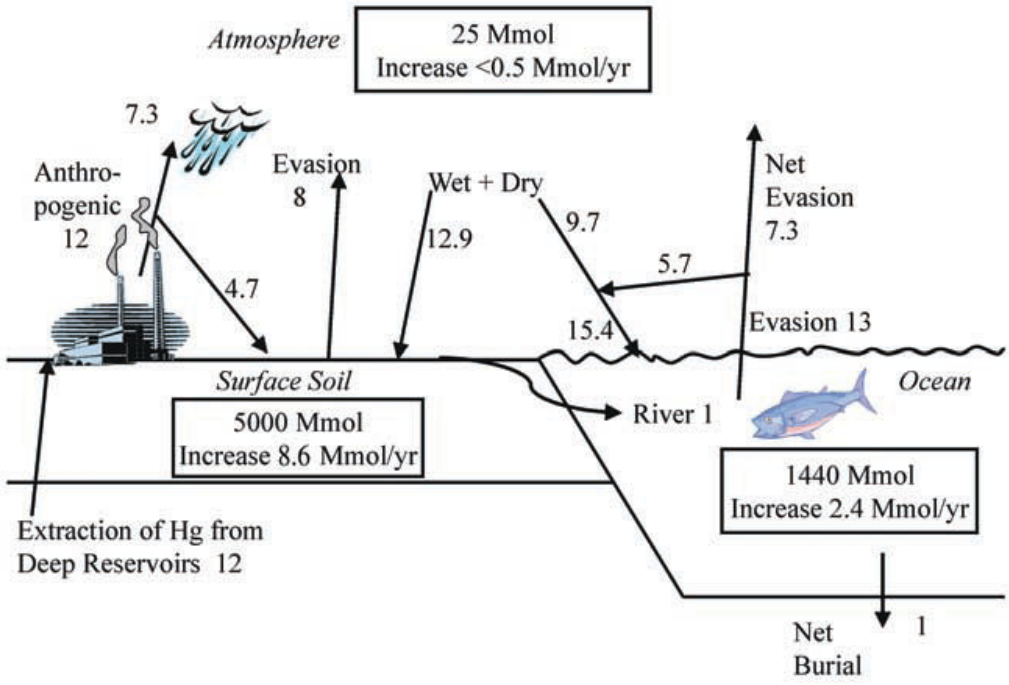

Figure 1.1 Mercury Cycle (Mason and Sheu, 2002)

While Hg evasion from both the ocean and terrestrial environment is considered mainly to be in the form of Hg (0), deposition is a more complicated process given the Hg speciation (Mason and Sheu, 2002, Lindberg and Stratton 1998). The depositional flux at a particular site depends on the individual concentrations of different mercury species as well as constituents involved in the removal process mentioned above, temperature, and rainfall. In air containing high concentrations of Hg (II) and particulate Hg (Hg-P) (>100 pg/ cubic meter), these species will dominate in both wet and dry deposition (Schroeder and Munthe, 1997). When the concentrations of Hg (II) and Hg-P are lower, the wet deposition mainly depends upon the oxidation of Hg (0) in gas or aqueous phases.

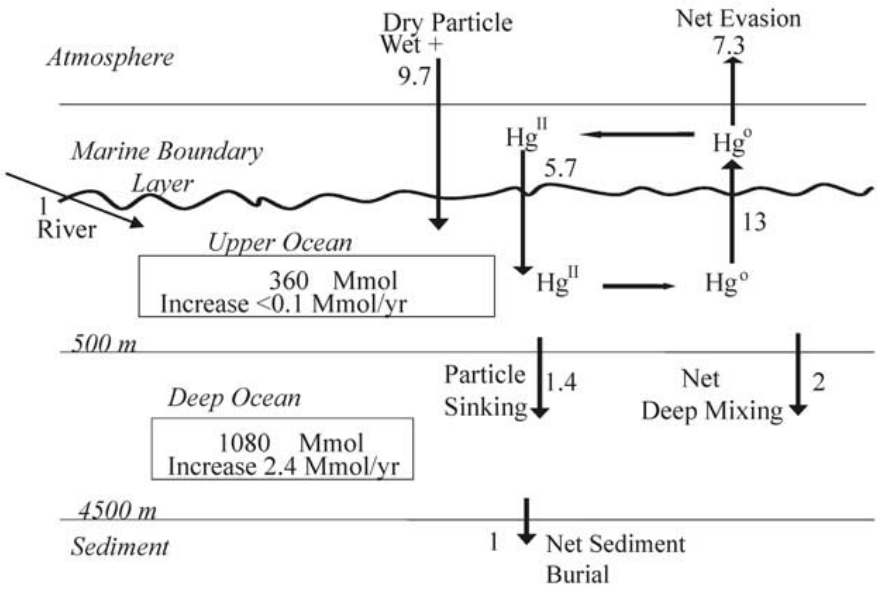

Figure 1.2 Hg cycle at the marine boundary layer (Mason and Sheu 2002). All fluxes in Mmol/year

Figure 1.2 is a box model representation of the mercury cycling and fluxes of mercury within the ocean and marine boundary layer (MBL) (Mason and Sheu, 2002). Most of the Hg deposited in the ocean is lost via gas evasion and probably cycles between the

surface ocean and the MBL before being lost to the atmosphere or the deep ocean. The overall balance for the deep ocean suggests that 30% of the flux to the deep ocean is preserved in sediments. Evasion is the main factor for loss of mercury from the upper ocean. However, some fraction of the evaded Hg is oxidized in the marine boundary layer and is re-deposited.

All currently existing models of the mercury cycle are based on studies on flux and concentration variation of mercury. There still remain uncertainties regarding the relative amounts of the various natural and anthropogenic emissions, the atmospheric depositional rates and the spatial variations of atmospheric mercury (Schroeder and Munthe, 1997).

1.4 Theory of Isotopic Fractionation

The spectrum of an atom consists of discrete nuclear energy levels. These energy levels depend on several factors, for example, nuclear charge, mass, volume, shape, distribution of neutrons in the nucleus and a host of other properties arising out of interaction of the electrons in the atom with the nuclear charge, magnetic moment etc. Out of these, the factor that primarily determines the atomic energy levels is the nuclear charge. All other effects contribute a small amount of modification to these energy levels. These changes are generally termed as “hyperfine structures”. Isotope shifts are a class of hyperfine structures. The important causes of isotopic effects are described below. These effects may occur together.

1.4.1 Mass Fractionation

Mass effect arises due to the fact that atomic energy levels depend on the mass of the nucleus. All isotopes of an element have the same electronic structure and hence have the same chemical characteristics. Molecules containing different isotopes of the same element however have different physical characteristics like their internal energy, heat

capacity and entropy. This is because molecules differing only in isotopic constituents have different translational, vibrational and rotational energies.

In reactions involving condensed phases, the difference of translational and rotational energy is more or less the same in products and reactants. Therefore, the predominant source of isotopic mass effects in condensed phases is the difference in the vibrational energy. Lighter isotopomers of mercury have higher vibrational frequencies and hence, the reaction rates of these molecules are faster than their heavier counterparts. As a result, in a kinetic fractionation process, the products are depleted in heavier isotopes relative to the reactants. The degree of fractionation depends on the relative mass difference between the molecules, the degree of completion of the reaction, the reaction path and the temperature. Temperature affects the vibrational frequencies of the molecules. As the absolute frequencies increase, the relative differences in frequencies between the lighter and the heavier molecules become smaller. As the temperature increases, the extent of isotopic fractionation decreases.

Mass fractionation effects are important for lighter elements such as H, O, N, C and S. For heavier elements such as mercury with a high mass number, the relative mass difference between the seven stable isotopes is small. Consequently, the isotopic effect produced by these mass differences is therefore very small. In case of these heavier elements, it is therefore important to also consider the effects of small changes in nuclear shape and structure. (Breit, 1958)

1.4.2 Mass Independent Fractionation

Mass-independent isotopic fractionation (MIF) was first demonstrated in the formation of ozone by Thiemens and Heidenreich (1983). Since then, investigations of MIF found in oxygen and sulfur (Farquhar et al., 2000) have led to a better understanding of earth's natural systems, in particular its atmosphere.

There are at least two important MIF mechanisms that can produce an odd-N isotope effect. In a multi isotope plot against the delta values, the even isotopes define a mass proportional curve whereas the odd isotopes deviate from this curve. This odd-N effect has now been reported by Bergquist and Blum (2007), Ghosh and Odom, 2007; Das and Odom, 2007; Ghosh et al. (2008); Gehrke et al. ,(2009); Biswas et al, (2008); Das et al, (2009) and Carignan et al (2009) , in the seven stable isotopes of mercury.

1.4.2.1 Magnetic Isotope Effect (MIE)

The magnetic isotope effect selects the nuclei according to their spins and magnetic moments (Buchachenko et al, 1976). The magnitude of the spin angular momentum of a particle is determined by the spin quantum number, which is an integral or a half-integral number that is characteristic of the particle (Turro, 1983). The spin quantum number for an electron is always +1/2. The spin quantum number of a nucleus can be both integral and half integral. Nuclei such as ^{198}Hg, ^{200}Hg, ^{202}Hg and ^{204}Hg with even mass numbers have spin value zero. Nuclei with odd mass numbers, however, have spin with half-integral values. The nuclear spin values for ^{199}Hg and ^{201}Hg are 1/2 and 3/2 respectively. The interaction of the magnetic moment of a nucleus with the magnetic moment of the atomic electrons, which is described as the nuclear-electronic hyperfine coupling provides the mechanism by which the nucleus influences chemical reactions. These interactions are small and do not influence the chemical equilibrium, but introduce a kinetic magnetic isotope effect, which allows the chemical reactions of isotopes with different spins to proceed at different rates (Turro, 1983).

Chemical reactions are spin selective. They are allowed only when the total spin states of the reactants is equal to the spin state of the product. In reactions involving radical pair intermediates, transitions may occur where spin may not be conserved. Here, the electronic spins of the unpaired radicals may be oriented so that they cancel each other completely corresponding to a net electronic spin of “0”. This spin state is called a “singlet state” because it remains a single state in the presence of a magnetic field. Alternatively, the spin of unpaired radicals may be oriented so that the net spin may be in multiples of one. This is called the “triplet state” because the electron spin vector can be oriented in three ways in a magnetic field. The three sublevels of the triplet state are T_+ (both individual spins are “up”), T_0 (one “up” and one “down”) and T_- (both are “down”). A schematic representation of the singlet state and triplet state is shown in figure 1.3. Through hyperfine coupling, the nuclear spin can influence the rate of singlet-triplet and triplet-singlet conversions known as intersystem crossings (ISC) in a radical pair during a chemical reaction.

These spin state conversions may be time dependent. In the presence of a magnetic field, which applies a torque, the electron spin vectors, which are weakly bound to each other but strongly bound to the magnetic field, may over a period of time change their orientation. Figure 1.4 is a schematic representation of a triplet-singlet ISC over time $t= \pi/2\Delta\omega$, where ω is the precession frequency. The nuclear spin effects can hence take place only for suitably long-lived radical pairs.

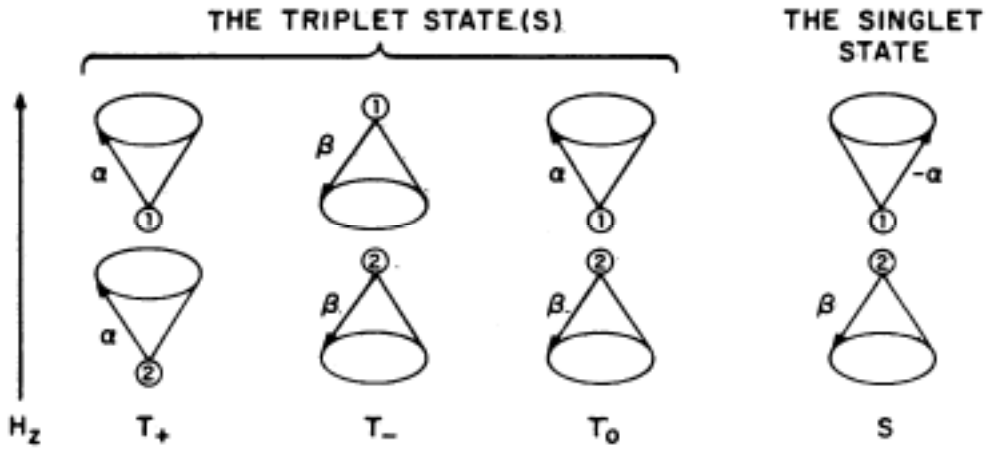

Figure 1.3 Schematic representation of a triplet state and a singlet state (Turro, 1983).

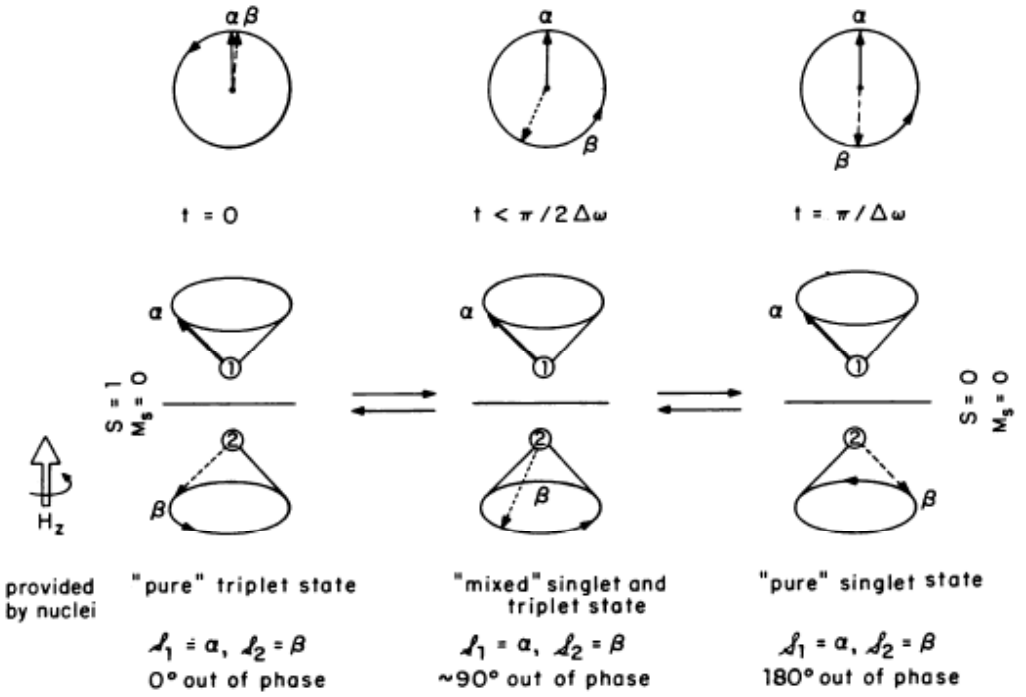

Figure 1.4 A magnetic field applies a torque on the spin vector, causing it to precess at a different rate than its counterpart so that over a period of time $\pi/2\Delta\omega$, a triplet state evolves into a singlet state (Turro, 1983).

1.4.2.2 Nuclear Volume Fractionation (NV)

Nuclear volume fractionation is caused due to a change in the nuclear charge distribution with a change in the number of neutrons. Isotope shift in heavy nuclei may arise due to nuclear size. The nucleus has positively charged protons that are distributed over the nuclear volume. Since the charge Z for different isotopes of the same element is the same, the nuclear charge is distributed over a larger volume in case of the heavier isotope than for the lighter isotope. Empirically, the radius of the nucleus varies with mass number A as $A^{1/3}$.

When we add one neutron to a nucleus, the mass number increases from A to A+1 so that the change in radius becomes

$$\Delta r = (A+1)^{1/3} - A^{1/3} \qquad \text{--- Equation 1}$$

Thus if we consider an atom with mean mass number A=200, the change in the radius on addition of a neutron is about 1/600 of the original radius. Typical nuclear radii are expressed in Fermi which is 10^{-15} m (Breit, 1958). The radius of mercury 200 nucleus is approximately 7 Fermi. Thus, the change in radius of mercury on addition of one neutron is less $2X10^{-18}$ m. The simplest way to consider nuclear size effect is to consider the nuclear charge distributed over a sphere of radius given by the above. The interaction between a positive and a negative charge is given by Coulomb's law - $Ze^2/4\pi\varepsilon_0 r^2$ (where ε_0 is the electric constant and r is the distance between the point charges). This assumes that the positive and the negative charges are point charges (no size) separated by a distance r. The corresponding potential energy is $-Ze^2/4\pi\varepsilon_0 r$. For a point nucleus as the distance becomes closer the energy goes to minus infinity. However, for a non-zero size nucleus the interaction energy curve goes to a finite negative value at r=0. When isotopic mass increases the radius increases, the value of the energy also increases. Since the potential energy is more for heavier isotope total energy is also higher. Thus the isotope shift for heavier isotope is expected to be higher.

The lowest energy of a molecule is achieved when smaller isotopes (higher nuclear charge density) occupy bonds with higher electron densities, i.e. bonds involving *s* electrons.

The spin angular momentum of a nucleon is measured in units of Planck's constant h divided by 2π, usually denoted by ħ. The intrinsic value of the spin angular momentum of a nucleon is ħ/2. It is conventional to omit the factor ħ and say that a proton, neutron or an electron has spin ½. Angular momentum is a vector and one can measure its component along any direction like a classical vector.

Unlike in the classical case, the projection of the angular momentum can only take discrete values. If the spin value is S, the projection can take any of the values –S to +S in steps of 1. Thus the spin of a nucleon being ½, its components can only take values -1/2 and +1/2. When we add any odd number of spins we get the minimum value ½ whereas if we add even numbers we get the minimum value 0. In a magnetic field, spin S level splits into 2S+1 levels. Thus the lowest level of odd isotopes will split into two levels called doublets whereas the lowest level of even isotopes will be a single level (2S+1=1), i.e a singlet. This is the primary reason why the even series is different from odd series. Figure 1.5 is a schematic representation of this nuclear energy split for the odd isotope ^{199}Hg.

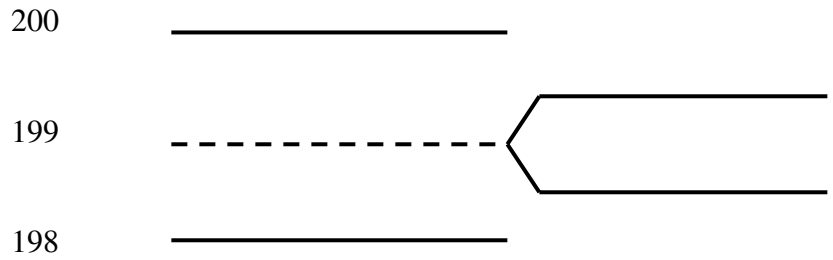

Figure 1.5 Schematic representation of energy levels of three isotopes of mercury. Dotted line represents the weighted mean energy of the levels for the odd isotopes. (Adapted from Breit, 1958)

1.5 Fractionation of Mercury Isotopes in terrestrial systems

Recent use of multicollector Inductively Coupled Plasma Mass Spectrometer (MC-ICP-MS) has enabled the precise measurement of Hg isotopes in many natural materials and has aided experimental studies in the fractionation of mercury isotopes. Mass dependent fractionation (MDF) of mercury isotopes was reported in hydrothermal systems (Hintelmann and Lu, 2003; Smith et al, 2005) and were reported to show a fractionation range of about 5 ‰. Mass Independent Fractionation (MIF) was first reported by Bergquist and Blum, 2007. They reported δ^A Hg values with respect to NIST SRM 3133 standard, where,

$$\delta^{A}Hg = \left[\frac{\left(\frac{^{A}Hg}{^{198}Hg} \right)_{SAMPLE}}{\left(\frac{^{A}Hg}{^{198}Hg} \right)_{NIST\,3133}} - 1 \right] \times 1000 \text{ ‰}$$

In the fish tissues analyzed in their study, they reported that ^{199}Hg and ^{201}Hg deviated from a mass dependent fractionation law and showed up to 4‰ enrichment with respect to the other isotopes. This anomaly is denoted as $\Delta\ ^{199}$Hg and $\Delta\ ^{201}$Hg. The observed MIF signature in the odd isotopes is attributed to the magnetic isotope effect or the nuclear volume effect explained in the previous section.

1.5.1 Biswas et al, 2008

Biswas et al. (2008) measured coal deposits from 30 different regions in the United States, Russia and China to determine their Hg isotopic composition. They reported a mass dependent fractionation (MDF) range of 2.8‰ in δ^{202}Hg values and a negative odd isotope (Δ^{201}Hg and Δ^{199}Hg) anomaly with the range -0.15 ‰ to -0.6 ‰. The slope of Δ^{201}Hg versus Δ^{199}Hg is 1.1 which is similar to that expected from photo-reduction of Hg (II). They further report a unique signature for each of the measured deposits indicating

that Hg isotopic composition of these deposits might be helpful in tracing sources of mercury pollution.

1.5.2 Ghosh et al 2008

Ghosh et al. (2008) measured mercury isotopes in Penido Vello peat bog which is an ombrotrophic peat bog in Spain. They reported MIF values in the peat where the Δ^{199}Hg values ranged between – 0.2 to – 0.5 ‰. They also reported a very small positive MIF of the order of 0.2 ‰ for Δ^{199}Hg in peat from Patagonia.

1.5.3 Das et al 2009

Das et al. (2009) conducted a study on fish of different trophic levels from Lake Jackson in Florida. The fish samples were collected at three locations around the lake, including near two sinkholes. During dry periods, the sinkholes can drain into the Florida aquifer. Several fish species belonging to different trophic levels were sampled over a short duration and comparative isotopic study was performed. The trophic levels of fish species were previously determined by gut contents and nitrogen isotopic compositions of the specimens by Aresco (2005). The authors found an increase in the magnitude of the MIF effect with increasing trophic level and argued that the MIF isotope effect resulted from metabolic processes.

1.5.4 Gehrke et al 2009

Gehrke et al. (2009) measured mercury isotopic composition of a Mid Pleistocene Mediterranean sea sapropel. They measured concentration of trace metals such as Ni, Cu, Zn, Mo, Ba, Re, U and Hg. In the organic rich layers there was a greater concentration of the trace metals. In terms of their mercury isotopic signature, the sapropels (organic rich sediments) demonstrate a δ^{202}Hg value of -0.91 ‰ and Δ^{199}Hg value of 0.11 ‰. The background sediment signature is indistinguishable from this with

a δ^{202}Hg value of -0.76 ‰. This has been interpreted to represent the isotopic composition of the Tyrrhenian sea in the mid-Pleistocene.

1.5.5 Carignan et al 2009

Carignan et al. (2009) measured the isotopic signature of mercury in lichens collected in France, Northern Quebec and the Swiss Alps. The lichen samples show a MIF effect of Δ^{199}Hg and Δ^{201}Hg of the order of -0.3 to -0.9 ‰. On a Δ^{199}Hg versus Δ^{201}Hg plot the samples define a slope of 1.1, characteristic of magnetic isotope effect. The authors conclude that the negative signature recorded by lichen is inherited from the atmosphere and they can be used as a proxy for measuring atmospheric mercury composition.

1.6 Laboratory Experiments

A few laboratory experiments have been undertaken to better understand the processes that cause the isotope effects found in nature. Some of the important recently published work is summarized below.

1.6.1 Bergquist and Blum 2007:

Bergquist and Blum (2007) conducted photoreduction experiments on aqueous Hg^{2+} and MeHg in the presence of dissolved organic carbon (DOC) that yielded both MDF as well as MIF. Experiments followed the Rayleigh fractionation process in which lighter isotopes are preferentially removed. Concentrations of 60- 100 ng/g were used for the experiments. The reduced elemental mercury was continually removed from the reaction chamber which inhibits photo-oxidation of the Hg^0. These two factors are considered in interpretation as the experimental conditions do not necessarily reflect

environmental conditions. Up to 2.5‰ enrichment of odd isotopes was reported with respect to the even isotopes in photoreduction of Hg2+. The degree of MIF was greater on the photoreduction of MeHg than in Hg^{2+}. The dark experiments yielded only MDF and no MIF. The authors also note that an increase in the concentration of DOC resulted in a larger magnitude of MIF.

1.6.2 Zheng et al 2007, 2008

Zheng et al. (2007and 2008) conducted a set of experiments to determine the magnitude of isotopic fractionation during the volatilization of Hg^0 from an aqueous phase. Hg^{+2} in solution was purged with $SnCl_2$ to generate Hg^0 which was then bubbled into a solution of 316 μM $KMnO_4$ with 0.9 M Sulfuric acid. The δ^{202} Hg values were determined for the fraction of Hg remaining in solution (f_R) as well as the fraction of Hg in the trapping solution (f_T). The first experiment measured the fractionation between the fraction of remaining Hg and the total accumulated Hg^0. The second experiment measured the fractionation between the remaining Hg and Hg vapour produced instantaneously. The fractionation was determined to be of Rayleigh type where the lighter isotopes were preferentially removed in the volatilized phase. The δ^{202} Hg increased exponentially as $f_R \rightarrow 0$. For f_R =0.036, δ^{202}Hg = 1.48‰. The δ^{202} Hg of the accumulated Hg vapor varied from -0.647 ‰ to -0.058 ‰. In the second set of experiments, δ^{202} Hg of the Hg vapour increased from -0.743 ‰ for f_R =0.966 to 0.683 ‰ for f_R =0.068. No MIF isotope effect was produced during the volatilization process.

In a later work, Zheng and Hintelmann (2009) performed key experiments to determine the significance of DOM-Hg complexes in the production of Hg isotope fractionations. They attempted to answer two fundamental questions in this work:

1) How do Hg isotopes fractionate in both reactant and product phases as photo-reduction proceeds?
2) What is the effect of Hg/DOC ratios on the isotopic fractionation?

Their study yielded both MDF and MIF with ^{199}Hg and ^{201}Hg showing a enrichment in the aqueous phase. Natural lake water from Lake Harp in Ontario, Canada with a DOC concentration of 12 mg/L and an initial Hg concentration of 8.9 ng/L was spiked with NIST 3133 to attain variable concentrations of Hg and therefore different Hg/DOC ratios. The reactor was maintained at constant temperature of 18 to 22ºC and irradiated by simulated sunlight to activate photoreduction of Hg(II) in the aqueous phase to vapor Hg(0). This was bubbled with Ar gas and the product was trapped in $KMnO_4$. Both the reactant and product were sampled in 2 hour intervals and analyzed for Hg fractionation. With increasing Hg/DOC ratios, a significant increase in the magnitude of the mass independent fractionation of the odd isotopes ^{199}Hg and ^{201}Hg was observed, presumably by the magnetic isotope effect. No significant dependence of mass dependent fractionation was observed on the Hg/DOC ratios for the even isotopes.

Reduction experiment in the presence of DOM conducted in dark conditions produced a MIF signature with a $\Delta^{199}Hg/\Delta^{201}Hg$ ratio of 1.5-1.6. The reaction pathways and fractionation process is abiotic and not photochemical in nature and is attributed to nuclear field shift effect (Zheng and Hintelmann, 2009).

1.6.3 Yang and Sturgeon, 2008

Yang and Sturgeon (2008) studied isotopic fractionation of mercury during reduction and ethylation processes. Hg^{+2} was reduced to Hg^0 by different methods for comparison. A working concentration of 100ng/g was used for the experiments using ultra pure reagents. The δ^{202} Hg was measured after 85-90% of reduction was complete with respect to the original composition of NIST SRM 3133. The first method of reduction is by purging Hg^{+2} with $SnCl_2$. This yielded a δ^{202} Hg value of 1.17 ‰. Reduction by $NaBH_4$ produced a δ^{202} Hg value of 1.08 ‰. UV photolysis in the presence of formic acid produced a δ^{202} Hg value of 1.34 ‰. And ethylation of Hg2+ with $NaBEt_4$ yielded a δ^{202} Hg value of 3.59 ‰. No significant MIF was found during any of the reduction processes or chemical ethylation processes.

1.6.4 Estrade et al, 2009

Estrade et al, (2009) conducted mercury liquid-vapor evaporation experiments to determine the isotopic fractionation of mercury. Two sets of experiments were conducted, one under equilibrium conditions and other under dynamic conditions. The equilibrium experiments were conducted in a temperature range of 0-22^0 C in a closed glass apparatus sealed by Teflon lined septum. When chemical equilibrium was reached the vapor above the liquid Hg was removed using a syringe. The average δ^{202} Hg of the vapor collected was -0.86 ‰.

In a separate system two sets of dynamic experiments were conducted under 10^{-5} bar vacuum. In one set 10mg of liquid Hg was evaporated at a temperature of 22^{0}C for 6-24 hours so it followed Rayleigh distillation process. The vapor was condensed on to a cold trap. In the second set of dynamic experiments, liquid Hg was evaporated between 22^{0}C to 100^{0}C and the condensed vapor fractions were analyzed. Also observed are odd isotope anomalies. The equilibrium experiment yielded Δ^{199}Hg/ Δ^{201}Hg ratio of 2.0, with the magnitude of Δ^{199}Hg being 0.12 ‰ and the magnitude of Δ^{201}Hg being 0.07 ‰. In the dynamic experiments, the ratio of Δ^{199}Hg/ Δ^{201}Hg was lower at 1.2 where the negative anomalies were in residual liquid fractions and the positive anomalies were in the cold trap. Magnitude for Δ^{199}Hg was between -0.12 to -0.02 ‰ in the residual liquid.

1.6.5 Kritee et al (2007)

Kritee et al conducted experiments to determine the isotopic composition of Hg during the reduction of Hg(II) to Hg(0) by mercury resistant bacteria. The main premise of this experiment was that Hg resistant bacteria that contain mercury reductase (merA) enzyme and reduce Hg (II) to Hg (0) produce kinetic fractionation of Hg isotopes preferentially up-taking lighter isotopes and enriching the remaining solution with heavy isotopes. It is acknowledged that the fractionation process may be species specific and may also depend on other environmental factors. Hg in an acidic solution was spiked with pure e coli culture and this was analyzed for Hg isotopic composition at

temperatures of 37º C, 30º C and 22º C. Working concentration of Hg in the initial solution was 600 ng/g. At 37º C the solution underwent a Rayleigh type fractionation process. When remaining fraction of Hg (II) was about 0.1, the δ^{202}Hg was approximately 3 ‰. In a subsequent study Kritee et al (2008) studied isotopic fractionation during mer-mediated microbial degradation of monomethyl mercury and reported an absence of MIF during mer-mediated Hg transformations.

CHAPTER 2

Isotopic Signature of Mercury in Air

2.1 Mercury in the atmosphere

In the atmosphere, approximately 99% mercury exists in the gaseous form, commonly referred to as total gaseous mercury (TGM) out of which 97% is elemental Hg vapor, i.e. Hg (0). The fact that mercury exists in the atmosphere mainly in vapor form distinguishes it from other common metals that tend to be associated with particulate matter. Its high volatility means that it can be subsequently re-emitted into the atmosphere after being deposited, as a result of several natural processes such as soil evasion, evasion from oceans and other inland water bodies as well as from plants. The residence time of mercury in the atmosphere has been determined to be of the order of 6 months to 2 years. This is considerably higher than most other metals present in the atmosphere that are associated with aerosols, which tend to have residence times between a few days to a few weeks depending on the properties of the associated aerosols. This, combined with the fact that it is extremely toxic has resulted in mercury being termed as a “global pollutant” (Schroeder and Munthe, 1998).

Mercury buried in deep reservoirs unavailable for natural cycling prior to the industrial revolution was extracted and made available to the environment as a result of human interference. This mercury directly or indirectly accounts for almost two thirds of the mercury flux as a result of subsequent reemission and deposition on the land and sea surface (Mason et.al 1994). In the present day, the atmospheric inventory of mercury has been estimated to be 25 Mmol, which is a three fold increase since the pre-industrial inventory estimated to be about 8 Mmol (Mason et al 1994). Currently, direct anthropogenic emission is estimated to contribute to as much as 36 % of the total flux of mercury into the atmosphere (Mason and Sheu, 2002). Out of this, almost 40% is due to

coal burning power plants (US EPA) and the rest is a product of waste incineration, metallurgy and manufacturing industries.

Hg can exist in three oxidation states of 0, +1and +2. It can exist as Hg (I) and Hg(II) in condensed atmospheric waters. Hg (I) in aqueous solutions such as in atmospheric waters is unstable as explained by the disproportionation reaction described by Munthe and McElroy (1992).

$$Hg_2^{2+}{}_{(aq)} \longleftrightarrow Hg^{2+}{}_{(aq)} + Hg^{0}{}_{(aq)}$$

Hg (I) cannot form stable complexes with common atmospheric ligands and in their presence will disproportionate to form Hg^{2+} and Hg^{0}. Even if it does exist, it is at much lower concentration than Hg (II). Due to this Hg (I) is of little consequence in atmospheric mercury cycle. Hg(II) is capable of forming stable complexes with ligands such as OH^-, Cl^-, Br^-, I^-, SO_3^- and CN^-.

Total gaseous mercury (TGM) which includes Hg (0) and gaseous divalent Hg (II) compounds and mercury associated with particulate matter (Hg-P) are the main species of mercury in the atmosphere. Tropospheric mercury mainly exists in the gaseous elemental vapor form, Hg (0), which remains mainly insoluble and non reactive unless converted to Hg (II) by photochemical redox reactions. This accounts for its long life time, which has been estimated to be 260 days for TGM and 16 days for Hg-P (Kvietkus & Sakalys, 2000). Transport behaviour and characteristics of TGM and Hg-P are different. TGM is quite well mixed in the troposphere. Gaseous mercury can be transported almost up to a global scale whereas Hg-P is usually deposited more or less close to its source.

Since the atmospheric inventory of mercury is increasing even in the most remote locations, it is critical to understand the biogeochemical cycle of mercury and the role

the atmosphere plays in it and to develop a tracer to remove the uncertainties regarding its sources and sinks of mercury.

2.2 Atmospheric pathways of mercury

The main pathways for introduction and removal of mercury from the atmosphere are wet and dry particle deposition and emission and reemission of TGM from oceans and lands by evasion (Mason et al. 1994). A comprehensive review of the various pathways and processes involving the oxidation and reduction of atmospheric mercury species have been described by Lin and Pehkonen (1999). A summary of the transformation pathways of various Hg species is described below.

2.2.1 Aqueous phase oxidation of Hg (0) to Hg (II) by ozone (Munthe 1992):

Ozone, produced from photochemical reactions, is a daytime oxidant and is scavenged from gaseous state into aqueous phases in atmospheric waters. This process is independent of temperature and pH and can be expressed as:

$$Hg^{0}_{(aq)} + O_{3(aq)} + H^{+} \rightarrow Hg^{2+}_{(aq)} + OH^{-}_{(aq)} + O_{2(aq)}$$

Hg^{0} by this process has a half life of approximately 40 seconds.

2.2.2 Gas phase oxidation of Hg (0) by ozone:

This process was first described by P'yankov (1949) and has since then been studied in detail by Slemr et al (1985), Schroeder et al (1991), Iverfeldt and Lindqvist (1986) and Hall (1995). The process can be expressed as:

$$Hg^{0}_{(g)} + O_{3(g)} \rightarrow HgO_{(g,s)} + O_{2(g)}$$

The half life of Hg^{0} due to this process is approximately one year. It was found that relative humidity does not play an important role in the reaction rate and that sunlight irradiation increases the reaction rate by six times (Hall, 1995).

2.2.3 Aqueous phase oxidation of Hg0 to Hg (II) by $^{\cdot}OH$ radicals (Lin and Pehkonen, 1997):

The hydroxyl radical can be produced in clouds as a result of photolysis of ferric-hydroxide complexes, H_2O_2, HNO_3 and HONO (Finlayson-Pitts and Pitts, 1986; Faust and Hoigne, 1990 and Faust and Allen, 1993) or can be scavenged into atmospheric waters from the gaseous state. Like ozone, the $^{\cdot}OH$ radical is a day time oxidant and the half life of Hg 0 by this process is approximately 6 minutes. This oxidation process is expressed as:

$$Hg^0_{(aq)} + {}^{\cdot}OH_{(aq)} \rightarrow Hg^{+}_{(aq)} + OH^{-}_{(aq)}$$

$$Hg^{+}_{(aq)} + {}^{\cdot}OH \rightarrow Hg^{2+}_{(aq)} + OH^{-}_{(aq)}$$

2.2.4 Aqueous phase oxidation of Hg^0 by Chlorine (Kobayashi, 1987; Lin and Pehkonen, 1998)

Chlorine may exist as hypochlorous acid (HOCl) and Hypochlorite ion (OCl^-) depending on the pH of the aqueous solution. Since it can easily undergo photolysis, it is an important night time oxidant that is of great consequence in the marine atmosphere. Reactive chlorine species can be produced as a result of photolysis of ozone and sea salt particles in the marine atmosphere (Oum et. al, 1998) as well as through the volatilization of sea salt particles during wave breaking (Keene et al, 1996). It enters the aqueous phase through scavenging and the half life of Hg^0 by this process is approximately 0.5 minutes (Lin and Pehkonen, 1999). Oxidation of Hg0 by reactive chlorine is described as:

$$HOCl_{(aq)} + Hg^0_{(aq)} \rightarrow Hg^{2+}_{(aq)} + Cl^{-}_{(aq)} + OH^{-}$$

$$OCl^{-}_{(aq)} + Hg^0_{(aq)} + H^{+} \rightarrow Hg^{2+}_{(aq)} + Cl^{-}_{(aq)} + OH^{-}_{(aq)}$$

2.2.5 Gas phase oxidation of Hg0 by nitrate radical

The nitrate radical can be produced in the atmosphere through the interaction of ozone and nitrogen dioxide and can undergo rapid photolysis in sunlight and is thus a night time oxidant (Finlayson-Pitts and Pitts, 1986). The oxidation reaction as given by Sommar et al 1997 is:

$$Hg^0_{(g)} + NO^{\cdot}_{3(g)} \rightarrow HgO_{(g,)} + NO_{2(g)}$$

Half life of Hg^0 through this pathway is approximately 20 days.

2.2.6 Gas phase oxidation of Hg^0 by H_2O_2

H_2O_2 can be produced in the atmosphere through the photo-oxidation of formaldehyde and hydrocarbons (Finlayson-Pitts and Pitts, 1986) and is day time oxidant. The oxidation reaction given by Seigneur et al (1994) is:

$$Hg^0_{(g)} + H_2O_{2(g)} \rightarrow Hg(OH)_{(g,s)}$$

The lifetime of Hg0 by this process is approximately 1.5 years.

2.2.7 Photolytic reduction of Hg (II) in the presence of organic matter

Dissolved organic matter (DOM) which consists mostly of humic substances and mixture of unidentifiable compounds, is present in all aquatic environments and tends to bind trace metals such as mercury thus affecting its speciation. Mercury forms strong ionic bonds with reduced sulfur species (sulfides and thiols) in organic matter (less than 2% by weight). Reduction of Hg2+ to Hg 0 is significantly increased in the presence of dissolved organic matter in aquatic environments (Allard and Arsenie, 1991; Costa and Liss, 1999). Mercury may be sequestered by photoloytic reduction of Hg (II) to Hg (0) in the presence of phytoplankton in soil, experimental studies have confirmed this process (Carpi and Lindberg, 1998; Zhang and Lindberg, 1999).

2.2.8 Aqueous phase photoreduction of Hg (II)

Though the photoreduction of many halide-Hg (II) and organo-Hg (II) complexes have been well documented, the wavelengths of UV required to effect photoreduction are not known to exist in the troposphere. Aqueous phase photo-reduction of Hg(II)-formate, acetate and oxalate is also not possible under tropospheric UV of $\lambda > 290$ nm (Pehkonen and Lin, 1998).

$Hg(OH)_2$ and HgS_2^{2-} can undergo photoreduction under $\lambda > 290$ nm (Xiao et. al, 1994). However, photoreduction of $Hg(OH)_2$ produces Hg^0 at a rate four times faster than HgS_2^{2-} . The proposed reaction mechanism for this process is:

$$Hg(OH)_{2(aq)} \xrightarrow{h\nu} [Hg\ (OH)^*]$$

$$\longrightarrow Hg\ (OH)_{(aq)} + {}^{\cdot}OH(aq)$$

$$\longrightarrow Hg^0{}_{(aq)} + Products$$

The half life of $Hg(OH)_2$ is approximately a month, therefore this process is not very significant in the production of Hg^0.

2.2.9 Aqueous phase reduction of Hg (II) by Sulfites

Munthe et al (1991) first described the reduction of Hg (II) by sulfites. In this process an intermediate unstable complex, $HgSO_3$, is produced which rapidly reduces to Hg^0. This can be expressed as:

$$Hg^{2+} + SO_3^{2-} \longleftrightarrow HgSO3$$

$$HgSO_{3(aq)} \longrightarrow Hg^0{}_{(aq)} + Products$$

Though $HgSO_3$ is a very unstable complex, it is important to note that other Hg-SO_3 species have different reactivity. Where $HgSO_3$ is unstable, Hg $(SO_3)_2^{2-}$ is very stable and will not produce Hg^0. Sulfite is introduced into atmospheric water by scavenging of SO_2. This process is dependent of pH and increases with increasing pH. SO_2 is not

produced via chemical processes in the atmosphere but is a major pollutant. The lifetime of SO_2 is only a few hours in clouds as it can be easily oxidized and will only yield a few hours worth of Hg^0 unless there is a constant source of SO_2 in to the clouds.

2.2.10 Aqueous phase reduction of Hg(II) by $HO_2^{\cdot}$

$HO_2^{\cdot}$ is produced by photochemical processes in the atmosphere. It can be produced in clouds or can be scavenged from the gas phase (Schwartz, 1984; Arakaki et al, 1995). The process of reduction of Hg (II) by $HO_2^{\cdot}$ is expressed as:

$$HO_2^{\cdot}{}_{(aq)} + Hg(II)_{(aq)} \rightarrow Hg\ (I)_{(aq)} + O_{2(aq)} + H+_{(aq)}$$

$$HO_2^{\cdot}{}_{(aq)} + Hg(I)_{(aq)} \rightarrow Hg^0{}_{(aq)} + O_{2(aq)} + H^+{}_{(aq)}$$

The half life of Hg (II) by this process is approximately 1.5 hours.

2.3 Sampling Methods

A method was developed to directly characterize the signature of atmospheric mercury. A refined procedure permitting precise isotopic analyses of as little as 7ng of mercury has made it possible to characterize atmospheric mercury vapor directly. The Hg sampling procedure is based on the principle that elemental mercury readily forms amalgams with most metals such as gold and silver. The sampling instrument includes a simple aquarium pump which is modified to connect a tube at the inlet perforation. This instrument pumps air at the rate of 1.2-1.5 liter / minute. This tubing is connected to a quartz tube filled with gold plated quartz sand, plugged by quartz wool so as to allow passage of air. Another tube filled with $CaSO_4$ is connected in series, which is used to absorb moisture from the air and does not interfere with the Hg collection. Air is passed through the gold trap by the pump, and the mercury vapor from the atmosphere forms an amalgam with the gold in the sampling tube. In the initial phases of the experiment, a flow meter was used to monitor the flow rate of the air through the tube. Figure 2 is a schematic representation of the collection process.

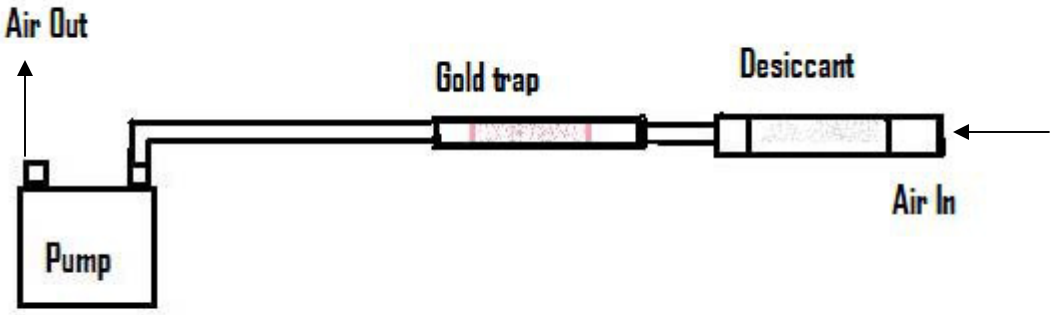

Figure 2.1 Schematic representation of the sampling unit

Air sampling units were deployed in several locations to compare the background Hg isotopic composition of the atmosphere in a local, regional and global scale. To ensure that anthropogenic input was at its minimum, sampling was not conducted in industrialized areas, or near coal powered plants and remote locations were preferred. For study in a local scale, sampling was conducted in two locations (roof of the FSU Love Building, Meteorology Department, Tallahassee, FL and the FSU Marine Laboratory at Turkey Point, FL) at various intervals over a period of one year to highlight any seasonal changes, if at all. A sampling unit was set up in Pensacola, Florida, close to a coal fired power plant which can contribute to local sources of mercury contamination. This sampling unit was set up to highlight any differences, if at all, between the regional isotopic signature and that of the Hg near the power plant. Sampling units were deployed at various locations in the United States to cover a regional study area as well as the NOAA Global Monitoring observatories in Trinidad Head (California), Mauna Loa (Hawaii), American Samoa and the South Pole. At Mauna Loa, one collection was conducted only during the night, between dusk to dawn, to demonstrate if at all there is any difference in the composition of atmospheric mercury in the absence of photochemistry. The wind field around the Mauna Loa observatory was studied by Ryan (1997). During the day, heating results in upslope radiation winds that

may have local a component. Nighttime winds are free far field down-slope tropospheric air devoid of any local component.

Assuming the lower limit of atmospheric concentration to be 3ng/cubic meter, and a flow rate through the gold trap (figure 9) to be set at 1 litre/min, the time required to trap 10ng of mercury is approximately 56 hours. Higher concentrations (approximately 30-40ng) are required for replicate analyses. This would take up to 1 week of sampling. For a better precision most samples from the NOAA base observatories are collected over a period of two weeks. The South Pole sample, due to very low expected concentration, was collected over a longer period of time. Due to the reported spring mercury depletion events reported in Arctic and Antarctic Polar Regions, the South Pole samples were collected two months before the onset of spring in the South Pole.

Once the sampling was complete, the gold trap was heated and purged by helium gas and bubbled into 3:1 14N HNO_3 to 12N HCl solution where it is completely oxidized to Hg (II). The acidity of the solution is decreased to approximately 1.5N by adding NaOH into the solution. This solution is introduced into the CETAC-HGX 200, which is installed as a sample introduction system into Thermo Finnigan's *Neptune*, which is a multi collector inductively coupled plasma mass spectrometer (MC-ICPMS). The CETAC HGX-200 is a hydride or cold vapor generation system, which enhances the sensitivity for a variety of elements. The mercury in solution is in the oxidation state of +2 or +1 (which is not a stable state due to disproportionation) because of the oxidizing nature of Aqua Regia. This is introduced into the cold vapor generator along with 2 % $SnCl_2$ in a 1N HCl matrix, which reduces the solution and releases elemental mercury in gaseous phase. The HGX-200 system has a U-shaped frosted glass gas-liquid phase separator which enhances the efficiency of gas-liquid phase exchange of Hg(0). This Hg(0) cold vapor is introduced into the plasma of the MC-ICPMS by argon gas. Sample solution is pumped into the cold vapor generator via a Perimax Spectec peristaltic pump which is controlled at 15 rotations per minute. This introduces a solution volume of approximately 0.9 ml/minute into the system. In between samples the system is washed with a 1N HCl solution till the mercury signal resumes background levels. Sample intensity ranges

from 500 mV to 4 V for ^{202}Hg. Background intensity is approximately 6mV which is lower than 1% of the signal intensity for most samples. Waste solution from the sample runs is analyzed periodically. It shows that the mercury in waste solution is at a background level and indicates a complete reduction of mercury by $SnCl_2$.

The Neptune has eight movable Faraday cups and one fixed center cup. Due to a very low abundance of ^{196}Hg, the mercury isotopes that are measured are ^{198}Hg, ^{199}Hg, ^{200}Hg, ^{201}Hg, ^{202}Hg and ^{204}Hg in cups L2, L1, C, H1, H2 and H3 respectively. Efficiency of the Faraday cups is calibrated by performing a gain calibration at the beginning of each day of sample run. The isobaric interference of ^{204}Pb on ^{204}Hg was monitored at mass 206 (^{206}Pb) on cup H4. There was, however, no observable interference on this mass. The Neptune has a 10^{11} Ω resistor and for a 1ppb Hg standard solution, the signal varies between 650 mV to 750 mV for the most abundant isotope, ^{202}Hg. Signal was tuned for intensity as well as stability to optimize external reproducibility of the standard. Signal intensities were converted to raw isotope ratios of ^{198}Hg/^{200}Hg, ^{199}Hg/^{200}Hg, ^{201}Hg/^{200}Hg, ^{202}Hg/^{200}Hg and ^{204}Hg/^{200}Hg, acquired in one block of 50 cycles with an integration time of 8.418 seconds (method developed by Sanghamitra Ghosh; Ghosh, 2008, dissertation). At the beginning of each measurement, peak centering is performed and baseline is calibrated by defocusing of the beam for 90 seconds while collecting 30 ratios. The time taken for each measurement is 510 seconds. Precise measurements can be performed with as low as 7ng of mercury in 7 ml of solution. This concentration yields between 650-750 mV signal intensity for ^{202}Hg and allows 50 cycles of measurement of isotopic ratios. To reduce the effects of instrumental fractionation, the isotope ratios were corrected by a sample-standard bracketing technique. The mercury isotope ratios are reported relative to NIST SRM 3133 Hg standard δ (‰) notation where,

$$\delta^{n}\text{Hg} = \left(\frac{Rsample}{Rstd} - 1\right)1000\,‰ \qquad \text{---Equation 2}$$

Where R= $\frac{^{n}Hg}{^{200}Hg}$ measured for the isotopes ^{198}Hg, ^{199}Hg, ^{200}Hg, ^{201}Hg, ^{202}Hg and ^{204}Hg.

Any deviation of the odd isotopes from the mass dependent behavior is denoted by Δ ^{199}Hg and Δ ^{201}Hg. Here Δ ^{199}Hg is defined as,

Δ ^{199}Hg= $\delta^{199}Hg_{observed}$- $\delta^{199}Hg_{MDF}$ ‰ ---Equation 3

2.4 Standard and Reagent preparation

Reagents used are 2% Stannous Chloride ($SnCl_2$) which is the reducing agent and 1 N HCl (wash solution). The stannous chloride solution is prepared using 98% $SnCl_2.2H_2O$ (ACROS) salt in 1N HCl. Stannous chloride instantly reduces any mercury that may be present in the solution. Compressed helium is passed through a series of gold plated sand traps to remove mercury from the lines and is bubbled into the reagent for approximately 30-40 minutes to purge the solution of any mercury from the reagent solution. 1N HCl was prepared by diluting Optima grade Fisher Scientific 12 N HCl.

The standard used in this study is the NIST SRM 3133. Appropriate amount of the stock solution of this standard with a concentration of 10,000 ppm is diluted in 1N HCl to make a solution of 9.72 ppm mercury concentration. This standard solution is stored in a Teflon PFA bottle in a refrigerator. Fresh standard solution of a concentration 1ppb (1ng/ml) is prepared from this solution before each day of sample run.

2.5 Experimental

An experiment was conducted to determine the influence of the sampling procedure and the subsequent thermal purging on the isotopic composition of the mercury collected.

2.5.1 Technique

Liquid mercury is contained in a conical flask that is submerged in a water bath maintained at 22ºC and ambient atmospheric pressure. This flask is sealed with a Teflon lined septum. Evaporation of liquid mercury at these conditions produces Hg vapor that is in equilibrium with the liquid. The first part of the experiment involves direct isotopic measurement of the mercury vapor. The Hg^0 vapor is collected by a Hamilton Gastight syringe. The mercury vapor is bubbled into 3:1 HNO3 : HCl. The Hg^0 is completely oxidized to Hg (II) in solution. Concentrated NaOH is added to this to bring the acidity of the solution down to about 1.5 N. A series of solutions with dissolved mercury vapor were prepared for isotopic analysis. Isotopic composition of the initial mercury is thus determined.

The second part of the experiment involves loading of the mercury on to the gold trap. Before starting the experiment gold traps were heated and purged of any mercury present in them. Mercury is collected into the syringe and is then introduced into tubing connected to the gold trap via a Teflon lined septum on the tubing. The vapor is carried into the trap by compressed ultra pure helium. Once the mercury is loaded into the gold trap, the trap is heated and bubbled into the 3:1 HNO3 : HCl solution. This process simulates the sampling procedure of mercury from the air. Comparison of the isotopic composition of mercury from the first part of the experiment and that of the second one allows us to determine if any fractionation is induced during the sampling procedure.

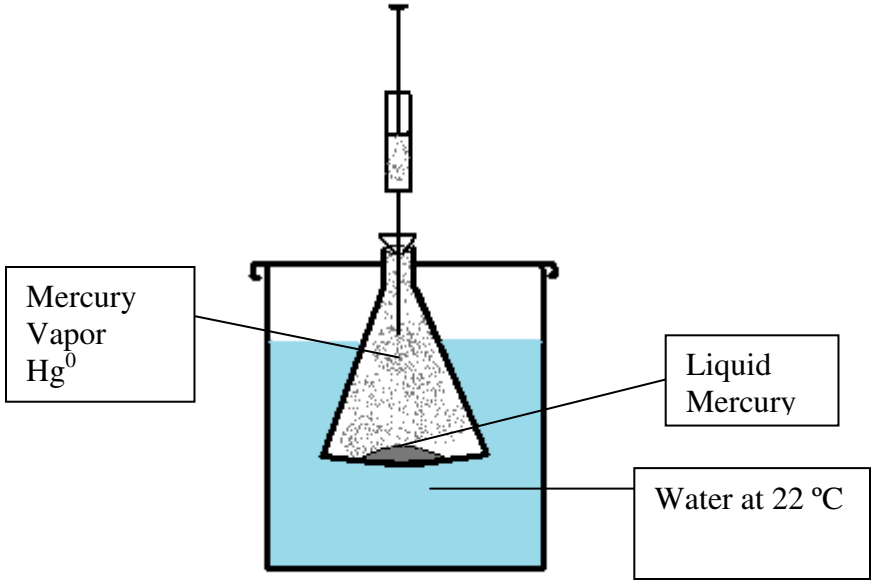

Figure 2.2 Mercury liquid-vapor bath apparatus

2.5.2 Results of vapor-gold trap experiment

The mercury vapor in equilibrium with the liquid mercury in the flask shows an enrichment of light isotopes with respect to the heavy isotopes (figure 2.3) .This isotopic composition is predicted by Estrade et al 2009. The mean δ^{198}Hg for the direct vapor measurement is 1.46 ‰ and for vapor sampled via the gold trap and thermally purging it is 1.60 ‰. However, all samples via the gold trap, including the most fractionated ones lie within $\pm 2\sigma$ of the isotopic composition of the mean direct vapor and the two cannot be distinguished (Figure 2.5). The Δ^{199}Hg and Δ^{201}Hg values of the direct vapor are 0.11 and 0.024 respectively. The Δ^{199}Hg and Δ^{201}Hg values of the Hg via gold trap are 0.19 and 0.09, but are within $\pm 2\sigma$ of that of the direct vapor (figure 2.6 a and 2.6 b). It is inferred that any difference in the isotopic composition are within analytical uncertainty and the sampling process does not introduce any detectable mass dependent or mass independent effect in the samples.

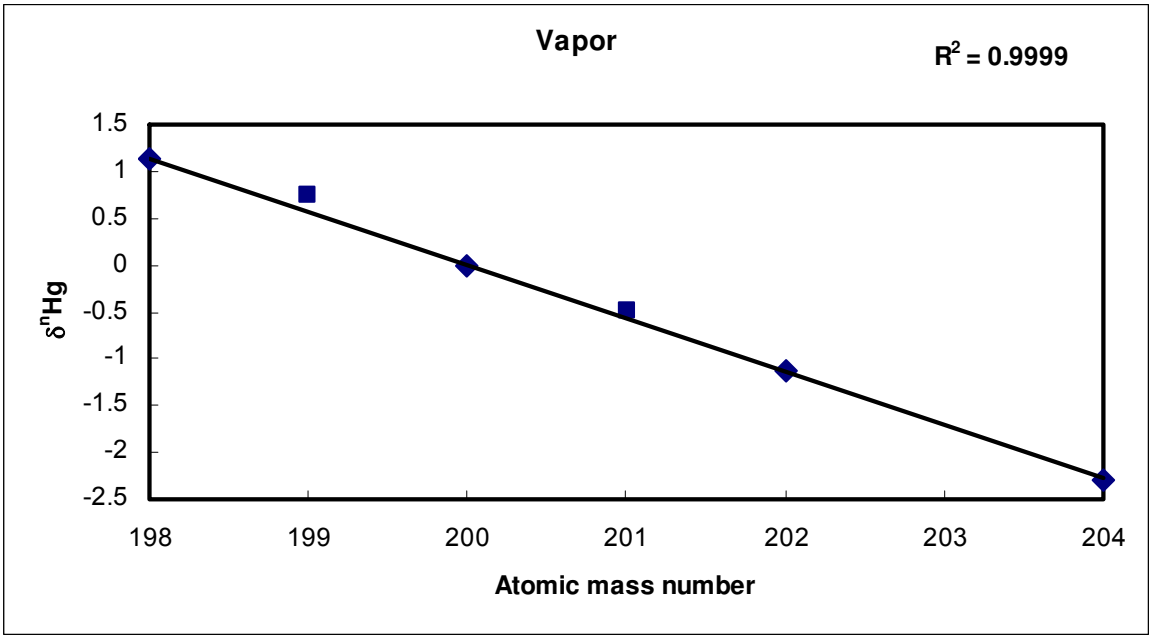

Figure 2.3 Mercury signature of the vapor sampled directly

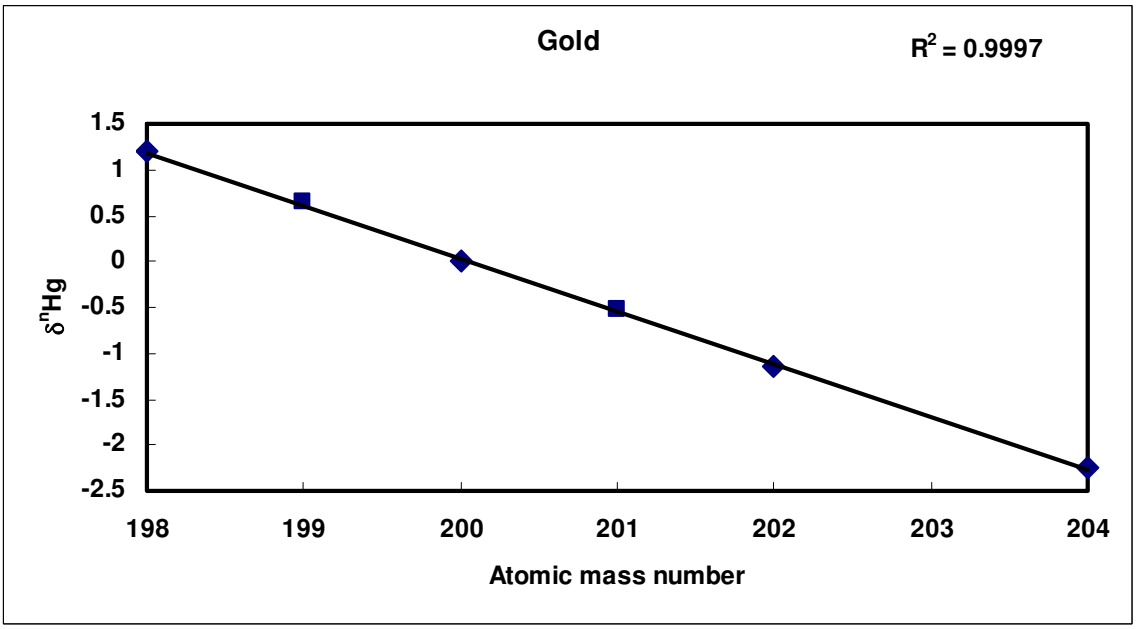

Figure 2.4 Mercury signature of the vapor introduced into a gold trap and subsequently thermally purged

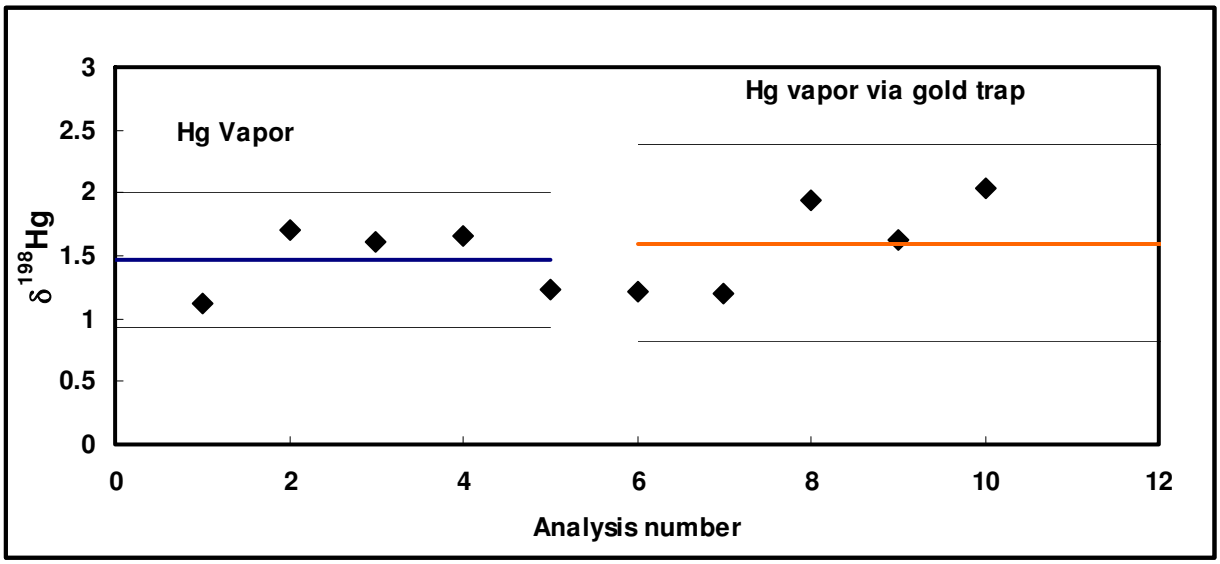

Figure 2.5 δ^{198}Hg of the Hg vapor and the Hg vapor via the gold trap. The blue line is the average δ^{198}Hg of the Hg Vapor; the yellow line is the average δ^{198}Hg of the Hg sampled via the gold trap and the black lines represent $\pm 2\sigma$

a)

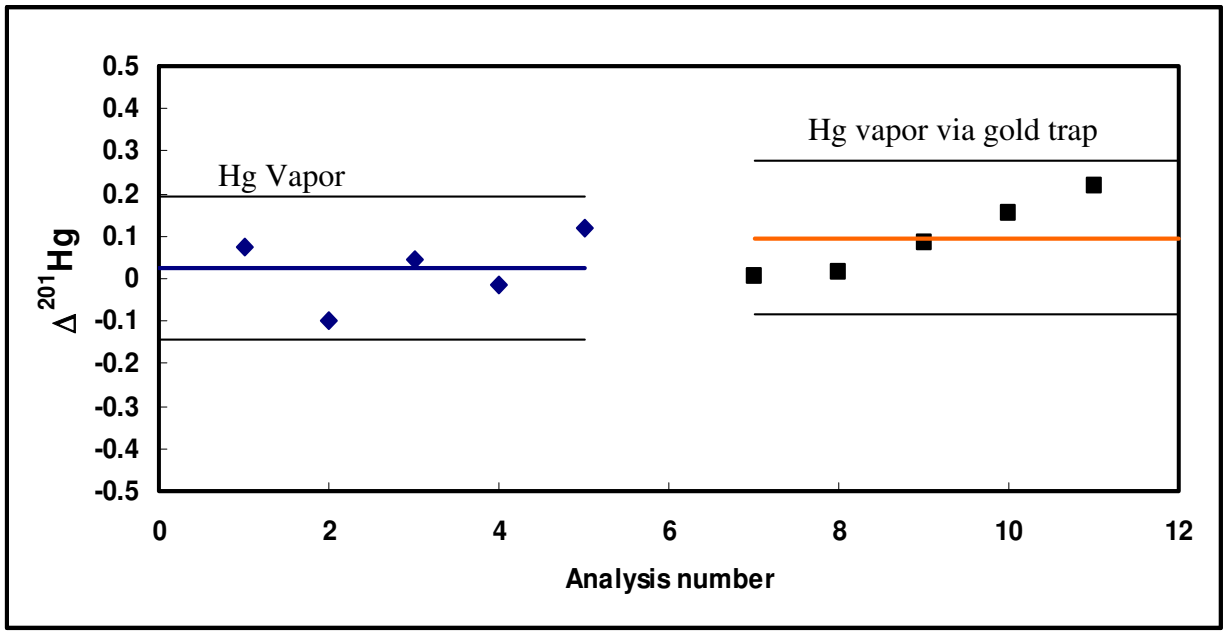

b)

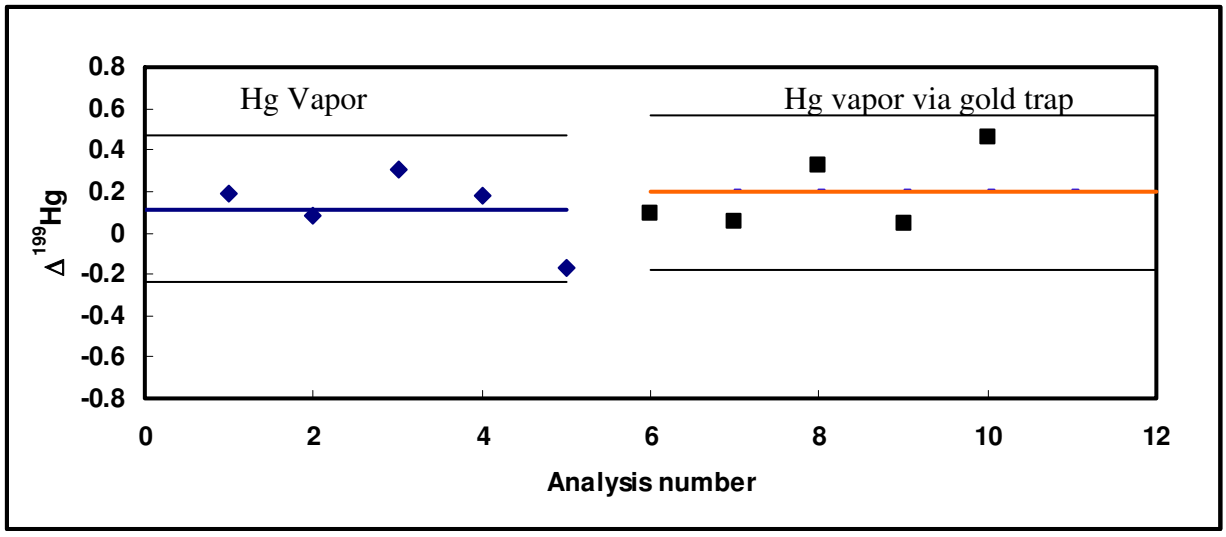

Figure 2.6 a) Δ^{201}Hg of the Hg vapor and the Hg vapor via the gold trap. b) Δ^{199}Hg of the Hg vapor and the Hg vapor via the gold trap. The blue line is the average Δ^{199}Hg and Δ^{201}Hg of the Hg Vapor; the yellow line is the average Δ^{199}Hg and Δ^{201}Hg of the Hg sampled via the gold trap and the black lines represent $\pm 2\sigma$

2.6 External reproducibility

To monitor the reproducibility of the Hg isotopic measurements, an external standard, Almaden cinnabar was used. 1ng/ml Almaden solution was prepared in 1N HCl. The cinnabar is fractionated with respect to the NIST SRM 3133 standard with an enrichment of the light isotopes (Figure 2.7). Linear scaling of the even isotopes also shows a small positive anomaly for the ^{199}Hg and ^{201}Hg isotopes. The mean δ^{198}Hg of the cinnabar is 0.22 ‰ and they are measured to a precision of 0.16 ‰ (2σ) (Figure 2.8). For the odd isotopes, the deviation from the MDF, mean Δ^{199}Hg is 0.13 ‰ measured to a precision of 0.08 ‰ (2σ) (Figure 2.9), and the mean Δ^{201}Hg is 0.09 ‰ $\pm$ 0.1 ‰ (2σ) (Figure 2.10).

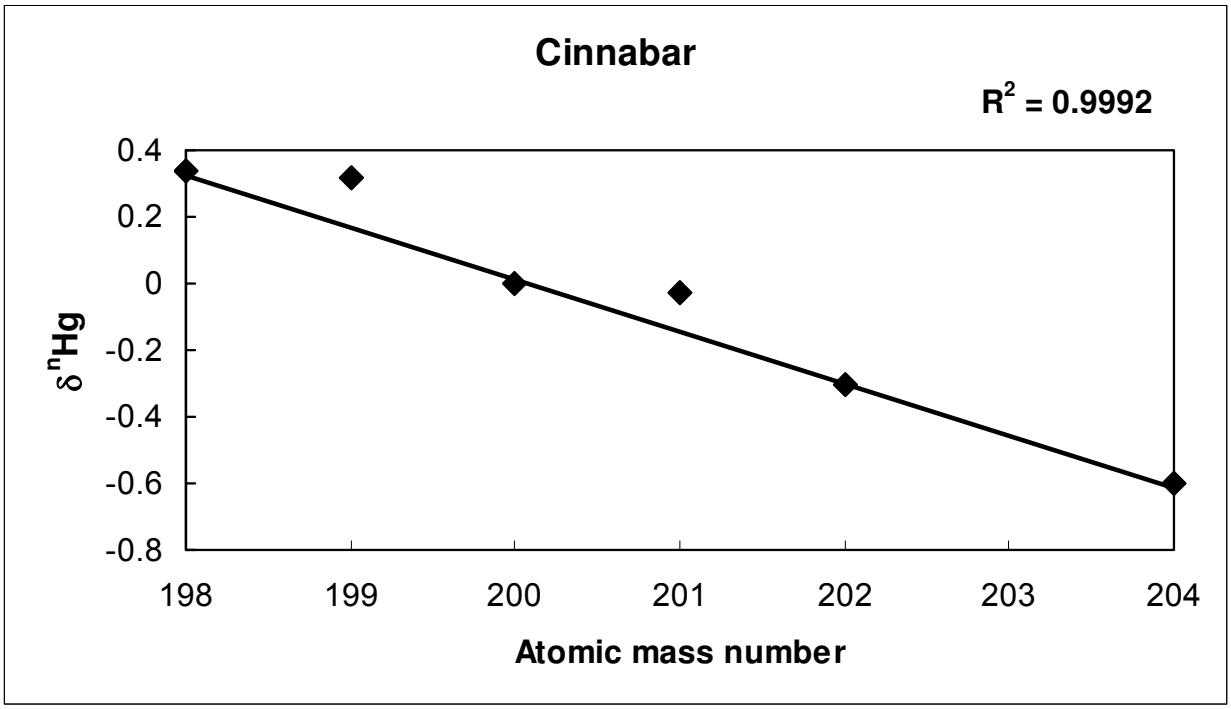

Figure 2.7 Isotopic composition of cinnabar on a multi-isotopic plot

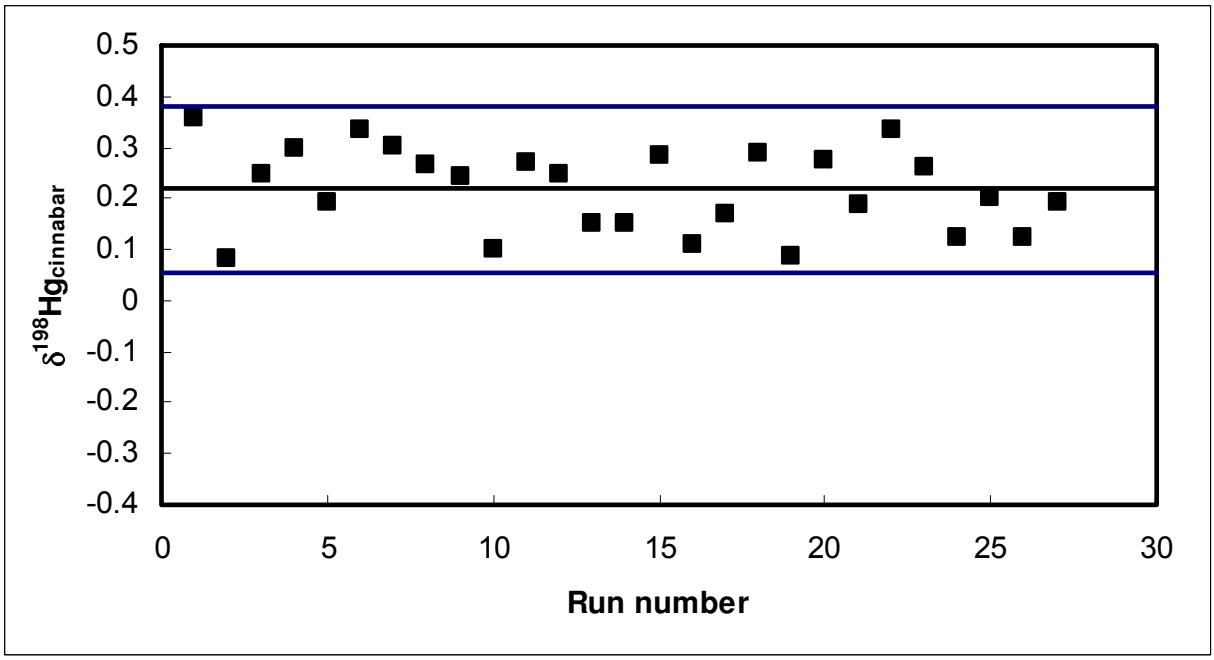

Figure 2.8 Reproducibility of δ^{198}Hg of Almaden Cinnabar. The black line represents the mean δ^{198}Hg and the blue lines represent $\pm$ 2σ

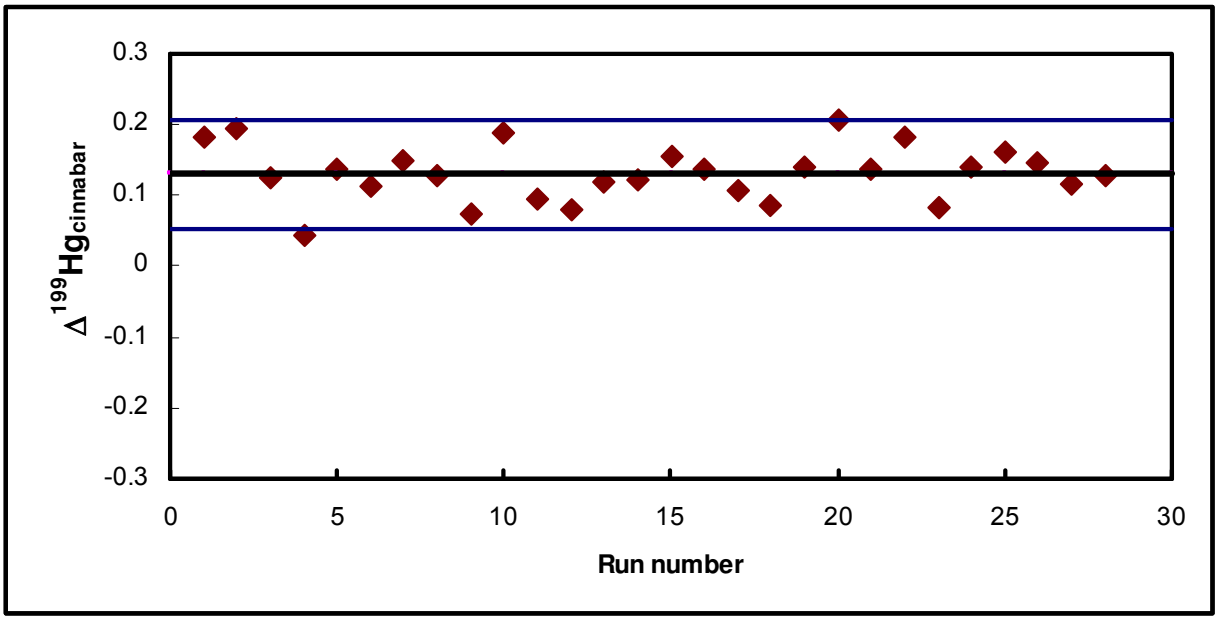

Figure 2.9 Reproducibility of Δ^{199}Hg of Almaden Cinnabar. The black line represents the mean Δ^{199}Hg and the blue lines represent $\pm$ 2σ

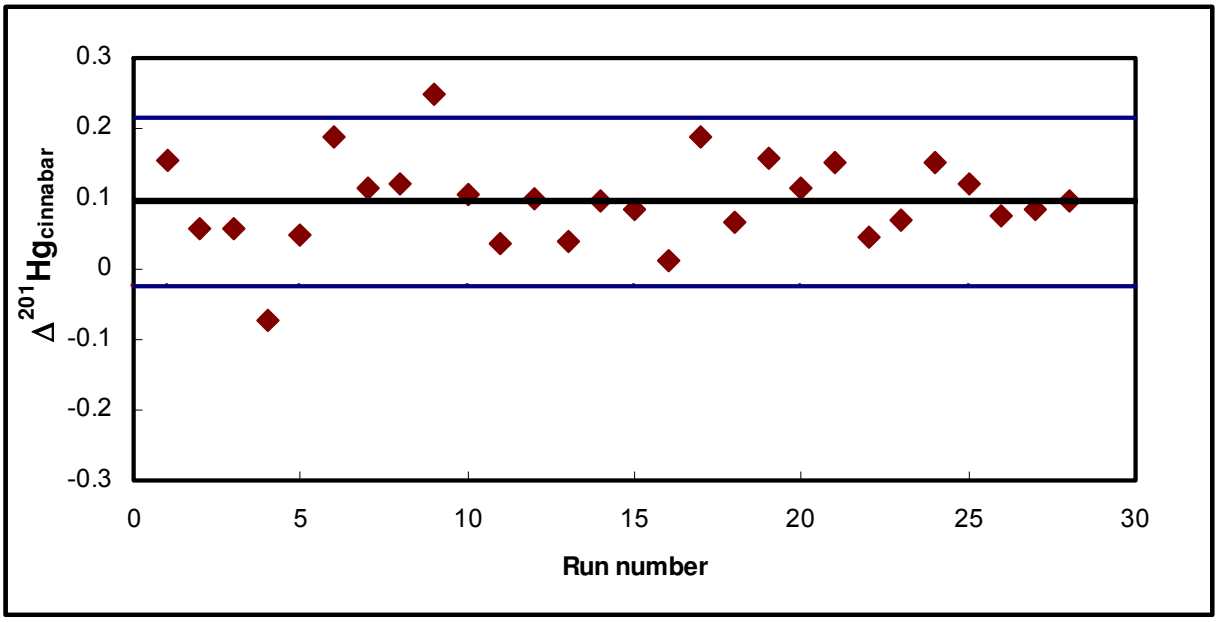

Figure 2.10 Reproducibility of Δ^{201}Hg of Almaden Cinnabar. The black line represents the mean Δ^{201}Hg and the blue lines represent $\pm$ 2σ

Table 2.1 Isotopic composition of Almaden Cinnabar with respect to NIST SRM 3133

Cinnabar	$\delta^{198}Hg$	$\delta^{199}Hg$	$\delta^{200}Hg$	$\delta^{201}Hg$	$\delta^{202}Hg$	$\delta^{204}Hg$	$\Delta^{199}Hg$	$\Delta^{201}Hg$
1	-0.31	0.02	0.00	0.28	0.25	0.57	0.18	0.16
2	0.36	0.36	0.00	-0.17	-0.46	-0.80	0.19	0.06
3	0.08	0.15	0.00	-0.03	-0.17	-0.24	0.12	0.06
4	0.25	0.16	0.00	-0.14	-0.23	-0.29	0.04	-0.07
5	0.30	0.29	0.00	-0.06	-0.27	-0.48	0.14	0.05
6	0.19	0.20	0.00	-0.01	-0.34	-0.64	0.11	0.19
7	0.34	0.32	0.00	-0.03	-0.30	-0.60	0.15	0.11
8	0.30	0.29	0.00	-0.02	-0.26	-0.62	0.13	0.12
9	0.27	0.21	0.00	0.07	-0.31	-0.69	0.07	0.25
10	0.24	0.31	0.00	-0.01	-0.24	-0.45	0.19	0.10
11	0.10	0.14	0.00	-0.02	-0.12	-0.21	0.09	0.04
12	0.27	0.21	0.00	-0.01	-0.28	-0.45	0.08	0.10
13	0.25	0.24	0.00	-0.04	-0.20	-0.36	0.12	0.04
14	0.15	0.19	0.00	0.02	-0.21	-0.24	0.12	0.10
15	0.15	0.21	0.00	-0.10	-0.38	-0.52	0.16	0.09
16	0.29	0.27	0.00	-0.12	-0.32	-0.49	0.14	0.01
17	0.11	0.17	0.00	0.11	-0.11	-0.29	0.11	0.19
18	0.17	0.17	0.00	-0.02	-0.17	-0.35	0.09	0.07
19	0.29	0.30	0.00	0.02	-0.19	-0.65	0.14	0.16
20	0.09	0.25	0.00	0.04	-0.12	-0.28	0.21	0.12
21	0.27	0.27	0.00	0.07	-0.22	-0.39	0.14	0.15
22	0.19	0.27	0.00	-0.09	-0.26	-0.46	0.18	0.05
23	0.34	0.25	0.00	-0.02	-0.24	-0.46	0.08	0.07
24	0.26	0.28	0.00	0.02	-0.23	-0.57	0.14	0.15
25	0.12	0.22	0.00	0.03	-0.17	-0.31	0.16	0.12

Table 2.1 Isotopic composition of Almaden Cinnabar with respect to NIST SRM 3133

Cinnabar	$\delta^{198}Hg$	$\delta^{199}Hg$	$\delta^{200}Hg$	$\delta^{201}Hg$	$\delta^{202}Hg$	$\delta^{204}Hg$	$\Delta^{199}Hg$	$\Delta^{201}Hg$
26	0.20	0.24	0.00	-0.05	-0.28	-0.44	0.15	0.07
27	0.12	0.17	0.00	-0.01	-0.20	-0.31	0.11	0.08
28	0.19	0.22	0.00	-0.01	-0.21	-0.41	0.13	0.10
Mean	0.22	0.24	0.00	-0.02	-0.24	-0.44	0.13	0.10
σ	0.08	0.06	0.00	0.06	0.08	0.15	0.04	0.06
2 σ	0.16	0.11	0.00	0.13	0.16	0.31	0.08	0.13

2.7 Results

All air samples analyzed show a Mass Dependent Fractionation effect where the light isotopes are enriched over the heavier isotopes. The delta values defined as

$$\delta^{n}\text{Hg} = (\frac{Rsample}{Rstd} - 1)1000\,‰$$

where $R=\frac{^{n}Hg}{^{200}Hg}$ were measured for the isotopes ^{198}Hg, ^{199}Hg, ^{200}Hg, ^{201}Hg, ^{202}Hg and ^{204}Hg relative to NIST SRM 3133. On a multiple isotope plot, even mass number isotopes form a highly linear array (Figure 2.11). Also observed is a very small enrichment of the odd isotopes ^{199}Hg and ^{201}Hg with respect to the mass dependent fractionation line. This anomaly given by $\Delta\ ^{199}$Hg and $\Delta\ ^{201}$Hg (defined in equation 3) is of the magnitude of +0.1 to +0.3 ‰. This effect is reproducible in repeated analysis of the same sample, between different samples collected at the same location over a month's time, and between all samples collected from the Gulf of Mexico coast inland to Tallahassee (Table 2.2).

A plot of $\Delta\ ^{201}$Hg Vs $\Delta\ ^{199}$Hg for all analyzed atmospheric Hg-vapor samples in Figure 2.14 shows scatter and it is difficult to resolve the effect of magnetic isotope effect and nuclear volume effect. It is clear that the anomalies are not due to magnetic isotope effect alone.

Even isotopes δ^{198}Hg and δ^{204}Hg plotted against δ^{202}Hg of all air samples measured from all locations in Figure 2.12 (a and b), reveals a very tight fit which is a linear terrestrial mass dependent fractionation line. Odd isotopes δ^{199}Hg and δ^{201}Hg plotted against δ^{202}Hg in Figure 2.13 (a and b) of all air samples measured from all locations, reveals a fairly good fit on the terrestrial mass fractionation line. However they do show a bit more scatter than the even isotope plot indicating a very small deviation from the terrestrial mass fractionation line.

The mean δ^{198}Hg for the direct air Hg vapor measurement is 1.3$\pm$ 0.9 (2σ) ‰ for approximately 60 samples from locations in the Unites States as well as some around the world (Figure 2.15). The Δ^{199}Hg and Δ^{201}Hg values of the direct vapor are 0.13 and 0.08 ‰ (2σ) respectively (Figure 2.17 a and b). Isotopic composition of air samples collected in the area of Tallahassee alone over a period of one year gives a mean δ^{198}Hg of 1.1 $\pm$ 0.5 (2σ) ‰ (Figure 2.16).

The sample from Pensacola, Florida, that was set up near a coal fired power plant shows the smallest fractionation of all other air samples with a δ^{198}Hg of 0.43 ‰. This may be significant in the distinction of isotopic composition of polluted air masses.

In the Mauna Loa observatory, one sample was collected in night time (sample number 44/45) only to highlight any difference in the isotopic composition of mercury in the absence of photochemistry. The cumulative daytime and night time values for Hg gives a mean δ^{198}Hg of 1.8 $\pm$ 0.6 (2σ) ‰ which is among the most fractionated samples among all air samples. The night-time values gave a δ^{198}Hg of 2.3 ‰, higher than, but within the analytical uncertainty of the cumulative Hg isotopic composition. No significant difference in the Δ^{199}Hg and Δ^{201}Hg values were observed in these samples.

The magnitude of the mass dependent or mass independent fractionation cannot be distinguished geographically. So far only two locations in the Southern Hemisphere have been sampled for atmospheric mercury, the South Pole and American Samoa. Samples from American Samoa, with a mean δ^{198}Hg of 1.6 $\pm$ 0.5 (2σ) ‰ and samples from the South Pole, with a mean δ^{198}Hg of 1.3 $\pm$ 0.3 (2σ) ‰ are within the analytical uncertainty of the other samples and at this time cannot be isotopically distinguished from samples collected in the Northern Hemisphere and fall within 2σ of those samples. Also, no distinguishable odd isotope signature can be observed in the southern hemisphere samples that are distinct from the northern hemisphere.

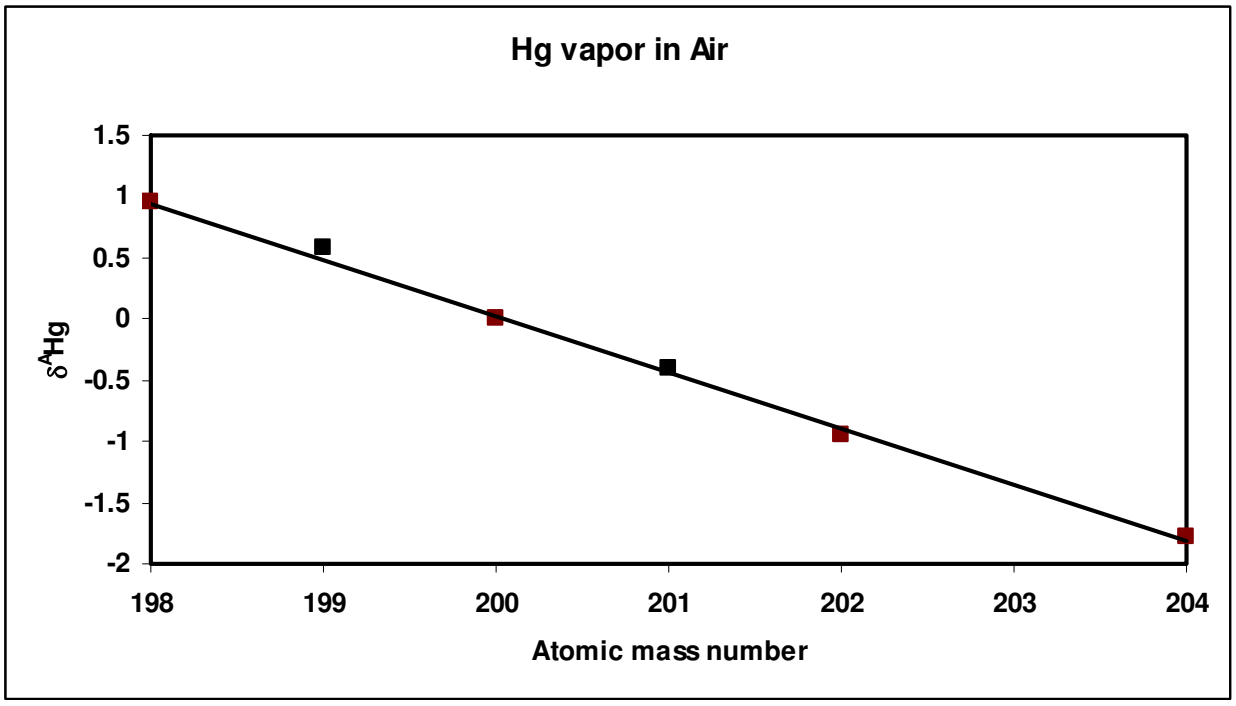

Figure 2.11 Isotopic composition of direct sampling of Hg vapor from the air. Linear scaling of even mass numbered isotopes reveal a very small, if any, deviation of odd-mass isotopes from the dependent array.

a)

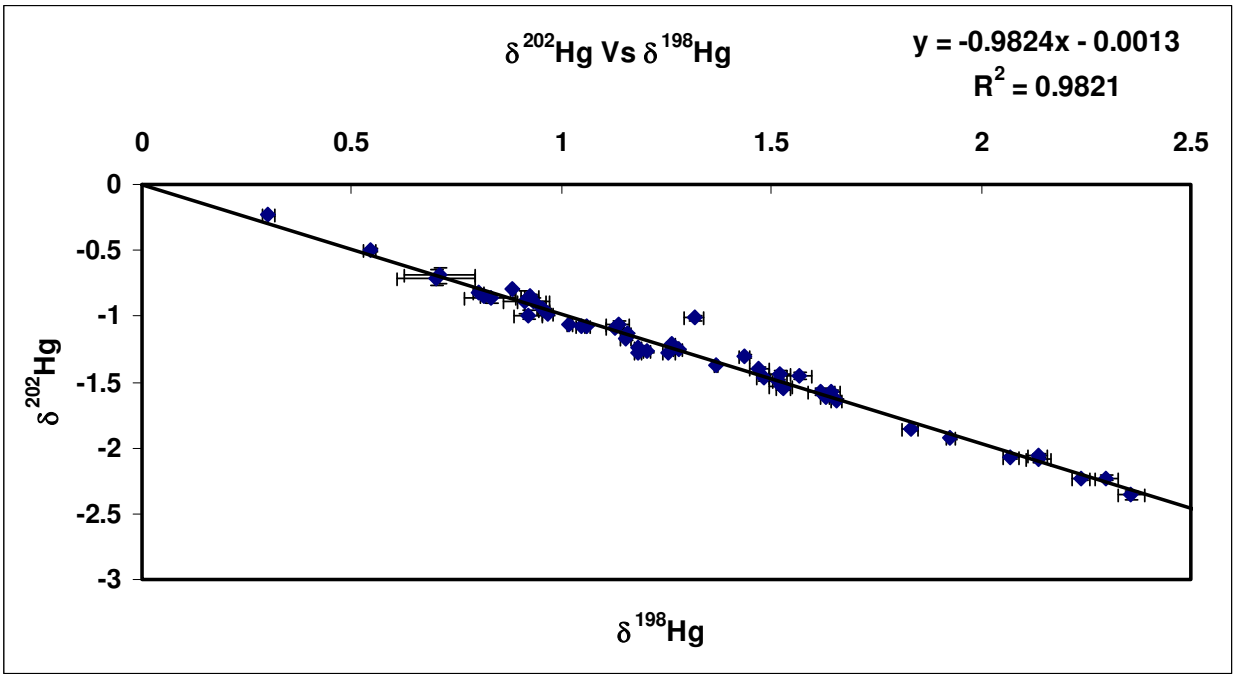

b)

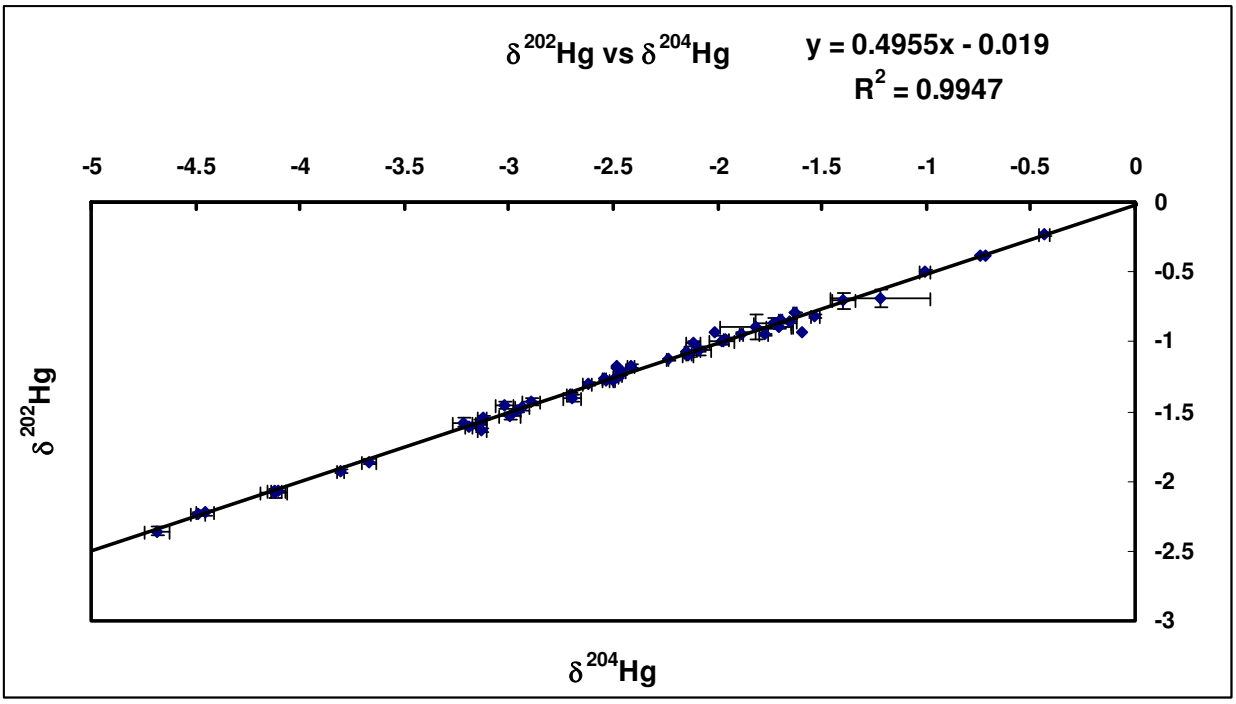

Figure 2.12 Even isotopes δ^{198}Hg and δ^{204}Hg plotted against δ^{202}Hg of all air samples measured from all locations. The internal precisions of measurement for the samples are given as 2SE on 50 ratios.

a)

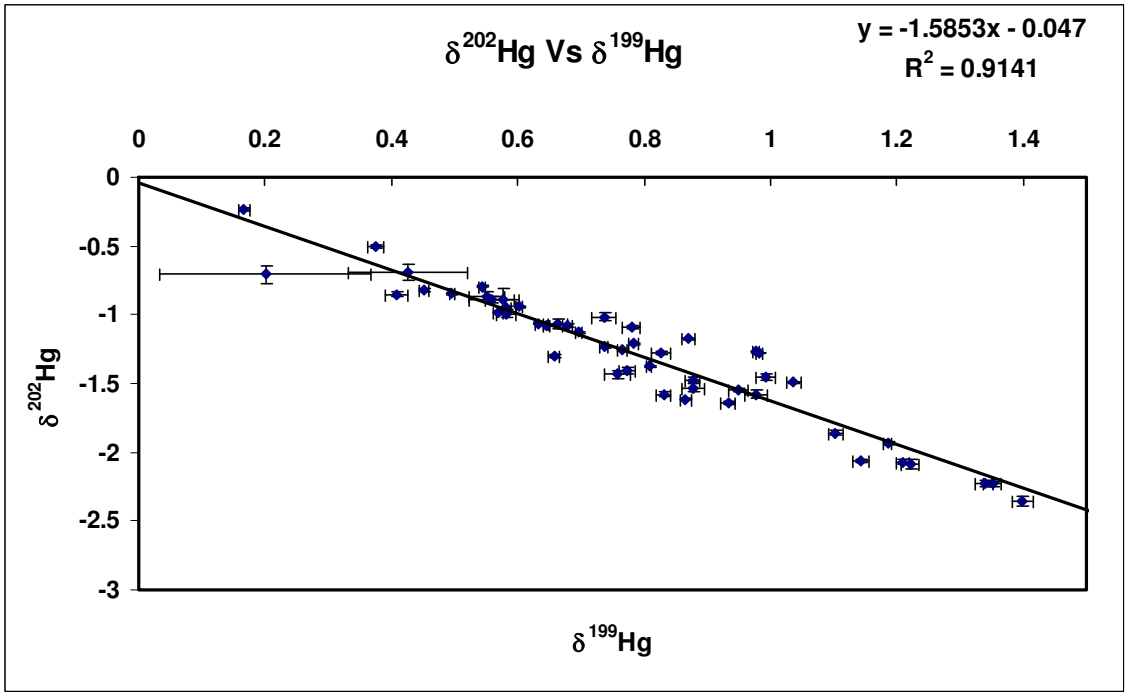

b)

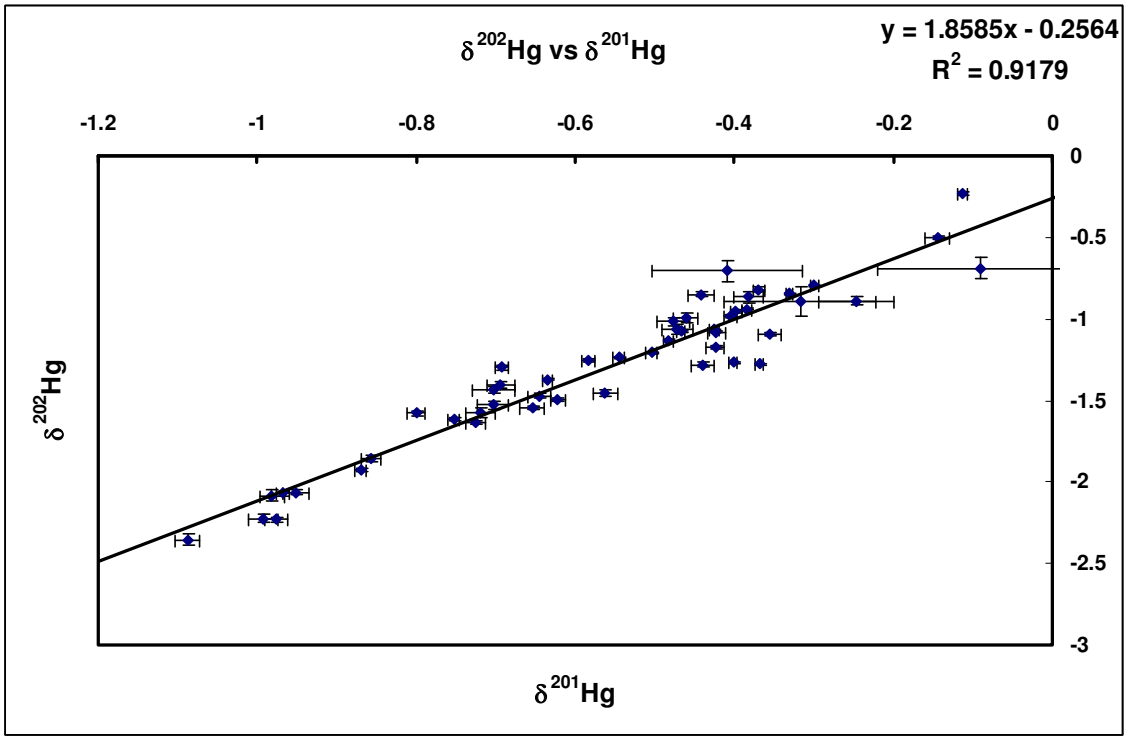

Figure 2.13 Odd isotopes δ^{199}Hg and δ^{201}Hg plotted against δ^{202}Hg of all air samples measured from all locations. The internal precisions of the measurements for the samples are given as 2SE on 50 ratios.

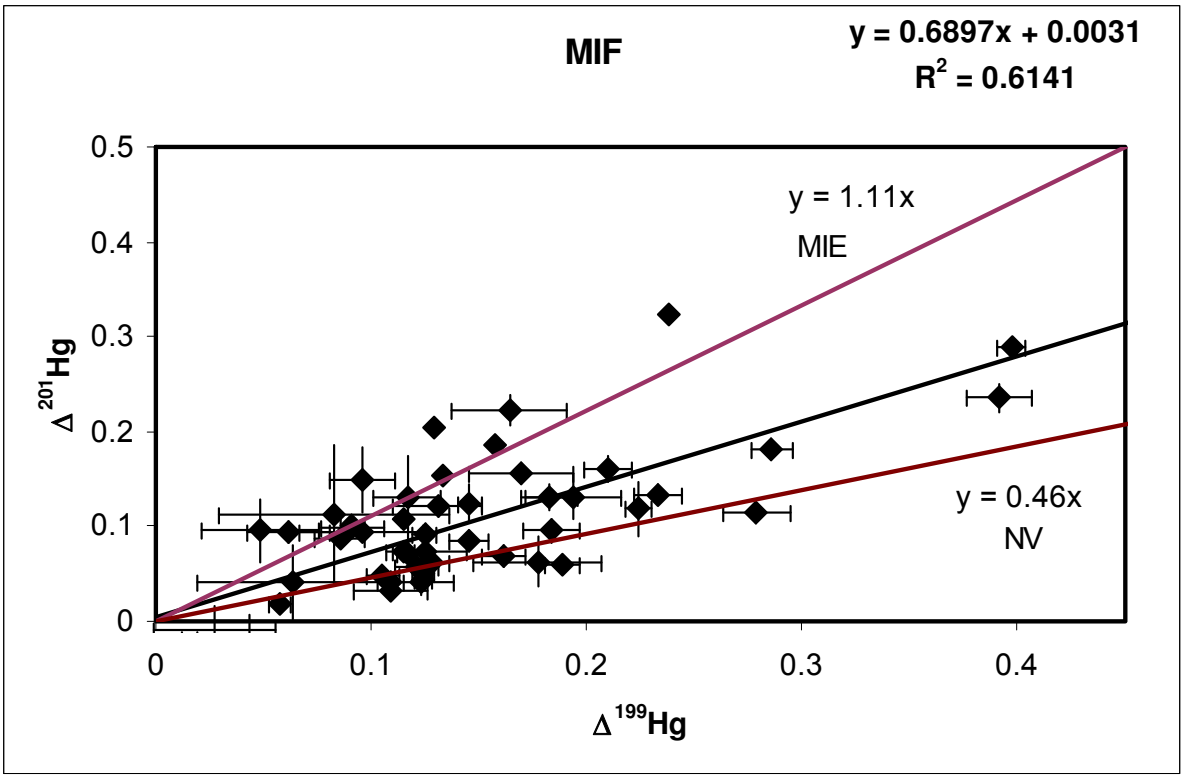

Figure 2.14 A plot of $\Delta\ ^{201}$Hg Vs $\Delta\ ^{199}$Hg for all analyzed atmospheric Hg-vapor samples. The internal precision of measurement is shown as 2SE on 50 ratios. Black line represents the best fit line of the data points. The purple and red lines indicate the theoretical lines for Magnetic Isotopic Effect and Nuclear Volume Effect respectively.

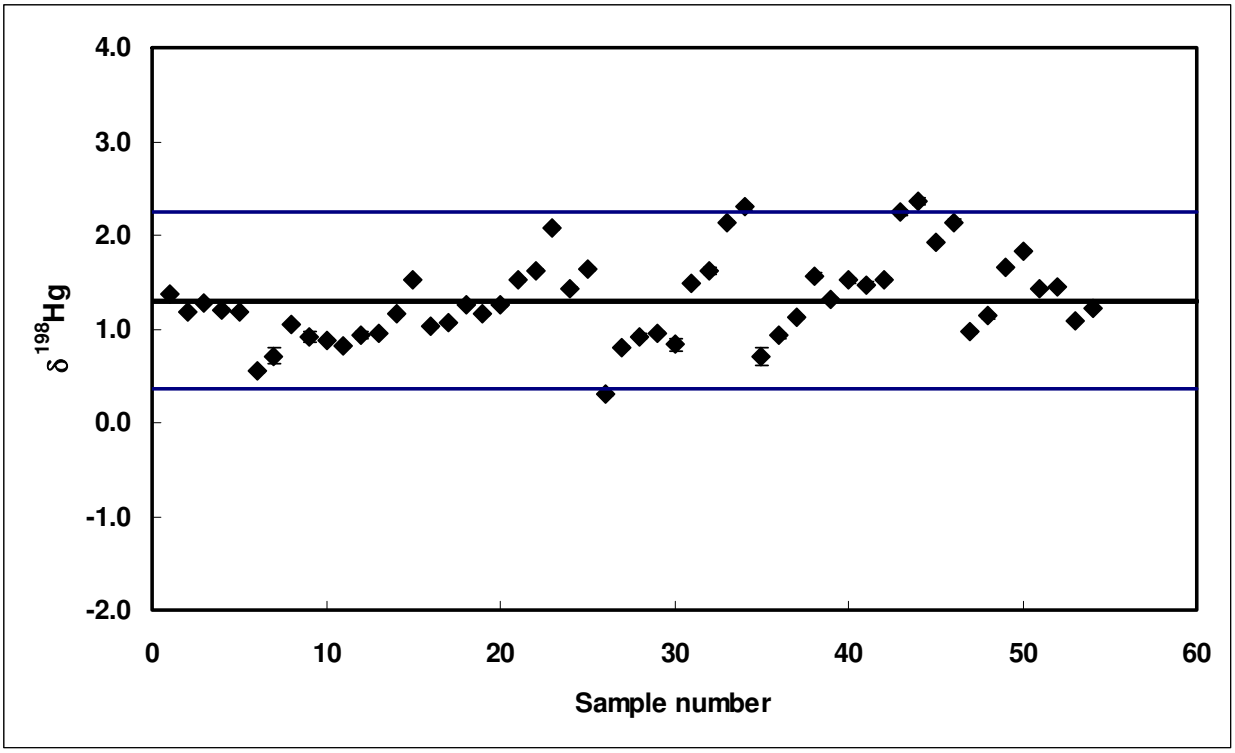

Figure 2.15 δ^{198}Hg of all air samples measured. The black line is the average δ^{198}Hg of the Hg Vapor; the blue lines represent $\pm 2\sigma$

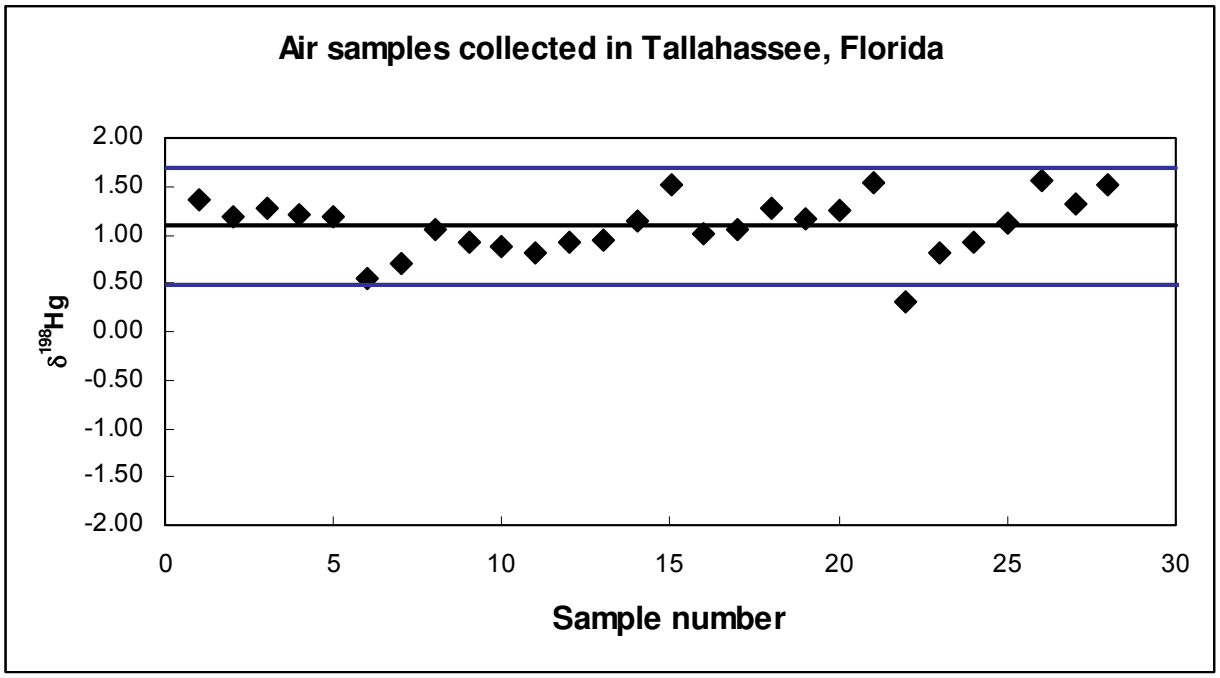

Figure 2.16 δ^{198}Hg of air samples collected in and around Tallahassee, Florida. The black line is the average δ^{198}Hg of the Hg Vapor; the blue lines represent $\pm 2\sigma$

a)

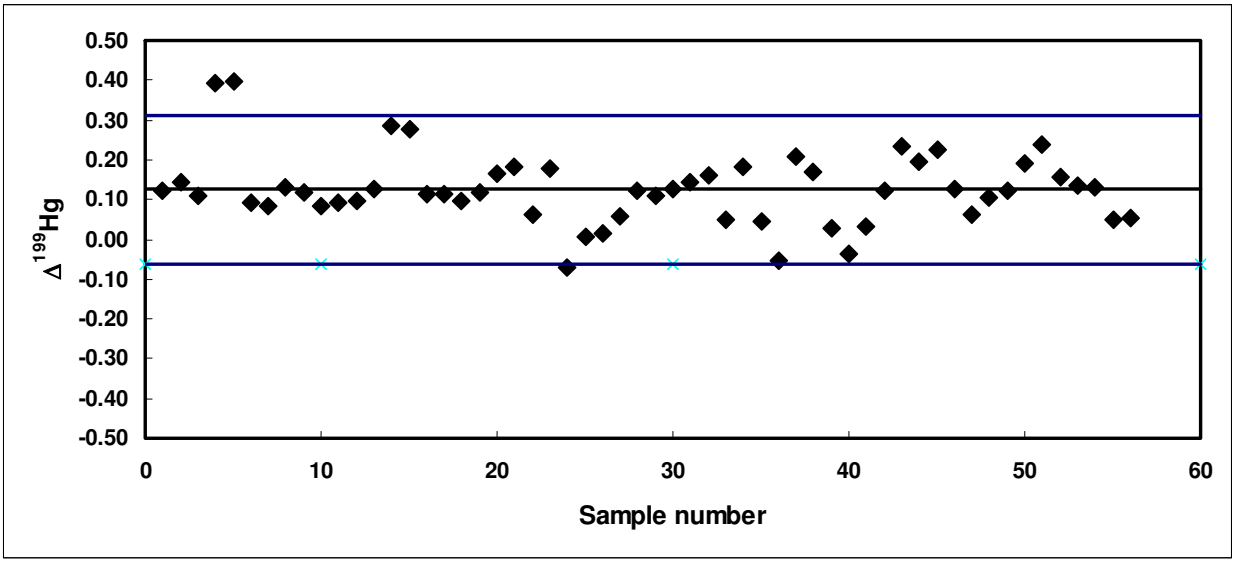

b)

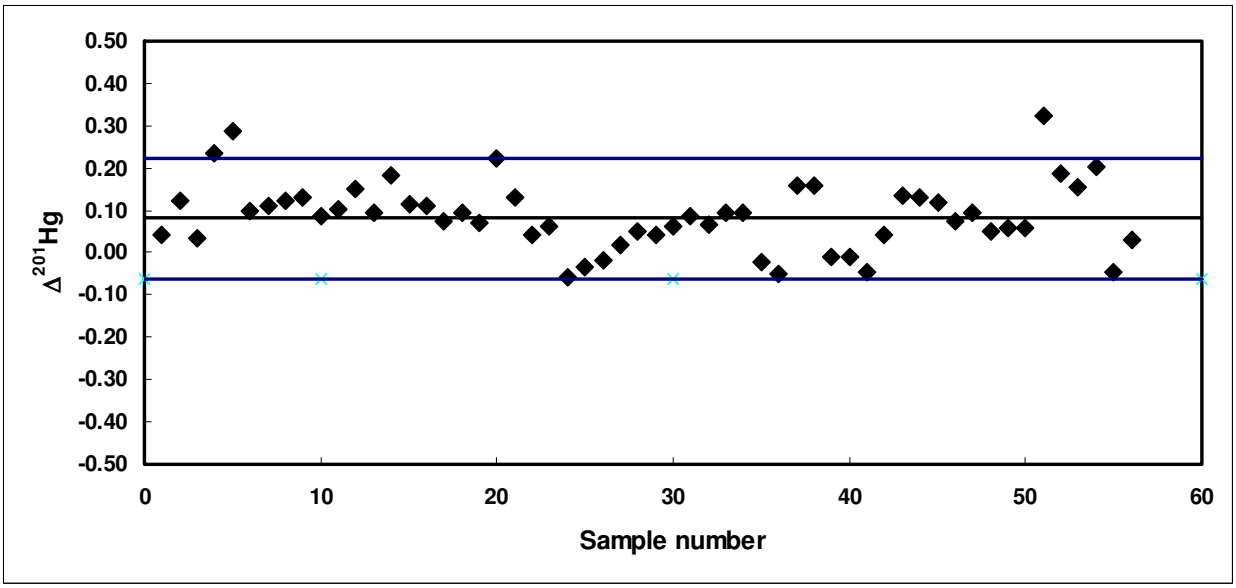

Figure 2.17 Δ^{199}Hg (a) and Δ^{201}Hg (b) of all air samples measured. The black line is the average Δ^{199}Hg and Δ^{201}Hg respectively of the Hg Vapor; the blue lines represent $\pm 2\sigma$

2.8 Discussion and Conclusions

The cardinal role of the atmosphere in the global dispersion of mercury and its deposition in aquatic environments and on land is well established. Readmission of mercury from waters and land is the major source of atmospheric mercury. If isotopic variations in Hg are to be used in developing a better understanding of the mercury cycle, experimental studies of the isotope effects of those processes that induce mercury transformations from one species to another and its transition in and out of the atmosphere are critical. Knowledge of the isotopic composition of atmospheric mercury is also a key.

The residence time of Hg^0 which comprises of approximately 98% of the total mercury in the atmosphere has been variously estimated to be between 0.6 and 2.0 years. Both the horizontal and vertical mixing times of the troposphere are approximately one month (vertical mixing can be much faster). Accordingly, we suspect that atmospheric mercury might closely approach isotopic homogeneity on a hemispherical scale (mixing times between the northern and southern hemispheres might well exceed a year).

From this study it is concluded that the atmosphere comes close to an isotopically uniform reservoir of mercury $(IUR)_{Hg}$, on which local and temporary effects are likely imposed. Future work involving measurement of atmospheric mercury in a dense network around the globe could perhaps reveal some of these local/ temporary effects. The $(IUR)_{Hg}$ provides an anchor around which models of the global mercury cycle could be constrained.

Table 2.2 Isotopic composition of mercury in measured air samples

Sample #	Location	$\delta^{198}Hg$	$\delta^{199}Hg$	$\delta^{200}Hg$	$\delta^{201}Hg$	$\delta^{202}Hg$	$\delta^{204}Hg$	$\Delta^{199}Hg$	$\Delta^{201}Hg$
1	Alumni Village, Tallahassee	1.37	0.81	0.00	-0.63	-1.37	-2.71	0.12	0.04
2	Alumni Village, Tallahassee	1.18	0.74	0.00	-0.55	-1.24	-2.47	0.15	0.12
3	Alumni Village, Tallahassee	1.28	0.76	0.00	-0.58	-1.26	-2.49	0.11	0.03
4	Alumni Village, Tallahassee	1.20	0.98	0.00	-0.40	-1.27	-2.54	0.39	0.24
5	Alumni Village, Tallahassee	1.18	0.98	0.00	-0.37	-1.28	-2.50	0.40	0.29
6	Alumni Village, Tallahassee	0.54	0.38	0.00	-0.14	-0.50	-1.01	0.09	0.10
7	Alumni Village, Tallahassee	0.71	0.43	0.00	-0.09	-0.69	-1.22	0.08	0.11
8	FSU Marine Lab, FL	1.05	0.68	0.00	-0.42	-1.08	-2.14	0.13	0.12
9	FSU Marine Lab, FL	0.91	0.58	0.00	-0.32	-0.89	-1.81	0.12	0.13
10	FSU Marine Lab, FL	0.88	0.54	0.00	-0.30	-0.79	-1.63	0.09	0.09
11	FSU Marine Lab, FL	0.81	0.50	0.00	-0.33	-0.85	-1.70	0.09	0.10
12	FSU Meteorology, FL	0.93	0.56	0.00	-0.25	-0.89	-1.71	0.10	0.15
13	FSU Meteorology, FL	0.95	0.60	0.00	-0.38	-0.94	-1.88	0.12	0.09
14	FSU Meteorology, FL	1.15	0.87	0.00	-0.42	-1.18	-2.41	0.29	0.18
15	FSU Meteorology, FL	1.52	1.04	0.00	-0.62	-1.49	-2.96	0.28	0.11
16	FSU Reservation, FL	1.02	0.63	0.00	-0.43	-1.06	-2.09	0.12	0.11
17	FSU Reservation, FL	1.06	0.64	0.00	-0.47	-1.08	-2.15	0.12	0.07
18	Tallahasse, Suburban	1.26	0.78	0.00	-0.50	-1.21	-2.45	0.10	0.09
19	Tallahasse, Suburban	1.16	0.70	0.00	-0.48	-1.13	-2.24	0.12	0.07
20	Tallahasse, Suburban	1.26	0.83	0.00	-0.44	-1.28	-2.53	0.16	0.22
21	Tallahasse, Suburban	1.53	0.95	0.00	-0.65	-1.55	-3.12	0.18	0.13
22	American Samoa	1.63	0.87	0.00	-0.75	-1.61	-3.19	0.06	0.04
23	American Samoa	2.07	1.21	0.00	-0.97	-2.07	-4.12	0.18	0.06
24	American Samoa	1.44	0.66	0.00	-0.69	-1.30	-2.62	-0.07	-0.06

Table 2.3 Isotopic composition of mercury in measured air samples

Sample #	Location	δ^{198}Hg	δ^{199}Hg	δ^{200}Hg	δ^{201}Hg	δ^{202}Hg	δ^{204}Hg	Δ^{199}Hg	Δ^{201}Hg
25	American Samoa	1.64	0.83	0.00	-0.80	-1.58	-3.14	0.01	-0.03
26	FSU Marine Lab, FL	0.30	0.17	0.00	-0.11	-0.23	-0.43	0.02	-0.02
27	FSU Marine Lab, FL	0.80	0.45	0.00	-0.37	-0.82	-1.53	0.06	0.02
28	FSU Marine Lab, FL	0.92	0.58	0.00	-0.46	-0.99	-1.98	0.12	0.05
29	Great Smokey NP, TN	0.96	0.58	0.00	-0.40	-0.95	-1.78	0.11	0.04
30	Great Smokey NP, TN	0.83	0.55	0.00	-0.38	-0.87	-1.74	0.13	0.06
31	Great Smokey NP, TN	1.48	0.88	0.00	-0.65	-1.47	-2.94	0.15	0.08
32	Great Smokey NP, TN	1.62	0.98	0.00	-0.72	-1.58	-3.21	0.16	0.07
33	Mammoth Cave NP, KY	2.14	1.14	0.00	-0.95	-2.06	-4.10	0.05	0.10
34	Mammoth Cave NP, KY	2.30	1.34	0.00	-0.99	-2.23	-4.45	0.18	0.10
35	Mammoth Cave NP, KY	0.70	0.20	0.00	-0.41	-0.71	-1.40	0.04	-0.02
36	Mammoth Cave NP, KY	0.92	0.41	0.00	-0.44	-0.85	-1.65	-0.05	-0.05
37	FSU Meteorology, FL	1.13	0.78	0.00	-0.36	-1.09	-2.14	0.21	0.16
38	FSU Meteorology, FL	1.57	0.99	0.00	-0.56	-1.45	-3.02	0.17	0.16
39	FSU Meteorology, FL	1.32	0.74	0.00	-0.48	-1.01	-2.12	0.03	-0.01
40	FSU Meteorology, FL	1.52	0.76	0.00	-0.70	-1.43	-2.89	-0.04	-0.01
41	Mauna Loa, HI	1.47	0.77	0.00	-0.69	-1.40	-2.70	0.03	-0.04
42	Mauna Loa, HI	1.52	0.88	0.00	-0.70	-1.53	-2.99	0.12	0.04
43	Mauna Loa, HI	2.24	1.35	0.00	-0.98	-2.23	-4.49	0.23	0.13
44	Mauna Loa, HI	2.36	1.40	0.00	-1.09	-2.36	-4.69	0.19	0.13
45	Mauna Loa, HI	1.93	1.19	0.00	-0.87	-1.93	-3.81	0.22	0.12
46	Mauna Loa, HI	2.14	1.22	0.00	-0.98	-2.08	-4.12	0.13	0.07
47	Trinidad Head	0.97	0.57	0.00	-0.40	-0.98	-1.96	0.06	0.09
48	Trinidad Head	1.13	0.66	0.00	-0.47	-1.06	-2.09	0.11	0.05

Table 2.4 Isotopic composition of mercury in measured air samples

Sample #	Location	δ^{198}Hg	δ^{199}Hg	δ^{200}Hg	δ^{201}Hg	δ^{202}Hg	δ^{204}Hg	Δ^{199}Hg	Δ^{201}Hg
49	Trinidad Head	1.65	0.93	0.00	-0.73	-1.64	-3.13	0.12	0.06
50	Trinidad Head	1.83	1.10	0.00	-0.86	-1.86	-3.67	0.19	0.06
51	South Pole	1.43	0.97	0.00	-0.25	-1.17	-2.48	0.24	0.32
52	South Pole	1.45	0.91	0.00	-0.37	-1.18	-2.48	0.16	0.19
53	South Pole	1.09	0.72	0.00	-0.31	-0.93	-2.01	0.13	0.15
54	Pensacola, FL	0.44	0.27	0.00	-0.21	-0.38	-0.72	0.05	-0.05
55	Pensacola, FL	0.44	0.27	0.00	-0.14	-0.38	-0.74	0.05	0.03

CHAPTER 3

Isotopic signature of mercury in wet deposition

3.1 Purpose of study

The global atmospheric reservoir is the principle source of mercury that is deposited in natural water bodies and on land. The study described in the previous chapter was an attempt to isotopically characterize this mercury reservoir. The process by which mercury is transferred from the atmospheric reservoir to waters and land surfaces primarily involves its oxidation to water soluble species and then rapid removal in precipitation. In order to determine what, if any isotopic effects might be associated with this transfer from atmosphere to surface, samples of rainwater have been collected and isotopically analyzed.

3.2 Mercury in Rainwater

Mercury is present in three predominant forms in the atmosphere; Hg (0), Hg (II) and Hg-P. Hg (II) is the most reactive species of mercury and is also known as Reactive Gaseous Mercury (RHg). Hg (II) is very water soluble and is the primary form of mercury in precipitation due to its tendency to get 'washed out'. Elemental mercury vapor in the atmosphere can photo-oxidize to Hg (II) or can be converted to Hg (II) by processes such as reaction with ozone, halogens and $OH^{\cdot}$ radicals (Lindqvist and Rhode, 1985). Deposition of Hg (II) is the most important process of removal of Hg from the atmosphere (Lindqvist and Rhode, 1985). Understanding the behavior of mercury in precipitation is therefore important in flux based models of the mercury cycle. Mercury in precipitation depends upon the availability of oxidizing agents in atmospheric waters as well as the availability of mercury in the atmosphere by way of re-emissions and

anthropogenic emissions. Pathways of transformation of RHg in atmospheric waters have been described in detail in chapter 3.

Lindqvist and Rhode (1985) summarized the then available data on atmospheric mercury, including that in precipitation. The lowest recorded Hg concentration in rainwater was observed in Samoa Islands and Japan where the concentration is lower than 1 ng/L. The average Hg concentration in rain water is of the order of 5-100 ng/L (Lindqvist and Rhode, 1985).

Between 1998 and 2002, significant cuts in mercury emissions (from 15.9 ton/year to 4.7 ton/year) have been achieved in the Northeastern US states as a result of a cooperative effort between the Northeastern states and the eastern Canadian provinces. Two studies have been published recently on the long term behavior of mercury in wet deposition. In a local study, Gratz et al (2009) have collected and analyzed precipitation samples from Underhill, VT for over a decade from 1995-2006. Their findings show no significant reduction in the concentration of mercury in the precipitation in this period even though significant emission cuts have been made in the region. This is due to the transport of anthropogenic mercury emitted from near by regions in the mid west and the east coast as well as long range sources such as increased emissions in Asia, and its eventual deposition. Years with lower concentrations of mercury were related to greater amount of precipitation due to El Niño Southern Oscillation cycles.

The Mercury Deposition Network (MDN), a subset of the National Atmospheric Deposition Network (NADP) is a cooperative effort by the United States and Canada to monitor long term mercury deposition in the continental scale that has been operational since 1995. Prestbo and Gay (2009) have studied the available data from the MDN from 1996-2005, specifically for a spatial or temporal patterns seen in wet deposition. The volume weighted mean concentration of mercury in the US south east especially in Florida is much higher than the average value in the rest of the network of 9.5 ng/L.

The Florida Atmospheric Mercury Study (the FAMS Project) was a 5-year study of the deposition of atmospheric mercury in Florida, its seasonal and geographical variability (Guentzel et al 1995). The study shows a marked difference in the Hg flux in the winter and summer months. Deposition rate in south Florida is 29% greater than that of north central Florida. Winter concentrations are in the range of 2 ng/L (low) to 25 ng/L (high). Summer concentrations are in the range of 7 ng/L (low) to 30 ng/L (high). Bulk deposition of mercury including wet and dry aerosol deposition showed no significant difference from just that of the wet deposition, implying a fairly low contribution of particulate matter in the total atmospheric deposition.

3.3 Sampling

Rainwater was collected using a Florida Atmospheric Mercury Study (FAMS) wet deposition sampler (Guentzel et.al, 1995). The apparatus comprises of Teflon lined polycarbonate funnel connected to FEP Teflon tubing which in turn is connected to a 2 Liter FEP Teflon receiving bottle. The apparatus is mounted on a large polyethylene trash container with a tight fitting lid. Rainwater for each measurement was collected over a period of a single rain event involving heavy rain storm integrated over 1-2 days. Rainwater was collected in Tallahassee, Florida. The apparatus is cleaned before and after each sampling event with 1 N HNO_3 to remove any particulate matter deposition in the funnel. Approximately, 2-3 liters of rain water is required for isotopic analysis of mercury. Once the sampling is complete, HCl is added to the rainwater so that the normality of the acid is 0.1 M. RHg in rainwater is converted to $HgCl_2$ upon reaction with HCl. This compound is a lot more stable than Hg (II) and is a lot less volatile. Rain water is stored in acid washed Pyrex glass bottles until they are ready to be processed. Due to the low concentration of mercury in rainwater, the solution is heated at a temperature of 70 C to evaporate the solution down to approximately 25 ml. The final solution is then introduced into the CETAC HGX 200 Cold Vapor generator.

This method only allows us to quantify the mass independent effect as the analytical procedure is expected to induce mass fractionation during the evaporation process. Any apparent mass dependent effect is therefore inconclusive at this stage. The analytical procedures, however, do not introduce a mass independent effect and therefore the MIF signature of rainwater can be used to compare the effect of wet deposition on the signature observed in Spanish moss.

3.4 Results and discussion

Not unlike the air samples, the rainwater shows a very linear array of the even mass isotopes on a multiple isotope plot (Figure 3.1). Rainwater also shows a small enrichment of the odd isotopes ^{199}Hg and ^{201}Hg with respect to the mass dependent fractionation line. This is denoted by Δ^{199}Hg and Δ^{201}Hg respectively as defined in equation 3. A plot of Δ^{201}Hg versus Δ^{199}Hg (Figure 4.2) shows no distinct pattern for either magnetic isotope effect or nuclear volume effect and is likely a combination of both or some other effect. Table 3.1 shows isotopic composition of all measured rain samples from Tallahassee, FL. The mean magnitude of this anomaly is 0.213 +/- 0.28 (2σ) ‰ for ^{199}Hg (Figure 4.3 a) and 0.18 +/- 0.24 (2σ) ‰ for ^{201}Hg (Figure 4.3.b) seen in all measured samples.

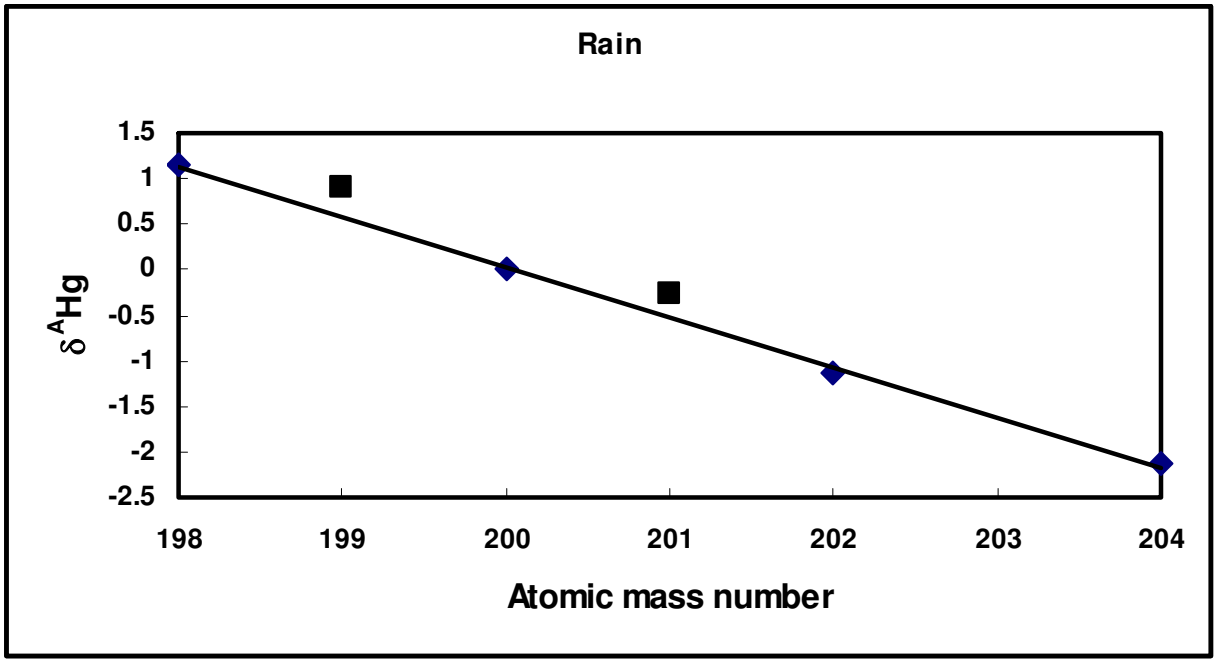

Figure 3.1 Isotopic composition of Hg (II) in precipitation. Linear scaling of even mass numbered isotopes reveal a very small deviation of odd isotopes from the dependent array.

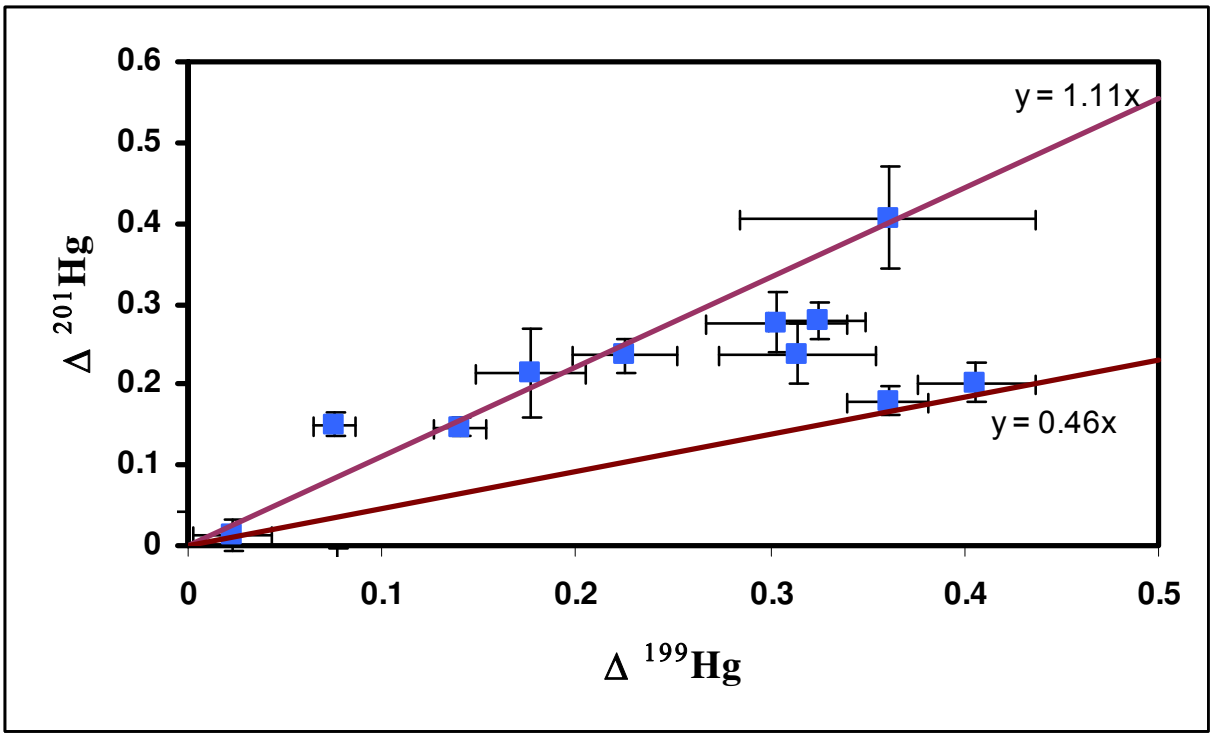

Figure 3.2 A plot of Δ^{201}Hg Vs Δ^{199}Hg. The internal precision of measurement is shown as 2SE on 50 ratios. The purple and red lines represent theoretical fractionation lines for magnetic isotope effect and nuclear volume effect. The plot shows scatter at this scale and it is difficult to resolve the effect of magnetic isotope effect and nuclear volume effect.

a)

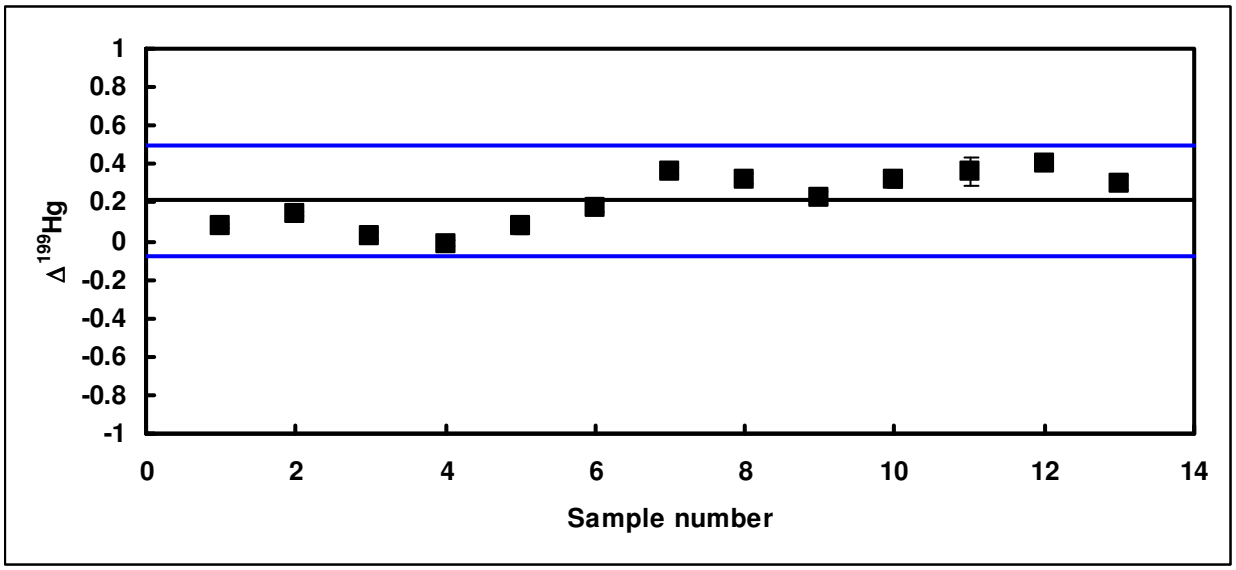

b)

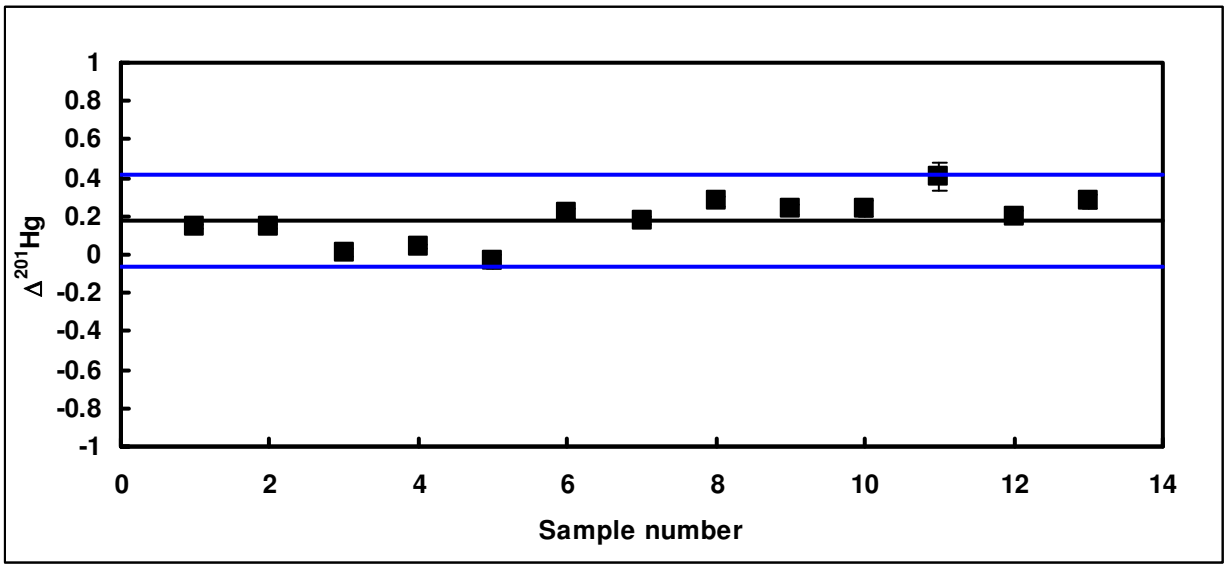

Figure 3.3 Δ^{199}Hg (a) and Δ^{201}Hg (b) of all rain samples measured. The black line is the average Δ^{199}Hg and Δ^{201}Hg respectively of the Hg in rain water; the blue lines represent $\pm 2\sigma$. The internal precision of measurement is shown as 2SE on 50 ratios.

Table 3.1 Isotopic composition of mercury in rainwater collected in Tallahassee, FL

Sample	$\delta^{198}Hg$	$\delta^{199}Hg$	$\delta^{200}Hg$	$\delta^{201}Hg$	$\delta^{202}Hg$	$\delta^{204}Hg$	$\Delta^{199}Hg$	$\Delta^{201}Hg$
1	1.60	0.88	0.00	-0.64	-1.59	-2.60	0.08	0.15
2	1.67	0.98	0.00	-0.63	-1.57	-2.64	0.14	0.15
3	1.51	0.75	0.00	-0.79	-1.62	-2.69	0.02	0.01
4	1.44	0.70	0.00	-0.70	-1.47	-2.40	-0.01	0.04
5	1.35	0.70	0.00	-0.65	-1.36	-2.31	0.08	-0.04
6	1.25	0.81	0.00	-0.36	-1.22	-2.30	0.18	0.21
7	1.02	0.85	0.00	-0.39	-1.14	-2.49	0.36	0.18
8	0.99	0.84	0.00	-0.39	-1.30	-2.76	0.32	0.28
9	0.90	0.77	0.00	-0.31	-1.11	-2.14	0.22	0.24
10	1.15	0.89	0.00	-0.26	-1.14	-2.14	0.31	0.24
11	1.86	1.32	0.00	-0.09	-1.24	-2.74	0.36	0.41
12	1.10	0.96	0.00	-0.42	-1.19	-2.39	0.41	0.20
13	1.04	0.81	0.00	-0.48	-1.34	-2.64	0.30	0.28
Mean	1.30	0.87	0.00	-0.47	-1.33	-2.48	0.21	0.18
Standard Deviation	0.30	0.16	0.00	0.20	0.18	0.22	0.14	0.12
2σ	0.60	0.32	0.00	0.40	0.36	0.43	0.28	0.24

CHAPTER 4

Use of Epiphytes as monitors for isotopic signature of atmospheric mercury

4.1 Epiphytes as isotopic tracers

Part of an ongoing effort to understand the isotopic composition of mercury in and deposited from the atmosphere has involved the use of epiphytes as monitors. The greatest advantage of these natural collectors is that a wide-spread, high-density network is possible at a low cost. Epiphytes are often referred to as “air plants” because they do not root in soil. These plants use host trees for physical support and access to sunlight but are non-parasitic. This study uses a regional network composed of samples of *Tillandsia usneoides*, commonly known as Spanish moss. Spanish moss is widely distributed in the Gulf and Atlantic Coastal Plains. They derive the necessary moisture and nutrients entirely from the atmosphere via air and rainfall and produce food by Crassulacean acid metabolism (CAM photosynthesis) (Martin and Siedow, 1981) C. Shaklette and Connor (1973) studied and analyzed Spanish moss samples from Southern United states for 38 elements including heavy metals such as mercury. They concluded that even though the concentration of elements collected and retained by Spanish moss does not completely reflect the concentration of elements in the ambient air mass, it can be a fast and economical method of estimating the relative concentration of airborne chemical elements among locations over a period of months or years and can be used as an indicator for air pollution. The purpose to this study is to test the use of epiphytes such as Spanish moss as a proxy for isotopic composition of atmospheric mercury.

4.2 Morphology

Spanish moss belongs to the bromeliad family (same as the pineapple family) and requires high humidity, warm climates and abundant sunlight to grow. It is believed to

have originated in the Peruvian Andes (Smith, 1934). Its distribution in the south eastern United States is likely related to storm paths and patterns that start in Mexico or in the Caribbean (Garth, 1964). The morphology and growth pattern of Spanish moss was extensively studied by R.E Garth (1964). Spanish moss is a flowering plant and shows a growth pattern of scorpioid dichotomy, wherein, each thin hair-like stem forks out to have one non-dominant leaf like branch and another dominant branch that continues to grow and fork. Its small yellow flowers grow on short branches that arise out of the leaf axils. The sensitivity of plants such as mosses and lichens to chemicals in the air has been discussed as early as 1863 by Nylander. Airborne chemical elements are absorbed by most plants via their foliage. The morphology of Spanish moss produces a plant with a relatively large foliar surface area with respect to its mass. Due to this, Spanish moss has an increased surface of absorption and is able to accumulate much larger amounts of airborne chemicals than other plants. Its ability for absorption is greatly enhanced by the presence of abundant minute translucent disc shaped scales attached to the stem and leaves, which pump water as well as salts into the moss (Mez, 1904; Aso, 1909). The plants essentially act as a filter, trapping elements and particles from the atmosphere. At any given time less than 45 cm of the plant is alive, most often the alive segment is 15 to 25 cm in length (Garth, 1964). Most often many small plants entangle with each other giving the illusion of much larger volume. The plants grow at the rate of 6 inches to a foot per year.

4.3 Hg in Spanish Moss

Spanish moss samples collected from FSU campus were analyzed for their mercury content in Florida State University's Department of Oceanography by Sara Cleveland. Samples were analyzed by Cold Vapor Atomic Florescence Spectrometry. The range of Hg concentration in multiple moss samples were determined to be between 10-60 ng/g of wet sample. Mercury preferentially binds to ligands of sulfur and therefore in biological material shows a particular affinity towards sulfur containing proteins such as cystine rich metallothioneins (Halbach 1995). Mercury in Spanish moss is likely strongly

bound with sulfur rich proteins that accumulate mercury within the plant which may effect biochemical reactions involving mercury within the plant.

4.4 Sampling

Moss samples were collected from along the eastern Coastal Plain of the U.S. from northern Florida to North Carolina. Samples were mainly collected from unindustrialized areas along rural roads. Samples were cleaned by air-dusting to remove dust and small insects that are common in Spanish moss. The moss was then torn in smaller pieces and eventually ground down using an agate mortar and pestle which is rinsed with 18 mega ohm de-ionized water before each sample is processed. Only wet samples were used for analyses. The samples were stored in sample containers in a freezer at approximately -20ºC to preserve its composition until they were ready to be processed. Prepared moss samples were digested in 50 ml PFA beakers that are cleaned in a solution of concentrated ultra pure reagent grade nitric acid and hydrochloric acid (1:1). Approximately, 1 gram of ground Spanish moss was mixed with 5 ml of aqua regia in the PFA beaker which was closed tight to prevent any loss of volatiles during the digestion process. The beaker was then placed overnight on a mechanical platform shaker. The samples were then placed in an ultrasonic bath for a total of 24 hours. This solution is then filtered through a 100 micron filter paper to remove the un-dissolved cellulose. NaOH was added to reduce the acidity of the sample solution to approximately 1.5 N. Also a few samples were digested with a smaller quantity of aqua regia in Parr microwave bombs for 10-15 seconds. Once dissolved, the solutions were diluted with 18 mega ohm water. Comparison of total microwave oven dissolution with that of leaching with aqua regia, indicates that the leaching technique removes all mercury from the moss and yields the same isotopic results. A detailed discussion of the analytical procedure and technique are described in chapter 2.

4.5 Results

4.5.1 Mass Dependent Fractionation

Spanish moss samples indicate a mass dependent isotopic signature for Mercury. The delta values defined as

$$\delta^{n}\text{Hg} = (\frac{Rsample}{Rstd} - 1)1000\ ‰ \quad \text{--- (1)}$$

where $R=\frac{^{n}Hg}{^{200}Hg}$ were measured for the isotopes ^{198}Hg, ^{199}Hg, ^{200}Hg, ^{201}Hg, ^{202}Hg and ^{204}Hg relative to NIST 3133. In all the measured moss samples, the delta values plotted against the respective isotopes define a linear curve. This is the expected mass fractionation line.

For most Spanish moss samples the δ^{198}Hg composition is of the order of 0.5 ‰. Some samples have a δ^{198}Hg of the order of -1‰ (Table 4.1). A discussion of analytical uncertainty of δ^{198}Hg and external reproducibility is also included in chapter 2. The mass dependent isotopic composition of Spanish moss when compared to the isotopic composition of ambient air with a δ^{198}Hg of 1.3 $\pm$ 0.8 ‰ suggests that the moss preferentially retains the heavier isotopes and releases the lighter isotopes possibly via exchange through its foliar surface.

4.5.2 Mass Independent Fractionation

The odd isotopes, δ^{199}Hg and δ^{201}Hg, however, deviate from this relationship and show a negative anomaly. This deviation of the odd isotopes from the mass dependent behavior is denoted by Δ^{199}Hg and Δ^{201}Hg as shown in figure 4.2.

Table 4.2 and Figure 4.4 (a and b) include Δ^{199}Hg and Δ^{201}Hg values of Spanish moss collected along south eastern United States. The average Δ^{199}Hg value is -0.5 $\pm$ 0.7 (2σ) ‰ and the average Δ^{201}Hg is -0.6 $\pm$ 0.8 ‰.

The measured Δ^{199}Hg /Δ^{201}Hg in the Spanish moss samples varies in the range 0.9 to 1.1. The trend line through all samples on a plot of Δ^{199}Hg versus Δ^{201}Hg has a slope of 1.04 (figure 4.3). Figure (4.5) includes isotopic data of Spanish moss as well as data obtained from residual Hg from photo reduction experiments conducted by Bergquist and Blum (2007). A regression line through both data sets indicates that the Spanish moss samples are complementary to the photo reduction data (see discussion).

4.6 Discussion

The plot of Δ^{201}Hg versus Δ^{199}Hg values (Figure 4.2) of the Spanish moss reveals an almost serendipitous pattern. In figure 4.2, dashed lines indicate theoretical fractionation lines for isotopes fractionated due to nuclear volume effect (Ghosh et al. 2008) and by magnetic isotope effect (Buchachenko, 2009). The ratio of the magnetic moments of ^{201}Hg and ^{199}Hg (0.56023 μ_B and 0.50589 μ_B respectively) is 1.11. All samples plot closely along a straight line passing through zero and having a slope of 1.04, which is within analytical error of the theoretical line for isotopes fractionated due to magnetic isotope effect. In the initial phases of this study, the isotopic signature of the moss was interpreted to reflect on the isotopic signature of the atmosphere. Moreover, the perfect complementary fit of the moss data with that of the data from photoreduction experiments by Bergquist and Blum (2007) was interpreted to imply that the atmosphere was a negative reservoir for odd-N mercury isotopes brought about by photoreduction from major water bodies. However, continued research suggests otherwise.

Comparison of the isotopic signature of the Hg (0) from the air mass shows a stark difference from the signature recorded in the epiphyte Spanish moss, implying that the moss does not record the signature of the ambient air mass in which it grows and receives its nutrients from.

The effect of magnetic fields on biological reactions and processes has been and remains to this day one of the more controversial areas of research. Magnetic spin effects arise from an endogenous magnetic field due to non-zero spin in certain nuclei. This effect in enzymatic and chemical reactions, by way of intermediate radical pair recombination involving a change of singlet-triplet or triplet-singlet states, has been demonstrated and studied in laboratories by many researchers (Buchachenko1995; 2004; 2007; 2008; Grissom 1995).

In photosynthetic reaction centers, a singlet state is generated when a photon is absorbed for ATP synthesis. Upon the absorption of the photon, an electron is donated to an acceptor and this forms an intermediate caged RP in the singlet state. This RP transfers an electron to a quinone acceptor and produces another RP without undergoing intersystem crossing (ISC), due to its low free energy (Grissom, 1995).

$$PIX \xrightarrow{hv} P*IX \longrightarrow {}^1(P^{+\cdot}\,{}^{-I}X) \longrightarrow {}^1(P^{+\cdot}I^{\cdot -x}) \quad \text{--- Equation 4}$$

Here, P is the electron donor, I is an intermediate electron acceptor and X is the stable quinone acceptor. If, however, the quinone acceptor in this step of this reaction chain is reduced so as to not allow it to accept the electron, the lifetime of the intermediate RP in the first step is increased and ISC to a triplet state is favored. This, however, is rare in the photosynthetic reaction centers in the absence of an external magnetic field.

$$P*IX^{-\cdot} \longrightarrow {}^1(P^{+\cdot}\,{}^{-I})X^{-\cdot} \longrightarrow {}^3(P^{+\cdot}\,{}^{-I})X^{-\cdot} \longrightarrow {}^3P*IX^{-\cdot} \quad \text{---Equation 5}$$

Magnetic field effects are particularly important in enzymatic reactions. During enzyme biochemistry, only the enzyme-substrate complex is capable of forming products. The conversion of the substrate to the product takes place by several intermediate smaller steps. If a simple enzymatic reaction is considered where a substrate ‘S’ is converted to a product ‘P’, the first step involves the binding of the enzyme ‘E’ to ‘S’. The enzyme-substrate complex ‘ES’ is then converted to a product ‘P’, which is governed by the rate

of catalysis of ES, k. This is an irreversible process (Grissom, 1995), generally following kinetic isotopic fractionation.

$$E + S \Leftrightarrow ES \xrightarrow{k} E + P \qquad \text{--- Equation 6}$$

If magnetic field effects due to an endogenous magnetic field, act on 'k' instead of kinetic isotope effects, an intermediate formation of radical pair before the formation of the product. In this case the reaction would proceed in the following way,

$$E + S \Leftrightarrow ES \Leftrightarrow E^{\cdot}\,^{\cdot}S \longrightarrow E + P \qquad \text{--- Equation 7}$$

For MFE to be induced in enzymatic reactions, it imperative for at least one step of this reaction to form spin correlated radical pair, that are weakly coupled and exists for a suitably long time. If the coupling is strong, it will not undergo intersystem crossing (Grissom, 1995).

Buchachenko et al (2004) experimentally demonstrated magnetic isotope effect in the odd isotopes of mercury in biochemical reactions during the ATP-synthesis of the enzyme creatine kinase by methylmercury chloride (MMC). An enrichment of the isotopes ^{199}Hg and ^{201}Hg was observed in the mercury bound to the enzyme. A significant component of the active creatine kinase enzyme is the cysteine residue. The thiol functional group (RSH) with in the cysteine residue is most reactive to methyl mercury chloride and is responsible for the spin selectivity of the reaction. In the mechanism suggested by the authors, the first step is the formation of the radical pair $CH_3^{\cdot}$ $^{\cdot}HgCl$ and $^{+\cdot}RSH$ in the singlet state. ISC can take place where the magnetic isotope change from singlet to triplet states faster than the non-magnetic isotopes and accumulate in the product. This positive MIF is dependent on the actual conditions of photolysis (Buchachenko et al, 2008).

Zheng and Hintelmann (2009) performed key experiments to determine the significance of DOM-Hg complexes in the production of Hg isotope fractionation, specifically, the

effect of Hg/DOC ratios on the isotopic fractionation. As previously stated, dissolved organic matter (DOM) consists of humic substances and other unidentifiable complex compounds and is present in all aquatic environments. DOM binds strongly with Hg and affects its speciation and transport behavior. Natural waters contain a Hg/DOC ratio of at the most 20 ng Hg/ mg DOC. Previous Hg photoreduction experiments were conducted in as much as Hg/DOC ratio of 10,000 to 100,000 ng/ mg. If fractionation of Hg isotopes depends on the Hg/DOC ratios of the environment, then these experiments do not necessarily reflect on natural conditions. Also, a dependence of Hg-DOM binding in the production of mass independent fractionation of Hg isotopes may also have strong implications on the actual nature of this MIF itself, i.e. if it is actually a reflection on organic material aiding in the production of magnetic isotope effects.

In aquatic environments, Hg may bind with either reduced S compounds or carboxyl groups. Hg forms very stable compounds with thiol groups and does not readily undergo photo-reduction. However, the abundance of reduced S compounds is much less than carboxyl compounds in DOM. Therefore reduction kinetics depends on the Hg concentration in the water body with respect to DOM. If the concentration of Hg is less than that of reduced S, all of the Hg preferentially binds with the reduced S, forming stable complexes and thus lowering the reduction rates. If the Hg concentration is much higher however, then a small proportion of Hg will bind with the available reduced S and the remaining Hg will bind with carboxyl groups resulting in compounds with much lower stability constants and thus much higher reduction rates. The point of saturation of S compounds by Hg depends on the concentration of reduced S in the DOM which in turn depends on the Hg/DOC ratios. For Hg/DOC ratios of 1000ng/mg the stability of the Hg-DOM complexes decreased dramatically. DOM is able to start a direct electron charge transfer via ligand to metal charge transfer (LMTC) during photolysis of DOM-Hg complexes, wherein Hg is reduced. This process produces intermediate radicals R. and Hg which as the radical pair intermediates needed to produce intersystem crossing to generate a magnetic isotope effect. The hyperfine coupling constants are different for different radical pair intermediates. Radical pairs produced during the LMCT of different DOM-Hg compounds have different recombination rates and hyperfine coupling

constants. At high Hg/DOC ratios intermediate radical produced are Hg+ and .OR, whereas at lower Hg/DOC, radicals produced are Hg+ and .SR. The .SR radical and Hg + radical form much more stable complexes and here a faster recombination is preferred rather than intersystem crossing, thereby not allowing MIE to be produced.

It is inferred from this work that the production of MIF in aquatic environments is dependent on a prerequisite of high Hg/DOC ratios (> 1000 ng /mg) and radical pair intermediates. This indicates that the main sources of mercury cycling such as atmosphere and oceans may not produce any significant MIF signatures. Oceans, for example have Hg/DOC ratios of 20ng/mg which hardly produces any MIF worth measuring so it cannot be the source for the MIF measured in previously analyzed fish tissues. Biological material higher up in the food chain as well as in plant material that can bio-concentrate or accumulate Hg may have the required amount of Hg-organic material binding to produce sufficient amount of measurable MIF in nature. Photoreduction experiments conducted by Bergquist and Blum (2007) used up to 10,000 to 100,000 ng/mg of Hg/DOC. These concentrations of Hg are ten to a hundred times greater than what is required to induce a magnetic isotope effect within the experimental chamber. The MIF that is measured in the residue of these photo-reduction experiments while valid for experimental conditions, do not apply to natural conditions.

4.7 Conclusion

The nature of the mass independent fractionation observed in multiple epiphyte samples, shows a clear and strong component of magnetic isotope effect. Epiphytes attain mercury from the atmosphere via direct absorption of Hg vapor from the air, wet deposition of Hg (II) via mercury in rainfall and a very small component of particulate mercury (Hg-P). Within the plant there are many biological influences such as cysteine containing proteins and metallothioniens which might contribute to the mass independent isotope effect observed in this study

The isotopic composition of Spanish moss is markedly distinct from that of the isotopic composition of the Hg (vapor) in the air and Hg(II) in the rain and suggests that the spanish moss does not inherit the isotopic composition of its mercury sources. This observation is significant as it reflects on the actual nature of the mechanism affecting the origin of the large negative odd isotopic anomalies recorded in the moss. The isotopic composition of mercury in Spanish moss is not inherited from the atmosphere but indicates a biological origin within the moss itself.

It is concluded from this study that though the magnetic isotopic effect recorded by the Spanish moss is significant in its nature, it does not reflect on the isotopic composition of either of the sources of mercury in the moss and thus cannot be used as a proxy for atmospheric mercury.

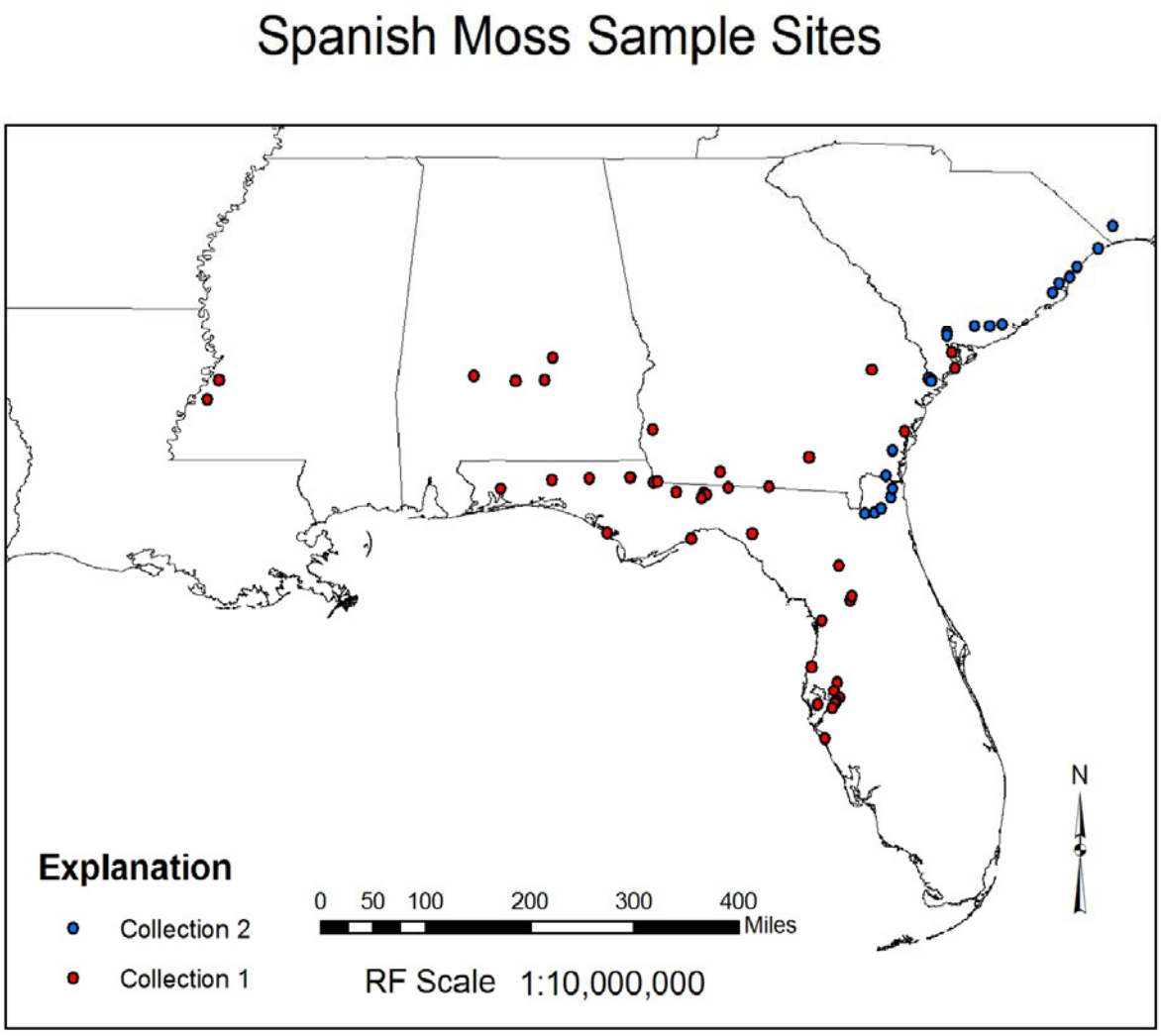

Figure 4.1 Map of south eastern United States showing sampling locations for Spanish moss. Collection 1 was conducted by Elizabeth Moulton in 2004 and collection 2 was conducted by the author in July 2007.

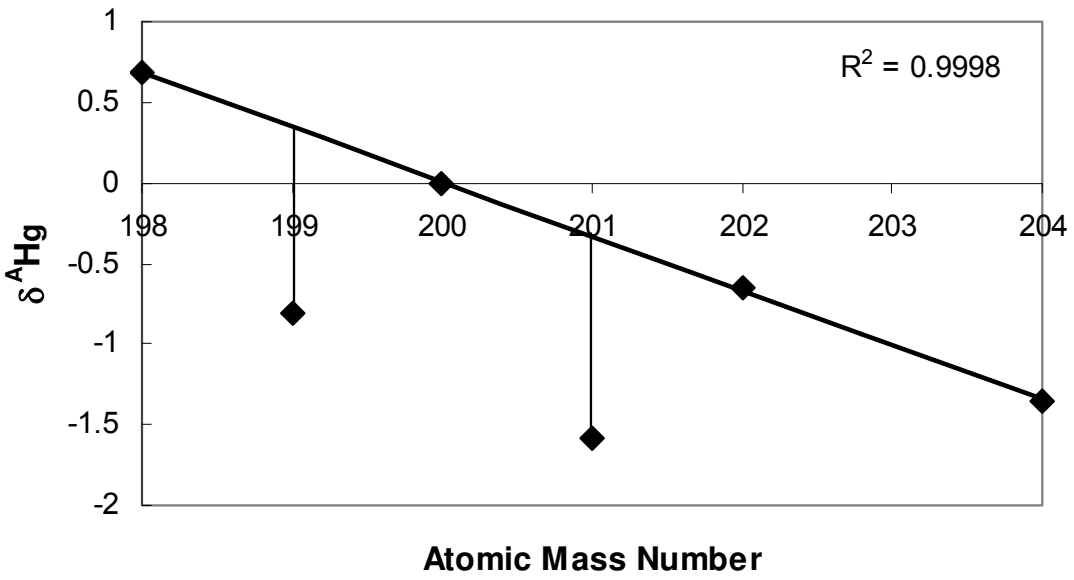

Figure 4.2 The Hg isotope plot for Spanish moss. Even isotopes plot on a linear curve and odd isotopes show a negative anomaly

Table 4.1 Isotopic composition of mercury measured in Spanish moss

Sample	$\delta^{198}Hg$	$\delta^{199}Hg$	$\delta^{200}Hg$	$\delta^{201}Hg$	$\delta^{202}Hg$	$\delta^{204}Hg$
su#1	-0.77	-1.47	0.00	-1.01	0.49	0.95
su#2	0.25	-0.64	0.00	-0.85	-0.21	-0.30
su#7	0.05	-0.84	0.00	-1.24	-0.15	-0.50
su#14	0.69	-0.81	0.00	-1.58	-0.65	-1.35
su#15	0.44	-0.58	0.00	-1.34	-0.71	-1.62
su#16	0.13	-0.76	0.00	-1.14	-0.35	-0.71
su#17	0.52	-0.77	0.00	-1.73	-0.85	-1.78
moss#1	0.38	-0.05	0.00	-0.57	-0.52	-0.96
moss#2	-0.39	-0.46	0.00	-0.07	0.30	0.73
moss#6	-0.36	-0.38	0.00	-0.08	0.30	0.69
moss#7	0.77	0.05	0.00	-0.77	-0.83	-1.62
moss#15	0.45	-0.07	0.00	-0.85	-0.55	-1.13
moss#16	0.95	0.37	0.00	-0.68	-0.97	-1.99
rez (bomb)	-0.39	-0.98	0.00	-0.78	0.22	0.36
Rezpl	-1.28	-1.54	0.00	-0.67	0.82	1.73
moss#10	0.47	-0.06	0.00	-0.70	-0.63	-1.29
moss#11	0.56	0.09	0.00	-0.55	-0.63	-1.24
moss#12	0.17	-0.17	0.00	-0.48	-0.32	-0.66
moss#13	0.71	0.34	0.00	-0.45	-0.80	-1.54
moss#18	-0.65	-0.60	0.00	-0.15	0.50	1.03
moss#19	-1.19	-0.79	0.00	0.31	1.02	2.06
moss#20	0.38	-0.04	0.00	-0.57	-0.53	-1.05

Table 4.2 Odd isotope anomalies measured in Spanish moss

Sample	$\Delta^{199}Hg$	$\Delta^{201}Hg$	2SE $\Delta^{199}Hg$	2SE $\Delta^{201}Hg$	Location
su#1	-1.19	-1.25	0.0951	0.0194	Jacksonville
su#2	-0.61	-0.71	0.0552	0.0283	Jacksonville
su#7	-1.01	-1.18	0.0331	0.0295	Waverly,GA
su#14	-1.15	-1.25	0.0282	0.0286	Ravenel,SC
su#15	-1.02	-0.96	0.0319	0.0332	Charleston,SC
su#16	-0.94	-0.96	0.0256	0.0180	Old Dock/Ash NC
su#17	-1.23	-1.30	0.0262	0.0236	Little River SC/NC
moss#1	-0.23	-0.30	0.0173	0.0145	Ocklocknee bay (south)
moss#2	-0.24	-0.23	0.0510	0.0295	Mexico Beach
moss#6	-0.18	-0.23	0.0482	0.0338	Marianna
moss#7	-0.33	-0.35	0.0130	0.0130	Sneads
moss#15	-0.29	-0.53	0.0163	0.0181	Ybor City
moss#16	-0.13	-0.18	0.0605	0.0189	South of Alafia river
rez (bomb)	-0.76	-0.80	0.0136	0.0176	FSU Reservation
Rezpl	-0.87	-0.99	0.0378	0.0550	FSU Reservation
moss#10	-0.40	-0.37	0.0262	0.0141	Quincy,GA
moss#11	-0.22	-0.23	0.0558	0.0193	Blakely,GA
moss#12	-0.33	-0.32	0.0295	0.0188	Perry,GA
moss#13	-0.41	-0.38	0.0179	0.0126	Crystal River,FL
moss#18	-0.34	-0.41	0.0209	0.0208	Tampa, FL
moss#19	-0.31	-0.22	0.0658	0.0303	Tampa,FL
moss#20	-0.30	-0.30	0.0211	0.0115	Sarasota, FL

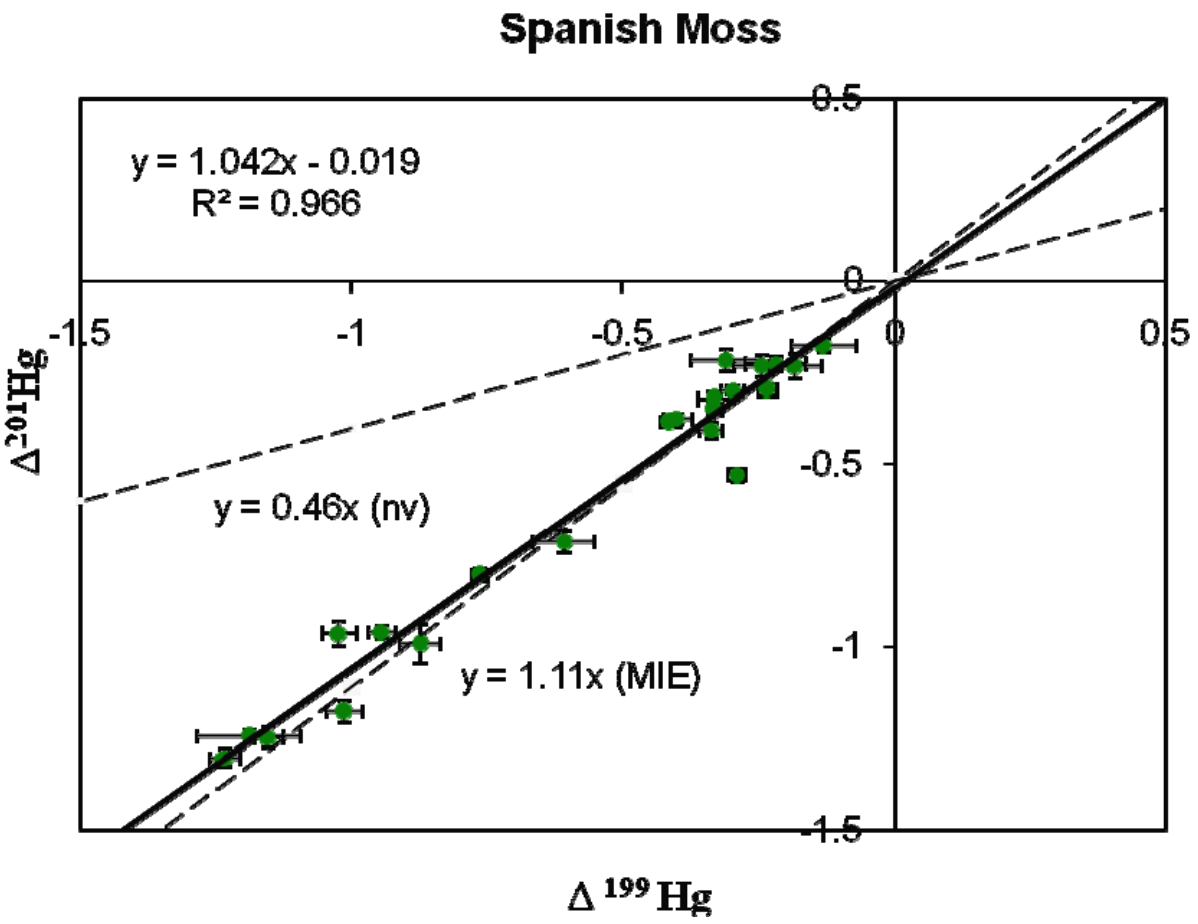

Figure 4.3 A plot of Δ ^{199}Hg versus Δ ^{201}Hg. Errors indicated are standard error of analysis. Dashed lines indicate theoretical isotopic fractionation lines due to nuclear volume effect (NV) and magnetic isotope effect (MIE)

a)

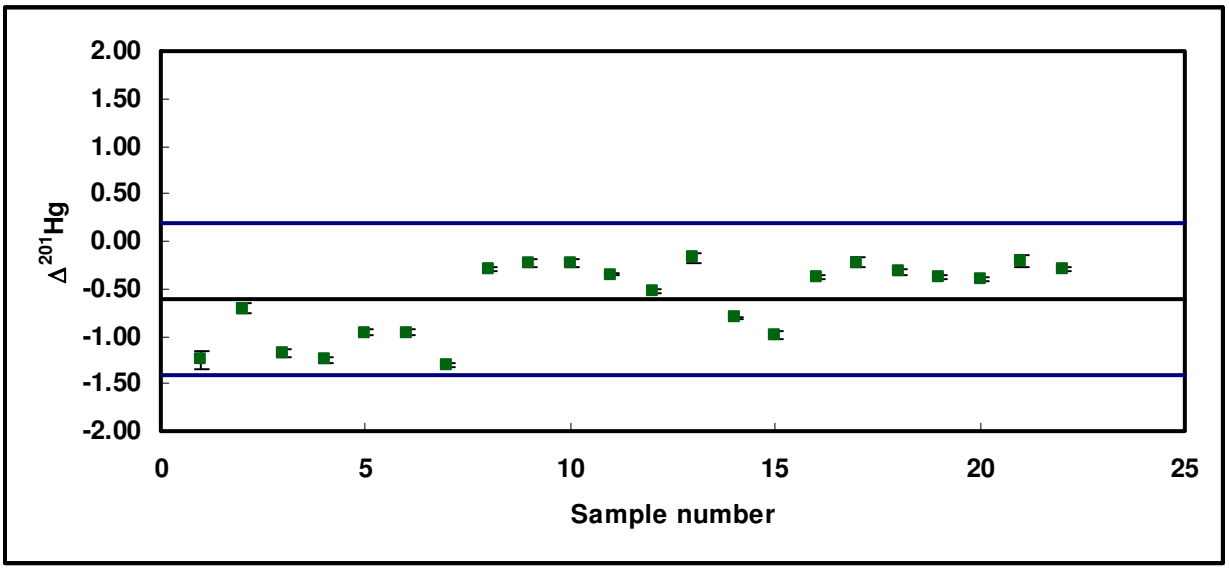

b)

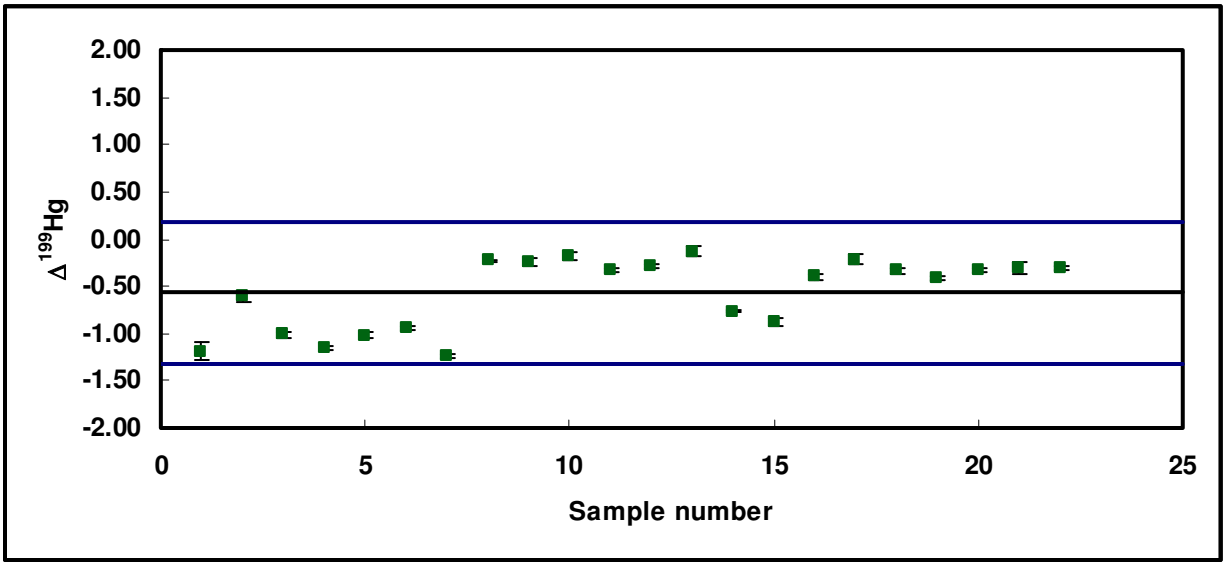

Figure 4.4 Δ^{199}Hg (a) and Δ^{201}Hg (b) of Spanish moss samples analyzed from the south eastern Atlantic and Gulf coast of The United States. Solid black lines represent mean Δ^{199}Hg and Δ^{201}Hg respectively. Blue lines represent 2σ.

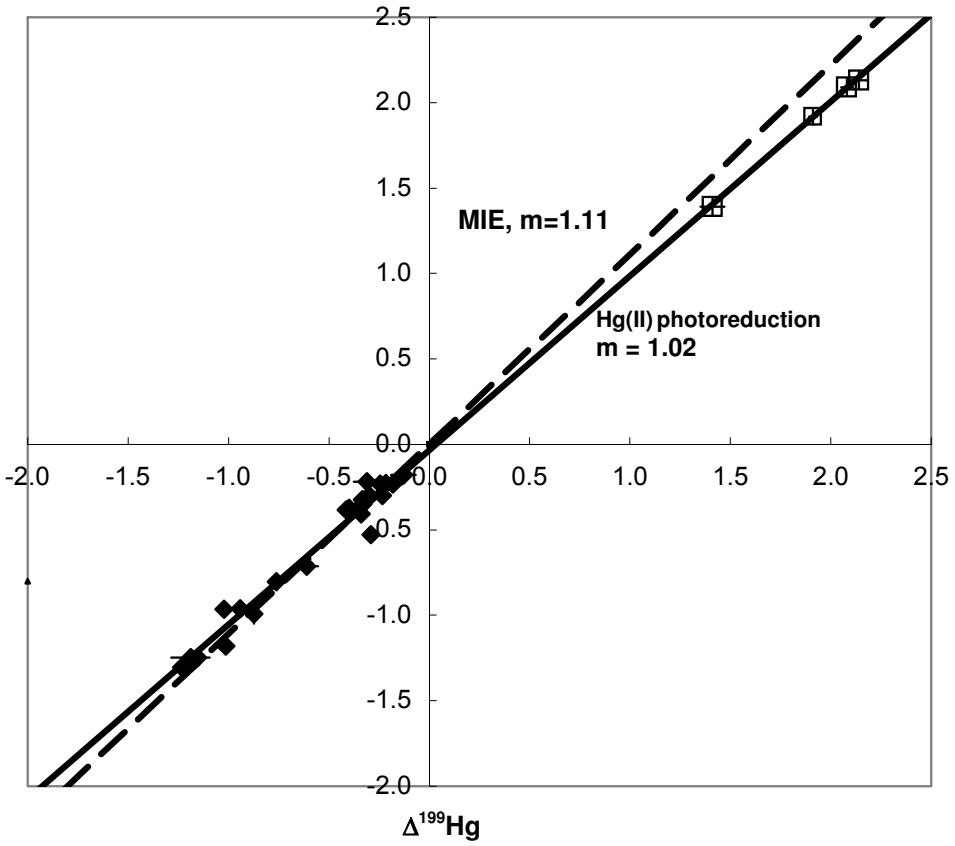

Figure 4.5 Plot of Δ^{199}Hg versus Δ^{201}Hg of Spanish moss (solid diamonds) and residual of photoreduction experiment conducted by Bergquist and Blum (2007) (open squares).

APPENDIX

Table A.1 Location of Spanish moss collection sites

Sample #	Location	Latitude			Longitude		
		Deg	Min	Sec	Deg	Min	Sec
Su #1	Baldwin near post office, FL	30	18	8	81	58	54
Su #2	Outskirts of Jacksonville, FL	30	18	77	81	50	88
Su #7	Off I 94 1 Mile south of Waverly, GA	31	8	12	81	35	70
Su #14	Hwy 17 Ravenel, SC	32	46	54	80	14	88
Su #15	Charleston, SC	32	47	75	80	4	62
Su #16	Between Old Dock & Ash, NC	34	5	65	78	32	81
Su #17	NC-SC border SC Visitor Center at Little River, SC	33	5	65	78	36	3
Moss#1	South side of Ochlocknee Bay on Hwy 98	29	57	37.4	84	23	6
Moss#2	West of Mexico beach on north side of Hwy 98	30	2	25.7	85	33	6.2
Moss#6	In Marianna	30	46	30.4	85	13	55
Moss#7	In Sneads	30	42	35.1	84	54	55.1
Moss#15	Ybor City off 39th Ave just north of SR 60	27	57	30.2	82	24	57.4
Moss#16	Off 301 south of Alafia River	27	51	38.9	82	19	38.7
Moss#10	In Quincy	30	35	7.9	84	35	48.2
Moss#11	North of Blakely on Hwy 27 in GA	31	23	54.2	84	55	25.7
Moss#12	South of Perry in Hwy 27	30	2	10	83	32	43.5
Moss#13	In Crystal River on US 98/19	28	53	39.8	82	35	7.6
Moss#18	Off CR-672, about 1/2 mile south of Tampa Electirc Big Bend Station	27	47	7.8	82	24	9.6
Moss#19	Off US 41 north of Ruskin, ~5 miles SSW of Tampa Electric	27	43	52.8	82	26	4.8
Moss#20	In Sarasota off US 41	27	19	44.8	82	32	17.4

Table A.2 Air collection dates for NOAA and NPS sampling locations

Trap ID	Location	Start	Stop	Latitude	Longitude
AS 01	American Samoa	2-Mar-09	16-Mar-09	14º19' S	170º 0' W
AS 02	American Samoa	16-Mar-09	30-Mar-09	14º19' S	170º 0' W
MLO 01	Mauna Loa	30-Apr-09	14-May-09	19º30'N	155º35'W
MLO 02	Mauna Loa	30-Apr-09	14-May-09	19º30'N	155º35'W
MLO 03	Mauna Loa	14-May-09	28-May-09	19º30'N	155º35'W
MLO 04	Mauna Loa	14-May-09	28-May-09	19º30'N	155º35'W
TH 01	Trinidad Head	3-Feb-09	31-Mar-09	41º03'N	124º09'W
TH 02	Trinidad Head	31-Mar-09	15-Apr-09	41º03'N	124º09'W
SP 01	South Pole	24-Jun-09	12-Aug-09	90ºS	
SP 02	South Pole	20-Jul-09	28-Aug-09	90ºS	
GS 01	Great Smoky NP	11-Aug-09	25-Aug-09	35º35'N	83º30'W
GS 02	Great Smoky NP	25-Aug-09	8-Sep-09	35º35'N	83º30'W
MACA 01	Mammoth Cave NP	14-Aug-09	28-Aug-09	37º08'N	86º13'W
MACA 02	Mammoth Cave NP	28-Aug-09	11-Sep-09	19º30'N	86º13'W

REFERENCES

Aiken G., Ravichandran M., Reddy M., Ryan J. and Tregellas J. (1998) Interaction of dissolved organic carbon with mercury in the Everglades, Florida. *Abstracts of papers* 216,

Allard B. and Arsenie I. (1991) Abiotic reduction of Mercury by humic substances in aquatic system- an important process for mercury cycle. *Water Air Soil Pollut.* 56, 457.

Arakaki T., Anastasio C., Shu P. and Faust B (1995) Aqueous- phase photoreduction of hydrogen- peroxide in authentic cloud waters – wavelength dependence, and effects of filtration and freeze-thaw cycles. *Atmos. Environ.* 29, 1697.

Aso, K. 1909. Konnen Bromeliaceen durch die Schuppen der Blatter Salze aufnehmen? Flora 100: 447-450

Bergquist B. and Blum J. (2007) Mass-dependent and -independent fractionation of Hg isotopes by photoreduction in aquatic systems. *Science* 318, 417.

Bergquist B. A., Blum J. D. and Jude D. (2008) Utilization of mass-dependent and -independent fractionation of mercury isotopes to understand mercury cycling and bioaccumulation in aquatic systems; Abstracts of the 18th annual V. M. Goldschmidt conference. *Geochim. Cosmochim. Acta* 72, A77.

Bigeleisen J. (1996) Nuclear size and shape effects in chemical reactions. Isotope chemistry of the heavy elements. *J. Am. Chem. Soc.* 118, 3676.

Biswas A., Blum J., Bergquist B., Keeler G. and Xie Z. (2008) Natural Mercury Isotope Variation in Coal Deposits and Organic Soils. *Environmental science technology* 42, 8303.

Biswas A., Blum J. D. and Bergquist B. A. (2007) Variation in natural mercury isotopic ratios of coal formations; Abstracts of the 17th annual V. M. Goldschmidt conference. *Geochim. Cosmochim. Acta* 71, A94.

Blum J. and Bergquist B. (2007) Reporting of variations in the natural isotopic composition of mercury. *Analytical and bioanalytical chemistry* 388, 353.

Breit G. (1958) Theory of isotope shift. *Reviews of modern physics* 30, 507-516.

Buchachenko A. (2009) Mercury isotope effects in the environmental chemistry and biochemistry of mercury-containing compounds. *Russian chemical reviews* 78, 319.

Buchachenko A., Ivanov V., Roznyatovskii V., Artamkina G. and Ustynyuk Y. (2007) Magnetic isotope effect for mercury nuclei in photolysis of bis(p-trifluoromethylbenzyl)mercury. *Doklady.Physical chemistry* 413, 39.

Buchachenko A., Ivanov V., Roznyatovskii V. and Ustynyuk Y. (2008) Inversion of the sign of the magnetic isotope effect of mercury in photolysis of substituted dibenzylmercury. *Doklady.Physical chemistry* 420, 85.

Buchachenko A., Kouznetsov D. and Shishkov A. (2004) Spin biochemistry: Magnetic isotope effect in the reaction of creatine kinase with CH3HgCl. *The journal of physical chemistry.A* 108, 707.

Buchachenko A., Ruban L., Step E. and Turro N (1995) Spin Catalysis of the radical recombination reaction. *Chemical Physics Letters* 233, 315.

Carignan J., Estrade N., Sonke J. and Donard O. (2009) Odd Isotope Deficits in Atmospheric Hg Measured in Lichens. *Environmental science technology* 43, 5660.

Carpi A. and Lindberg S. (1998) Application of a Teflon (TM) dynamic flux chamber for quantifying soil mercury flux: Tests and results over background soil. *Atmos. Environ.* 32, 873.

Costa M. and Liss P. (1999) Photoreduction of mercury in sea water and its possible implications for Hg-0 air-sea fluxes. *Mar. Chem.* 68, 87.

Das R., Salters V. and Odom A. (2009) A case for in vivo mass-independent fractionation of mercury isotopes in fish. *Geochem. Geophys. Geosyst.* 10, Q11012.

Dastoor A., Davignon D., Theys N., Van Roozendael M., Steffen A. and Ariya P. (2008) Modeling dynamic exchange of gaseous elemental mercury at polar sunrise. *Environmental science technology* 42, 5183-5188.

Estrade N., Carignan J., Sonke J. and Donard O. (2009) Mercury isotope fractionation during liquid-vapor evaporation experiments. *Geochim. Cosmochim. Acta* 73, 2693.

Faust B and Allen J (1993) Aqueous- phase photochemical formation of hydroxyl radical in authentic cloudwaters and fogwaters. *Environmental science technology* 27, 1221.

Faust B. and Hoigne J. (1990) Photolysis of Fe(II)- hydroxy complexes as sources of OH radicals in clouds, fog and rain. *Atmos. Environ.* 24, 79-89.

Finlayson-Pitts B., Ezell M., Wang S. and Grant C. (1986) Kinetics and mechanism of the reaction of hydroxyl radicals with nitrosyl chloride. *Abstracts of papers* 192,

Finlayson-Pitts B., Johnson S. and Wang S. (1986) Kinetics and mechanism of reaction of nitrogen dioxide with nitrosyl chloride. *Abstracts of papers* 192,

Finlayson Pitts and Pitts 1986 Finlayson-Pitts, B.J., Pitts, Jr., J.N., 1986. Atmospheric Chemistry: Fundamentals and Experimental Techniques. Wiley, New York.

Finlayson-Pitts B. and Pitts J. (1993) Atmospheric chemistry of tropospheric ozone formation: Scientific and regulatory implications. *Air Waste* 43, 1091.

Garth R. (1964) Ecology of Spanish Moss (Tillandsia Usneoides)- Its growth distribution. *Ecology* 45, 470.

Gehrke G., Blum J. and Meyers P. (2009) The geochemical behavior and isotopic composition of Hg in a mid-Pleistocene western Mediterranean sapropel. *Geochim. Cosmochim. Acta* 73, 1651.

Ghosh S. and Odom L. (2008) Mercury isotopic signature of the atmosphere. *Geochim. Cosmochim. Acta* 72, A307.

Ghosh S., Xu Y., Humayun M. and Odom L. (2008) Mass-independent fractionation of mercury isotopes in the environment. *Geochem. Geophys. Geosyst.* 9, Q03004.

Gratz L., Keeler G. and Miller E. (2009) Long-term relationships between mercury wet deposition and meteorology. *Atmos. Environ.* 43, 6218.

Grissom C. (1995) Magnetic- Field effects in biology- A survey of possible mechanisms with emphasis on radical- pair recombination. *Chem. Rev.* 95, 3.

Guentzel J., Landing W., Gill G. and Pollman C. (2001) Processes influencing rainfall deposition of mercury in Florida. *Environmental science technology* 35, 863.

Guentzel J., Landing W., Gill G. and Pollman C. (1995) Atmospheric deposition of mercury in Florida: The FAMS Project (1992-1994). (Originally published in Water, Air, and Soil Pollution 80: 393-402, 1995). *Mercury as a global pollutant*393.

Halbach S. (1995) Combined estimation of mercury species released from amalgam. *J. Dent. Res.* 74, 1103-1109.

Hall B. (1995) The gas- phase oxidation of elemental mercury by ozone. *Water, air, and soil pollution* 80, 301-315.

Hirdman D., Aspmo K., Burkhart J., Eckhardt S., Sodemann H. and Stohl A. (2009) Transport of mercury in the Arctic atmosphere: Evidence for a springtime net sink and summer-time source. *Geophys. Res. Lett.* 36, L12814.

Iverfeldt A. and Lindqvist O. (1986) Atmospheric oxidation of elemental mercury by ozone in the aqueous phase. *Atmos. Environ.* 20, 1567-1573.

Keene W. (1997) Chemical processes involving atmospheric sea salt: A global perspective. *Abstracts of papers* 214, 18.

Kobayashi 1987 Kobayashi, T., 1987. Oxidation of metallic mercury in aqueous solution by hydrogen peroxide and chlorine. Journal of Japan Society for Air Pollution 22, 230-236.

Kritee K., Barkay T. and Blum J. (2009) Mass dependent stable isotope fractionation of mercury during mer mediated microbial degradation of monomethylmercury. *Geochim. Cosmochim. Acta* 73, 1285.

Kritee K., Blum J. and Barkay T. (2008) Mercury Stable Isotope Fractionation during Reduction of Hg(II) by Different Microbial Pathways. *Environmental science technology* 42, 9171.

Kritee K., Blum J., Johnson M., Bergquist B. and Barkay T. (2007) Mercury stable isotope fractionation during reduction of Hg(II) to Hg(0) by mercury resistant microorganisms. *Environmental science technology* 41, 1889.

Kritee K., Blum J., Johnson M., Bergquist B. and Barkay T. (2007) Variation in the extent of mercury (Hg) stable isotope fractionation during reduction of Hg(II) to Hg(0) by different microbial strains. *Abstracts of the ...General Meeting of the American Society for Microbiology* 107, 439.

Kritee K., Blum J. D., Johnson M. W., Bergquist B. A. and Barkay T. (2007) Mercury Stable Isotope Fractionation during Reduction of Hg(II) to Hg(0) by Mercury Resistant Microorganisms. *Environ. Sci. Technol.* 41, 1889-1895.

Lalonde J., Amyot M., Kraepiel A. and Morel F. (2001) Photooxidation of Hg(0) in artificial and natural waters. *Environmental science technology* 35, 1367.

Li C., Cornett J., Willie S. and Lam J. (2009) Mercury in Arctic air: The long-term trend. *Sci. Total Environ.* 407, 2756-2759.

Lin C. and Pehkonen S. (1999) Aqueous phase reactions of mercury with free radicals and chlorine: Implications for atmospheric mercury chemistry. *Chemosphere* 38, 1253.

Lin C. and Pehkonen S. (1999) The chemistry of atmospheric mercury: a review. *Atmos. Environ.* 33, 2067.

Lin C. and Pehkonen S. (1998) Oxidation of elemental mercury by aqueous chlorine (HOCl/OCl-): Implications for tropospheric mercury chemistry. *Journal of geophysical research* 103, 28093.

Lin C. and Pehkonen S. (1998) Two-phase model of mercury chemistry in the atmosphere. *Atmos. Environ.* 32, 2543-2558.

Lin C., Pongprueks P., Bulock O. R., Lindberg S., Pehkonen S. and Jang C. (2007) Scientific uncertainties in atmospheric mercury models II: Sensitivity analysis in the CONUS domain. *Atmos. Environ.* 41, 6544-6560.

Lin C., Pongprueksa P., Lindberg S., Pehkonen S., Byun D. and Jang C. (2006) Scientific uncertainties in atmospheric mercury models I: Model science evaluation. *Atmos. Environ.* 40, 2911.

Lindqvist O. and Rodhe H. (1985) Atmoespheric mercury- A review. *Tellus.Series B, Chemical and physical meteorology* 37, 136.

Martin C. and Siedow J. (1981) Crassulacean acis metabolism in the epiphyte Tillandsia Usneoides L (Spanish moss)- responses of CO2 exchange to controlled environmental conditions. *Plant Physiol.* 68, 335.

Mason R. and Sheu G. (2002) Role of the ocean in the global mercury cycle. *Global Biogeochem. Cycles* 16, 1093.

Mez, C. 1904. Physiol Bromeliaceen-Studien. I. Die Wasser-Okonomie die extreme atmospharischen Tillandsien. Prings. Jahrb. f. Wissensch. Bot. 40: 157- 229.

Munthe J. (1992) The aqueous oxidation of elemental mercury by ozone. *Atmos. Environ.* 26, 1461.

Munthe J. and McElroy W. (1992) Some aqueous reactions of potential importance in the atmospheric chemistry of mercury. *Atmos. Environ.* 26, 553-557.

Munthe J., Xiao Z and Lindqvist O. (1991) The aqueous reduction of divalent mercury by sulfite. *Water Air Soil Pollut.* 56, 621.

Nguyen H., Kim K., Shon Z. and Hong S. (2009) A Review of Atmospheric Mercury in the Polar Environment. *Crit. Rev. Environ. Sci. Technol.* 39, 552-584.

Nylander W (1863) Lichens in J. Triana and J. E. Planchon: Prodromus florae Novo-Granatensis. Ann. Sci. Nat. IV. 19 (5/6), 286-382.

Oum K., Lakin M., DeHaan D., Brauers T. and Finlayson-Pitts B. (1998) Formation of molecular chlorine from the photolysis of ozone and aqueous sea-salt particles. *Science* 279, 74.

Pehkonen S. and Lin C. (1998) Aqueous photochemistry of mercury with organic acids. *Journal of the Air Waste Management Association* 48, 144.

Pehkonen S. and Lin C. (1998) Aqueous photochemistry of mercury with organic acids. *Journal of the Air Waste Management Association* 48, 144-150.

Prestbo E. and Gay D. (2009) Wet deposition of mercury in the US and Canada, 1996-2005: Results and analysis of the NADP mercury deposition network (MDN). *Atmos. Environ.* 43, 4223-4233

Ravichandran M. (2004) Interactions between mercury and dissolved organic matter - a review. *Chemosphere* 55, 319.

Ryan S. (1997) The wind field around Mauna Loa derived from surface and balloon observations. *Journal of geophysical research: Atmospheres* 102, 10711-10725.

Schauble E. and SCHAUBLE (2007) Role of nuclear volume in driving equilibrium stable isotope fractionation of mercury, thallium, and other very heavy elements. *Geochim. Cosmochim. Acta* 71, 2170.

Schroeder W., Lindqvist O., Munthe J. and Xiao Z. (1992) Volatilizatin of mercury from lake surfaces. *The Science of the total environment* 125, 47-66.

Schroeder W. and Munthe J. (1998) Atmospheric mercury - An overview. *Atmospheric environment* 32, 809.

Schroeder W., Munthe J. and Lindqvist O. (1989) Cycling of mercury betbeen water, air and soil compartments of the environment. *Water Air Soil Pollut.* 48, 337.

Schroeder W., Yarwood G., Niki H (1991) Transformation processes involving mercury species in the atmosphere- results from a literature survey. *Water Air Soil Pollut.* 56, 653-666.

Schwartz, S.E., 1984. Gas- and aqueous-phase chemistry of HO2 in liquid water cloud. Journal of Geophysical Research 86,11598-11946.

Schwartz, S.E., 1986. Mass transport considerations pertinent to aqueous phase reactions of gases in liquid-water clouds. In: Jaeschke, W. (Ed.), Chemistry of Multiphase Atmospheric Systems NATO ASI Series, vol. G6. Springer, New York, pp. 415-417.

Seigneur C. and Lohman K. (2008) Effect of bromine chemistry on the atmospheric mercury cycle. *Journal of geophysical research* 113, D23309.

Seigneur C., Wrobel J. and Constantinou E. (1994) A chemical kinetic mechanism for atmospheric inorganic mercury. *Environmental science technology* 28, 1589.

Selin N. (2009) Global Biogeochemical Cycling of Mercury: A Review. *Annual review of environment and resources* 34, 43.

Slemr F., Schuster G. and Seiler W. (1985) Distribution speciation, and budget of atmospheric mercury. *J. Atmos. Chem.* 3, 407-434.

Smith, L.B., 1934. Geographical evidence on the lines of evolution in the Bromeliaceae. Bot Jahrb. 66: 446- 468

Sommar J., Hallquist M., Ljungstrom E. and Lindqvist O. (1997) On the gas phase reactions between volatile biogenic mercury species and the nitrate radical. *J. Atmos. Chem.* 27, 233.

Turro N. (1983) Influence of nuclear spin on chemical reactions - magnetic isotope and magnetic field effects (a review). *Proc. Natl. Acad. Sci. U. S. A.* 80, 609.

Xiao Z., Munthe J., Stromberg D. and Lindqvist O. (1994) Photochemical behavior of the inorganic mercury compounds in aqueous solution. *Mercury pollution: Integration and synthesis*581.

Xiao Z., Stromberg D. and Lindqvist O. (1995) Influence of humic substances on photolysis of divalent mercury in aqueous- solution. *Water Air Soil Pollut.* 80, 789.

Yang L. and Sturgeon R. (2009) Isotopic fractionation of mercury induced by reduction and ethylation. *Analytical and bioanalytical chemistry* 393, 377.

Zheng W. and Hintelmann H. (2010) Nuclear Field Shift Effect in Isotope Fractionation of Mercury during Abiotic Reduction in the Absence of Light. *J. Phys. Chem* 114, 4238-4245.

Zheng W., Foucher D. and Hintelmann H. (2007) Mercury isotope fractionation during volatilization of Hg(0) from solution into the gas phase. *J. Anal. At. Spectrom.* 22, 1097.

Zheng W. and Hintelmann H. (2009) Mercury isotope fractionation during photoreduction in natural water is controlled by its Hg/DOC ratio. *Geochim. Cosmochim. Acta* 73, 6704.

BIOGRAPHICAL SKETCH

Sulata Ghosh received her Bachelor of Science degree in Geology from St Xavier's College, University of Mumbai in 2000. She completed her Master of Science degree in Geology from St Xavier's College, University of Mumbai in 2002. Her research interests lie in Environmental Geochemistry and intends to pursue a career in academics.